ANALYSIS OF STRESSORS CONTRIBUTING TO HYPOXIA IN LAKE ERIE USING DETERMINISTIC MODELS

by

Daniel Kenneth Rucinski

A dissertation submitted in partial fulfillment
of the requirements for the degree of
Doctor of Philosophy
(Natural Resources and Environment)
in the University of Michigan
2013

Doctoral Committee:

Professor Donald Scavia, Co-Chair
Adjunct Professor Joseph V. DePinto, Co-Chair
Professor J. David Allan
Associate Research Scientist Dmitry Beletsky
Professor George W. Kling

For my brothers

Acknowledgements

I have so many people to thank for helping me to complete this degree and accomplish a long-time dream. I have to first thank my committee co-chairs, Don Scavia and Joe DePinto. Throughout all of these years, they’ve both continued to support me and provide guidance and mentorship. Professor Scavia acted as both a co-chair, and my main academic advisor in SNRE. Not only did he provide me with a meaningful project to base my work on, but he has been incredibly understanding of my struggles to balance a full-time career with an in-depth academic pursuit. He also provided much of cost of education through his grants. Joe DePinto has been mentoring me since I began work at LimnoTech in 2003, and I will forever be grateful for his support of my dream to earn a doctorate degree. He provided me with an opportunity to pursue that dream and has never stopped supporting me in that pursuit, often times when I was myself questioning it. It’s been an honor to work alongside such prolific Great Lakes researchers for so long.

When I began considering “going back to school” after being in the consulting work force, I was worried that a long-term academic program would limit my ability to remain active in exciting and different project work at LimnoTech. I owe so much to all of the people there that put up with my flexible schedule, and provided time away from “billable” work to pursue my dream while maintaining a presence in the company. I’d particularly like to thank Paul Freedman and John Marr for seeing the value in investing in me and allowing me the freedom to attend classes and time off to work on this dissertation. I’d also like to thank all of the project

managers that worked around my ever changing schedule, especially Tad Slawecki and Todd Redder.

Iôd also like to thank the rest of my dissertation committee for all of the advice and guidance. Dmitry Beletsky has been extremely helpful in teaching my about hydrodynamics and lake circulation. I never intended to become an ocean physicist, but wanted to be able to understand enough to apply biological models in a hydrodynamic framework, and Dima has been excellent in understanding my goals. Professor Dave Allan has similarly helped me understand the land-based side of ecosystem modeling, and helped me to stay focused on not only the ecology in lakes, but also the rivers and watersheds that ñfeedò them. Professor George Kling has brought a valuable presence to my dissertation committee, as he has worked outside of the modeling aspect of this work, and kept me grounded in the science of limnology, as opposed to just the applications in modeling.

Of course I would not have been able to pursue this degree without considerable funding from the EcoFore grant provided by the NOAA Center for Sponsored Coastal Ocean Research, as well as a Graduate Student Research Assistant appointment from the School of Natural Resources and Environment.

Finally, I must thank all of my friends and family for not only supporting me in every way imaginable, but never letting me give up on myself and continually reminding me of what a special opportunity I had. Specifically, I want to thank my wonderful wife Kristyn for her never ending support. Through all of these years, this adventure has brought many stressful periods of time. And through all of them she has never wavered and continued to push me to work harder. I honestly would not have completed this work without her.

TABLE OF CONTENTS

LIST OF TABLES

LIST OF FIGURES

ABSTRACT

Lake Erie continues to experience hypoxia (dissolved oxygen concentrations $< 2\ \mathrm{mg \cdot L^{-1}}$), despite basin-wide reductions in total phosphorus loads intended to limit or eliminate hypoxia, as outlined in the Great Lakes Water Quality Agreement (GLWQA) in 1978. Despite initial success, periodic hypoxia in the central basin of Lake Erie persisted, and more recently, hypoxic area has enlarged and reemerged as a potential hazard to ecosystem health. The consequences of hypoxic conditions (e.g., loss of suitable fish habitat and decrease in fish abundance and growth rates) have therefore led to a renewal in interest in understanding the relative contributions to the stressors contributing to hypoxia in Lake Erie. This dissertation focuses on the impacts of nutrients and hydro-meteorological forcings

To analyze these stressors, a group of models was developed and applied in multiple management frameworks. First, a simple dissolved oxygen model was applied in a 1-dimensional, vertically stratified domain. Meteorological forcings determined temperature and mixing conditions, while the oxygen depletion rate within the water column was adjusted to match observed spatial and temporal dissolved oxygen concentrations, therefore determining if the water column oxygen demand has varied inter-annually. The model required an annually varying water column oxygen demand, suggesting that hypoxia is a function of variations in biological activity within the water column (e.g., organic carbon production), and not strictly a meteorological phenomenon. Second, a more robust lower-food web model was developed and calibrated, using the same 1-dimensional temperature and mixing conditions, but including nutrient loads and internal cycling to assess the effects of inter-annual variation in loading magnitude. The analysis suggests that a 46% reduction from the 2003-2011 average total phosphorus load and a 56% reduction from the current GLWQA target would be required to reduce hypoxic area to 2,000 km^2. Finally, several hypothetical scenarios were explored with the lower-food web model, representing variations in load seasonality and meteorological conditions; including two climate warming scenarios. This work suggests that while there has been significant variation in seasonal patterns of nutrient loads, meteorological conditions play an important role in the interannual variability due to its impact on stratification. The models developed here provide an estimate of expected hypoxic conditions as a function of loading; however, the forecast estimates must be applied within uncertainty bounds due to the importance of inter-annual meteorological variability.

CHAPTER 1: Introduction

Many aquatic systems suffer severe water quality issues as a result of excess organic carbon production, or eutrophication (Nixon 1995). There are two potential sources of the organic carbon: allochthonously derived (produced outside of the water body itself) and nutrient-driven autochthonous production driven from within the water body.

Autochthonous carbon production can be a result of increases in agriculture and urban development and the associated runoff (i.e., components of cultural eutrophication) and can increase the negative impacts on water quality considerably. Urban development tends to increases municipal or industrial point source discharges (Dolan 1993), while soil erosion and runoff containing excess fertilizers or manure tend to be related to agricultural practices (Calhoun et al. 2002).

Many large freshwater lakes near urban or agricultural areas have experienced degraded water quality, including poor clarity, taste and odor issues, harmful and nuisance algal blooms, and little to no dissolved oxygen in the hypolimnion (El-Shaarawi 1987; Rosa and Burns 1987; Cook et al. 1993; Chapra 1996; Breitburg 2002). The topic of this dissertation is to investigate theses natural and anthropogenic forcings that contribute to seasonal hypoxia (dissolved oxygen < 2 mg·L^{-1}) in the Central Basin of Lake Erie. While this dissertation focuses on the impacts of loading and meteorological stressors, it should be noted that some recent research has suggested that other phenomenon have the potential to influence the magnitude and duration of hypoxia, such as the roles of invasive filter feeders (Hecky et al. 2004) and the contribution of winter diatom growth to carbon production (Twiss et al. 2012). However, Bocaniov et al. (2013) demonstrated that the influence of filter feeders is strongest in near-shore areas, while generally limiting organic carbon production in offshore regions via the near shore shunt hypothesis. Additionally, it is not clear if winter carbon production does contribute to summer hypoxia (Twiss et al. 2012).

Lake Erie is the smallest and shallowest of the Laurentian Great Lakes; however, it has the highest drainage area to surface area ratio. Its drainage basin is the most populated, contains the highest proportion of agricultural lands, and contains several major urban areas, including Detroit, Toledo, and Cleveland. These physical characteristics and land use can lead to excessive amounts of nutrients entering the lake (Richards 2006; Richards and Baker 2002).

The morphology of Lake Erie is also conducive to hypoxia, as the spatial orientation and dominant flow patterns create a west-to-east transport of nutrients from the agricultural areas to the intermediate depths of the center of the lake. The lake has three distinct basins (Figure 1.1). The western basin is the shallowest, and rarely thermally stratifies. Therefore, the normally well-mixed western basin rarely experiences low oxygen conditions . Conversely, the eastern basin is very deep, and does experience strong stratification. However, its hypolimnion is so large that it is highly unlikely that the oxygen resources would be depleted; i.e., the amount of dissolved oxygen contained in the hypolimnion exceeds the potential oxygen demand from within the water column and the sediments. The central basin is a transitional zone between the shallow western and deep eastern basin. It has an intermediate depth, allowing it to stratify annually, but with a relatively small hypolimnion. Also, it receives a significant load of nutrients from the western basin, in addition to the load from tributaries and point sources entering the central basin directly. The thermal stratification inhibits oxygen transfer to the bottom waters, and decomposition of organic matter decreases oxygen conditions. As a result, the central basin is generally the only part of Lake Erie to experience hypoxia (Bertram 1993).

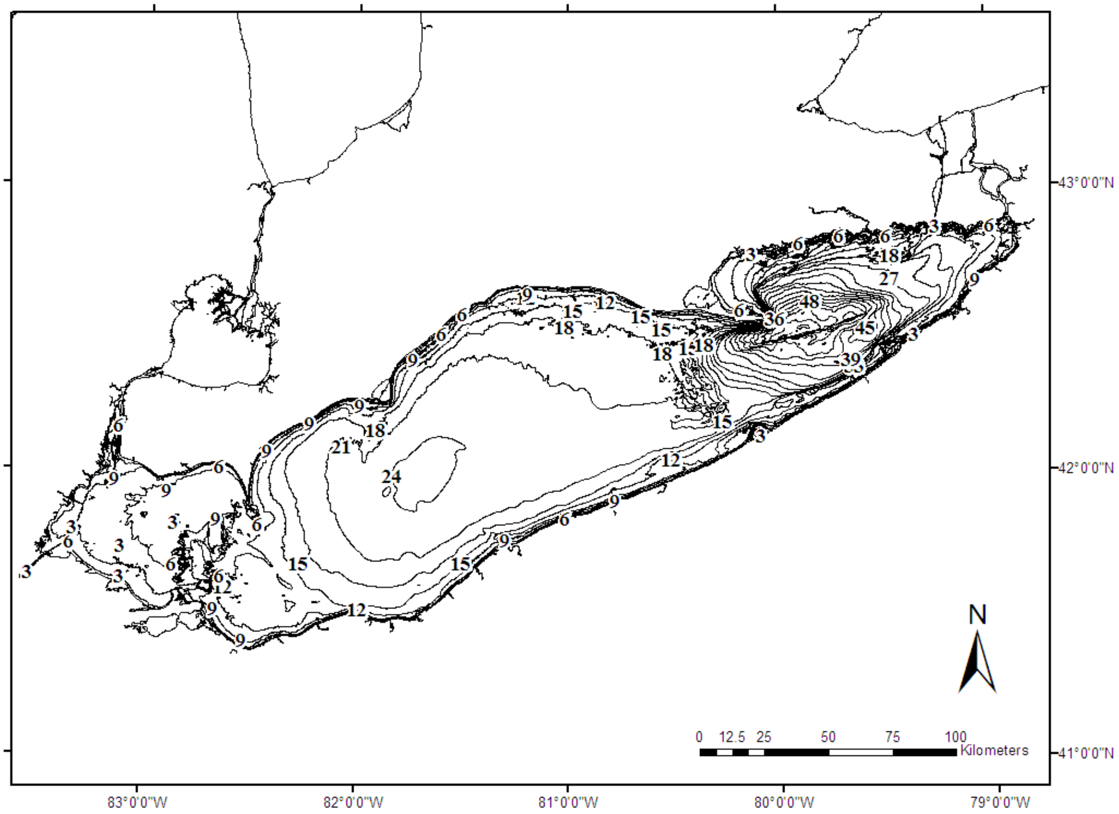

Figure 1.1: Morphology of Lake Erie

International concern about the consequences of hypoxia and cultural eutrophication led to extensive studies on the Lake Erie food web in the early 1970s, culminating in the Great Lakes Water Quality Agreement (GLWQA 1978) calling for an unprecedented total phosphorus load reduction (DePinto et al. 1986). Despite initial success, periodic hypoxia in the hypolimnion of the central basin of Lake Erie persisted, and more recently, the hypoxic area has enlarged and reemerged as a potential hazard to ecosystem health (Burns et al. 2005; Zhou et al. 2013).

Several studies have been performed previously investigating the observed oxygen dynamics in Lake Erie (Rosa and Burns 1987; Burns et al. 2005; and Chartlon 1980a), as well as early oxygen and algal growth forecasting models over decadal periods (Di Toro et al. 1987; Makarewicz 1993). In recent years, extensive sampling of the benthic food web and invasive species colonization has also occurred (IFYLE 2006). All of these efforts continue to help inform researchers and managers on aspects of the individual components of this complex system. However, the potential adverse effects of hypoxia present a need to better understand and quantify the factors that influence it. An integrated modeling analysis can help synthesize these data and observations, while combining the hydrometeorological effects that are also known to affect oxygen conditions. This dissertation explores many of the loading and hydrometeorological stressors affecting hypoxia in Lake Erie, and can provide critical guidance for stakeholders and lake managers attempting to reduce and limit hypoxia.

To investigate these impacts and stressors in Lake Erie, I have developed several models of the ecosystem, each focusing on different dynamics of the food web, climate, and with varying complexity. This approach allows me to gain insight into the significant stressors contributing to hypoxia, and also explore how the different models respond to variations in inputs, such as loads or hydrodynamics. Additionally, the models allow for the investigation of hypothetical situations, such as variation in nutrient load seasonality or increased regional air temperatures. The models developed in this effort are part of a combined framework of linked watershed, hydrodynamic, water quality, and fishery components (Scavia et al. in review). This dissertation focused on the lake water quality components of this framework.

This dissertation consists of 6 chapters, including this brief introduction. Chapter 2 contains a literature review of hypoxia as a general phenomenon as well a summary of relevant biogeochemical processes, focusing on large freshwater ecosystems, and especially Lake Erie. A review of previous hypoxia and lower food web modeling applications is included in Chapter 2. Chapter 3 demonstrates the development, calibration, and application of a simple 1-dimensional dissolved oxygen model for Lake Erie (Rucinski et al. 2010). This analysis indicates that while physical conditions are important, the autochthonous production of decomposable organic carbon driven by phosphorus loading is also necessary to capture inter-annual hypoxia variation in the central basin. Therefore, in Chapter 4 I have expanded the complexity of that model to include a traditional lower food web model. This more complex model is applied over a range of nutrient loading and hydrodynamic conditions to demonstrate expected reductions in hypoxia given certain model inputs (e.g., loads, air temperature regimes). Chapter 5 expands upon analysis of the drivers of the lower food web model, exploring not only a range of loads, but also a complete matrix of observed loading and hydrodynamic combinations. Additionally, hydrodynamic variability is further explored by applying the loading combinations under two hypothetical climate warming scenarios. Chapter 6 is a synthesis of these applications as well as comments on limitations, significant findings, and recommendations for future work.

CHAPTER 2: Literature Review

2.1 Hypoxia in Lake Erie

Lake Erie is far from the only ecosystem to suffer the effects of seasonal hypoxia. In fact, Bricker et al. (2007) combined several studies and estimated that 47-58% of US estuaries or other coastal water bodies (including the Great Lakes) currently exhibited seasonal hypoxia. This is an increase from approximately 38% in the 1980s (Whitledge 1985). While several smaller in-land lakes exhibit hypoxia or anoxia due to extreme cultural eutrophication, hypoxia in Lake Erie can be a naturally occurring phenomenon as a result of climate and circulation (Rao et al. 2008), although exacerbated via eutrophication. While many large marine ecosystems (e.g., Chesapeake Bay; Hagy et al. 2004, Gulf of Mexico; Rabalais et al. 2002, and estuaries around the world; Diaz 2001) also experience low DO, this literature review was focused on freshwater systems, where tidal and saline influences are not present. It should be noted that many of the same mechanisms are present in marine systems that experience hypoxia, including seasonal stratification, nutrient induced plankton growth, and antecedent sediment oxygen demand.

Density stratification creates two zones of relatively well-mixed waters in temperate dimictic lakes, with the upper layer (epilimnion) and lower layer (hypolimnion) separated by the thermocline. The thermocline contains a sharp density gradient that limits vertical transport between these layers. During the stratified period, the epilimnion can be highly productive, with generally high oxygen content as photosynthesis exceeds respiration. Often the epilimnion dissolved oxygen content can be at or above temperature-dependant saturation. Conversely, the hypolimnion often can be shielded from sunlight as a result of both organic and inorganic particulate matter (inhibiting photosynthesis in the deeper waters), and little or no oxygen is transported across the thermocline via diffusive or advective forces. The essentially isolated bottom waters can experience severe oxygen depletion if sufficient oxygen demanding materials are present in the either the water column or sediments. Sediment digenesis can deplete oxygen reserves further.

Several natural and anthropogenic factors are at least jointly responsible for exacerbating eutrophication. These include hydrology and climate (termed here as hydrometeorology) (Diaz 2001; Blumberg and Di Toro 1990), invasion of benthic filter feeders (e.g., zebra and quagga mussels; Hecky et al. 2004), and non-point and point source nutrient loading. Quantifying the relative impacts of these stressors is essential to being able to predict the timing, magnitude, and effects of low oxygen conditions, as well as manage the causes.

The timing of and strength of stratification is a function of climate characteristics, i.e., atmospheric heating, wind generated mixing, and hydrologic flows to the system. Early and hot summers can lead to a longer stratified period with a deeper thermocline. These circumstances can result in a small reservoir of oxygen in the bottom waters when stratification sets up and prolonging the duration of isolation from the surface. Both the timing and magnitude of hydrology is also a function of climate, as wetter periods can lead to more runoff and the associated nutrient loads stimulating phytoplankton growth. Therefore, normal variability in climate, as well as global and regional climate change, can considerably impact dissolved oxygen conditions, if sufficient organic matter is present in the system.

Eutrophication of lakes and estuaries has lead to many undesirable water quality conditions including poor clarity, nuisance algal blooms, and low oxygen (Vollenweider et al. 1980; Wetzel 2001). These consequences are partially a result of nutrient enrichment, which can occur naturally or be exacerbated by human influences. Nutrients stimulate primary productivity in surface waters, increasing phytoplankton biomass and decreasing light penetration. After the initial increase in algal growth, phytoplankton die or are consumed, creating sources of autochthonous organic matter. Under well-mixed conditions, this has relatively little impact on oxygen concentrations. However, if the water column is vertically stratified, with regard to density, then bottom waters can be isolated from oxygen sources at the surface and decomposition of that organic matter creates a significant oxygen demand (Rao and Jurkovic 1979; Helly and Levin 2004). In certain systems, hypoxic conditions can occur in the hypolimnion, with dramatic impact on water quality and ecosystem health, including altering both the lower and upper food web (Cook et al. 1993; Chapra 1996; Breitburg 2002; Diaz and Rosenberg 2008).

Another possible issue is the impact of invasive species on water quality. For example, the establishment of dreissenids, particularly in the Great Lakes, has significantly altered nutrient dynamics and water quality, particularly in the near shore areas (Hecky et al. 2004; Bocaniov et al. 2013). These filter feeders can increase water clarity, decrease phytoplankton concentrations, and excrete dissolved nutrients available for uptake by benthic alga. The resulting metabolism can also create an additional oxygen demand near the lake bottom. In areas of high colonization, it is possible for the severity of hypoxia to increase due to this metabolism. (Hecky et al. 2004).

Hypoxic conditions present potential stresses to many aquatic organisms. For example, benthivorous fish, such as yellow perch, rely on the cold, dark bottom waters of lakes and estuaries for refuge and habitat (Aku and Tonn 1997; Breitburg 2002). If the oxygen they require for survival is not present, the fish may be forced to consume less preferred prey, and otherwise inhabit less suitable thermal habitats (Arend et al. 2011; Roberts et al. 2009; Roberts et al. 2012; Vanderploeg et al. 2009).

2.2 Biogeochemical Processes

A eutrophication model of Lake Erie should incorporate relevant and important biogeochemical processes. This section provides a summary of the basic processes of biogeochemical cycles in freshwater systems.

2.2.1 The Carbon Cycle

Organic and inorganic carbon play important roles in the flow of energy in lakes. Inorganic carbon is an essential element for primary production, while organic carbon is cycled through the food web, including within the detritus pool. The amount and distribution of each can have a significant impact on the trophic structure and health of a lake.

2.2.1.1 Inorganic Carbon

Inorganic carbon is the primary source of carbon for photosynthesis. Primary producers (e.g., algae and cyanobacteria) use inorganic carbon to form organic substances (King 1970). Exchange with the atmosphere at the water surface and dissolution of minerals provide the source of inorganic carbon. It also plays an important role in the buffering capacity of lakes, via the carbonate-bicarbonate equilibrium.

2.2.1.1.1 Carbonate-Bicarbonate Equilibrium

CO_2 from the atmosphere is very soluble, and forms carbonic acid in the water column. Carbonic acid dissociates rapidly into bicarbonate and then carbonate. At equilibrium, the carbonate and bicarbonate ions dissociate forming hydroxyl ions. In systems that have high carbonate levels from runoff or groundwater inputs, the carbonic acid can solubilize carbonates, which can lead to excess hydroxyl ions. As long as the supply of excess hydroxyl ions is present, the water will maintain a buffering capacity against pH changes (Lampert and Sommer 1998).

2.2.1.1.2 Calcium carbonate Precipitation

During periods when CO_2 is lost at a rapid rate, such as during algal blooms, the equilibrium reactions can be thrown out of balance. Calcium bicarbonate ions will dissociate to replace CO_2, producing a calcium carbonate precipitate, often referred to as ñwhitingò (Otsuki and Wetzel 1972).

2.2.1.1.3 Photosynthetic Uptake

Primary producers convert inorganic carbon (primarily in the form of dissolved CO_2) to carbohydrates through photosynthesis. Under normal conditions, dissolved inorganic carbon is present in sufficient concentrations - so that CO_2 is in abundant supply, and rarely considered a limiting nutrient (Goldman et al. 1974). The carbonate complex reactions are generally at or near equilibrium, and photosynthesis will not be limited by the available CO_2. However, when uptake is occurring rapidly (e.g., during an algal bloom), pH increases above 8.5 can shift the equilibrium reactions resulting in CO_2 concentrations near zero. .

2.2.1.2 Organic Carbon and Detritus

Organic carbon pools consist of particulate organic carbon (POC) and dissolved organic carbon (DOC). Non-living POC (decomposing detritus) is generally much more abundant than living POC. POC can also be sub-categorized between fine (< 1µm) and course size classes (> 1µm). DOC generally represents greater than 60% of the total organic carbon pool; it can also flocculate to form fine POC.

.

2.2.1.2.1 Carbon in the Food Web

Carbon is cycled through the aquatic food web via photosynthesis and aerobic respiration (as described above) as well as heterotrophic consumption and decomposition (Wetzel 2001). Heterotrophic decomposition is the use of organic matter as the carbon substrate required for metabolism by bacteria and other primary and secondary consumers. During heterotrophic decomposition, CO_2 is produced. Most lakes are generally considered net heterotrophic (i.e., the system consumes more oxygen than it produces; Hanson et al. 2004; Urban et al. 2005)

2.2.2 The Nitrogen Cycle

The nitrogen cycle can be important in determining the productivity of a lake, and is driven by three main processes through the conversion of various forms of inorganic and organic nitrogen (assimilation, nitrogen fixation, denitrification), as outlined below.

2.2.2.1 Assimilation

Nitrate and ammonia are the primary inorganic forms of nitrogen taken up by microbes in lakes. Ammonia nitrogen is energetically more efficient for assimilation than nitrate uptake (Howarth et al. 1988).

Ammonia is generated by bacterial decomposition and is generally in low concentrations in lakes due to rapid uptake. Bacteria also oxidize the ammonia and convert it to nitrite and nitrate. Under anaerobic conditions, increases in ammonia may occur, as it cannot be oxidized directly by aerobic bacteria.

2.2.2.2 Nitrogen Fixation

Bacteria and some cyanobacteria have the ability to take up dissolved nitrogen gas (N_2) and convert it to ammonia for growth (Vitousek et al. 2002). Cyanobacteria typically account for much more of the nitrogen fixation than bacteria in a lake; however, bacterial fixation is greater in wetlands. Nitrogen fixation by cyanobacteria has been shown to be light dependant in most lakes. Fixation is less energetically efficient than either nitrate or ammonia assimilation, therefore, cyanobacteria generally only fix nitrogen when the ammonia and nitrate pools have been depleted.

2.2.2.3 Denitrification

Under anaerobic conditions, nitrate can be reduced to nitrogen gas by bacterial denitrification. This is a result of the absence of oxygen, and use of nitrate as a hydrogen acceptor in the oxidation of organic substances.

2.2.2.4 Organic Nitrogen

During primary production, inorganic forms of nitrogen (e.g., ammonia and nitrate) are assimilated into organic nitrogen. There are two forms of organic nitrogen in lakes, dissolved organic nitrogen (DON) and particulate organic nitrogen (PON), with DON typically comprising over half of all of the dissolved nitrogen in lakes. Most DON occurs as amino nitrogen compounds, while PON is essentially composed of algae, bacteria, and detritus.

2.2.3 The Phosphorus Cycle

Phosphorus is typically the growth-limiting nutrient in freshwater systems. Total phosphorus is made up of organic and inorganic species. While much of the total phosphorus in lakes in bound in the organic form, dissolved inorganic phosphorus (often referred to as soluble reactive phosphorus or orthophosphate) is the only form that is directly usable by algae and cyanobacteria in the water column.

2.2.3.1 Inorganic Phosphorus

Inorganic phosphorus is comprised of soluble reactive phosphorus (SRP), labile particulate inorganic phosphorus (LPIP), and refractory (or bound) particulate inorganic phosphorus (RPIP). Phosphates are highly reactive and can combine with many cations and precipitate out of the water column in alkaline conditions (Otsuki and Wetzel 1972). They can also sorb to inorganic colloids or clays, reducing the available pool.

2.2.3.1.1 Uptake Kinetics

The uptake of phosphorus is not only dependent on nutrient availability, but also environmental factors, such as light and pH. When light is abundant and phosphorus is not limited in availability, some algae can create internal stores (i.e., uptake can be more rapid than what is required for immediate growth, therefore excess phosphorus is stored intercellularly; Keenan and Auer 1974). This occurs mostly when nitrogen or carbon is limiting growth. Additionally, most algae exhibit optimal growth and uptake within a narrow pH range. Changes in pH may alter rates of phosphorus absorption by altering enzyme activity, or changing cell permeability.

2.2.3.2 Organic Phosphorus

The vast majority of phosphorus in lakes is bound or contained in cellular structure of organisms. Bacterial metabolism converts organic forms of phosphorus into inorganic forms through decomposition. The decomposition of organic materials can occur at different rates, and often a portion of the dissolved organic phosphorus cycles more rapidly.

2.2.3.3 Exchange at Sediment-Water Interface

Phosphorus diffusion through sediments can be slow except at the surface of the sediments because below the first few millimeters of sediments, exchange is controlled by low diffusion rates.

Under aerobic conditions near the sediment-water interface, an oxidized microzone forms. Below this zone, sediments are typically anoxic. Under anoxic conditions, phosphate and ferrous iron are released to the water column, due to iron being used for redox reactions. Normally, the oxic microzone prevents this release of sediment bound phosphate. However, in highly productive lakes, the release of phosphorus from the sediments can amount to 10-30% of the available pool (Auer et al. 1993).

2.2.4 Oxygen Resources

The oxygen cycle is driven by inputs from the atmosphere and photosynthesis, and losses from biotic respiration and chemical oxidation.

2.2.4.1 Atmospheric Inputs

Diffusion of oxygen at the air-water interface in a lake is a slow process. For equilibrium between dissolved oxygen (DO) and atmospheric oxygen to occur, turbulent mixing (from wind, waves, etc) is required (Ro et al. 2007). As temperature increase, the solubility of oxygen decreases. During ice cover, atmospheric inputs are essentially zero.

2.2.4.2 Photosynthesis and Respiration

Primary producers consume inorganic carbon and produce oxygen during photosynthesis, and during respiration organisms consume oxygen (Stern et al. 2003). In highly productive lakes, dissolved oxygen near the surface can be above saturated conditions during summer algal blooms. Considerable fluctuations can occur in DO levels throughout the day. These diurnal variations are a result of photosynthesis exceeding respiration in the presence of light (i.e., daytime) and respiration exceeding photosynthesis during the night.

2.2.4.3 Decomposition

Organic matter inputs to the lake add a demand for dissolved oxygen through bacterial respiration during decomposition. DO levels decrease progressively throughout the summer from the death and decomposition of organisms. Highly productive lakes generate a large amount of decomposing material, and this can lead to depletion of oxygen resources in the bottom waters, where light is unavailable for photosynthesis.

2.2.4.4 Sediment Interactions

Accumulation of dead and decomposing organic materials in the lake sediments can cause a significant loss of oxygen in the hypolimnion. This is primarily a problem during stratified periods, where the bottom waters are isolated from oxygen inputs. Oxygen consumption at the sediment water interface can be extremely intense, often leading to hypoxia and anoxia in productive systems (Effler 1996; Edwards et al. 2005).

2.2.5 Upper Food Web

2.2.5.1 Zooplankton

Zooplankton in lakes are composed primarily of three main groups: rotifers, cladocerans, and copepods. Rotifers are primarily sessile, although some species are planktonic. Most are non-predatory and consume bacteria, small algae, and detritus, although some rotifers feed on protozoa and other rotifers. Filtration of particles is the dominant feeding mechanism. Cladocerans mainly feed on algae and other particles filtered from the water column and are non-predatory, although a few species feed on other zooplankton. Copepods are comprised of two subgroups, calanoids and cyclopoids. Cyclopoids can be either carnivorous or herbivorous. Calanoids swim in circular motions to generate a current to carry particles to feed on.

2.2.5.2 Dreissinids

Dreissinids (e.g., zebra and quagga mussels) can have dramatic impacts of ecosystem health. Due to the very high filtering capabilities, they can reduce phytoplankton biomass, increase water clarity, increase benthic production, and the reduce biodiversity of other mollusks (Hecky et al. 2004; Effler 1998). Increased clarity appears to be a significant impact, as the increase in littoral photogenic area can shift algal production to benthic species (e.g., cladophora; Hecky et al. 2004). This can have a dramatic effect on how and where nutrients are taken up and where detritus accumulates. Additionally, there are very few predators of dreissenids, and they multiply and colonize areas at an astounding rate.

2.2.5.3 Planktivorous Fish

Planktivorous fish consume zooplankton and play an important role in controlling their abundance and size structure. Size selection for feeding is based on abundance; if prey are abundant, only larger plankton are preyed upon, and as abundance decreases, smaller prey are consumed (Vanderploeg et al. 2009). When certain zooplankton are preferred by fish, the community structure can be altered (e.g., larger cladocerans can be eliminated from lakes due to size preference). Characteristic species include rainbow smelt and the emerald shiner.

2.2.5.4 Piscivorous Fish

Piscivores prey mostly on other fish; however, some early life-stages begin as planktivores. Similar to the impacts that planktivores can have on determining community size and structure, piscivores can have the same effect. For example, when a community is dominated by large piscivores, the amount of planktivores decreases, and therefore the size of zooplankton increases. Characteristic species include walleye and yellow perch.

2.3 Review of Relevant Lower Food Web, Hypoxia, and Eutrophication Models

The models developed here are all deterministic, i.e. random variability in parameters and solutions is not included. The model described in Chapter 3 is a hybrid between a mechanistic thermal model (i.e., the solution is based on the processes involved in the system) and an empirical dissolved oxygen model (i.e. the solution is a function derived directly from a best fit to observations; Chapra 1997). The model incorporates a first-order oxygen loss rate that represents all biochemical processes, as well as time-variable thermal profile. However, this model was not adequate for describing the nutrient cycling and system response to loading. As a result, Chapters 4 and 5 use a mechanistic, deterministic modeling approach to estimate hypoxia. These models are developed by making assumptions on how the state variables interact with each other and with the driving forces. Generally the rate terms that define these interactions are obtained by calibration to best fit the observations. Often these types of models are termed ñmass balance models,ò as they conserve mass throughout the simulation (Chapra 1997). In the study performed for this dissertation, the model complexity varied in terms of how the biological processes of the food web were described; however, the spatial complexity was constrained to a 1-dimensional vertical profile of the central basin of Lake Erie. Many other models have been developed for related purposes, several of which are described below.

Dissolved oxygen is an integral component to any lower food web ecosystem model. There are dozens of standard lower food web models, all incorporating DO in some form. Many of these models are ñoff the shelfò (i.e., developed for use in multiple systems); however several have been developed specifically for use in a single system. This section will focus on a review of the biogeochemical cycles included in a handful of relevant models which fall in both categories, followed by a high level summary and historical review of important models that have been developed in the Great Lakes.

The Lake Ontario Ecological Model (Scavia 1980) contains a biomass and detritus based carbon cycle with constant stoichiometry. Phytoplankton and zooplankton biomass contains a constant Redfield ratio of the nutrient distribution. When detritus is decomposed, it is redistributed between the nutrient pools based on the Redfield ratio. Dissolved inorganic carbon is included in the model; however, it is not allowed to be a limiting nutrient. The model also simulates the carbonate precipitation system. If carbonate precipitation occurs, carbon is subject to settling, diffusion, and dissolution.

Three phosphorus pools are considered in this model, detrital phosphorus, phosphorus in biomass, and dissolved inorganic phosphorus. Phosphorus excreted during respiration is assumed to be in the dissolved inorganic form. This phosphorus submodel is fairly simplified. The particulate inorganic form is ignored, as well as dissolved organic phosphorus. Additionally, there is no capability for phosphorus release from the sediments during anaerobic conditions. The assumption that all excreted phosphorus is available may be overestimating phosphorus availability.

Dissolved oxygen sources in the Lake Ontario Ecological Model include reaeration, and photosynthesis. DO is lost through algal and zooplankton respiration, detritus respiration, and nitrification. Respiration of benthic invertebrates is assumed to be a temperature dependant function. Overall, the model appropriately represents the oxygen cycle in Lake Ontario.

DiToro and Connelly (1980) developed a compartmentalized biological model for Lake Erie, referred to as Lake1A. Two phosphorus state variables are included: unavailable phosphorus and soluble reactive phosphorus. The available fraction is used by both algal classes and returned to the water column pools through respiration and non-predatory mortality. Herbivorous zooplankton obtain phosphorus through predation and also return it to the water column pools though excretion and death. Phosphorus is also returned to the water column pools through carnivorous zooplankton excretion and death. The phosphorus cycle is relatively simple in Lake1A. The sediment flux of available phosphorus under anaerobic conditions is ignored, which may make application to highly eutrophic lakes troublesome. Additionally, decomposition from detrital organic matter is simplified.

In Lake1A, dissolved oxygen sources include reaeration and photosynthesis. Sinks include oxidation of detrital organic carbon, nitrification, respiration, and a sediment oxygen demand. The DO submodel in Lake1A is mechanistically similar to the theoretical cycle. Oxidation of detritus could be separated into different rate classes, but overall the oxygen model is appropriate for application under most situations.

One stand alone ñoff the shelfò model that is widely used is WASP5 (Ambrose 1993). In WASP5, DO is affected by reaeration (wind based), decomposition of organic matter (from dissolution of detritus pools), sediment oxygen demand, primary production, and respiration. Detritus pools are dissolved into three carbonaceous biochemical oxygen demand (CBOD) classes with varying rates. The three CBOD classes represent a fast, medium, and slowly decaying matter, respectively. Dissolved oxygen is also linked with nitrification of ammonia to nitrate. SOD is calculated internally from the detritus pool that settles to the sediments. The dissolved oxygen resources modeled in WASP are generally the same as the theoretical cycle.

2.3.1 History of Modeling the Great Lakes

Initial modeling efforts in the Great Lakes began in the 1970s, beginning with a nutrient-phytoplankton-zooplankton (NPZ) model of the western Basin of Lake Erie (Di Toro et al., 1973). This model was spatially segmented into seven segments; however, mixing between the segments was based on long-term steady state exchange values. Di Toro and Connolly (1980) then applied this NPZ model (although with additional state variables for multiple phytoplankton and zooplankton classes) to the entire Lake Erie system, using a very coarse 3-dimensional domain with seven ñstackedò and connected model segments. This model would help define phosphorus loading targets to Lake Erie under the GLWQA.

Around the same period of time, other researchers were developing more complete ecosystem models for other Great Lakes. The biological model from Di Toro and Connolly (1980) was applied to Lake Ontario, although the spatial segmentation consisted of 2 mixed layers representing the epilimnion and hypolimnion (Thomann et al. 1975; Thomann et al. 1976). An initial application of the model was also applied in 3 dimensions, however, the authors remarked on the difficulty in both computation and understanding of output (Thomann et al. 1975). As described previously, Scavia (1980) also developed an ecological model for Lake Ontario around the same time, although with more advanced biological components (multiple algal and zooplankton classes).

Lake Huron and Saginaw Bay were also the subject of early ecosystem modeling. The same lake model developed by for Lake Erie (DiToro and Connolly 1980) was applied to Lake Huron and Saginaw Bay (DiToro and Matystik 1980). Bierman et al. (1980) developed a multi-class phytoplankton model for Saginaw Bay, which included internal nutrient pools, a change from the other Great Lakes models developed at the time.

While many of the early modeling efforts were focused on single lakes, others developed eutrophication models for the entire Great Lakes basin. Vollenweider (1975) developed steady-state empirical relationships between loading and chlorophyll-a for each of the Great Lakes, which also helped guide the GLWQA. Chapra (1977) developed dynamic total phosphorus models for each of the Great Lakes, using a simple mass balance budget. This modeling approach (while improved upon) is still in use and was revisited by Chapra and Dolan (2012) with new loading estimates.

More recently, studies have focused on fine-scale coupled or linked hydrodynamic-eutrophication models. The credibility of these models is enhanced as they represent more realistic transport processes. Zhang et al. (2008) developed a longitudinal 2-dimensional ecosystem model for Lake Erie based on CE-QUAL-W2 (an ñoff the shelfò model). This model uses a hydrodynamic transport model, as well as an advanced ecosystem model that includes multiple phytoplankton and zooplankton classes, a full sediment diagenesis model, and the growth and metabolism of dreissenids. A model of similar biological complexity, referred to as the Advanced Aquatic Ecosystem Model (A2EM), was developed for the lower Maumee River and Maumee Bay in Lake Erie (LimnoTech 2010). This model is driven by an extremely fine-scale advanced 3-dimensional hydrodynamic model. A fine-scale 3-dimensional model of Lake Erie as a whole has recently been developed by Leon et al. (2011) and Bocaniov et al. (2013). This model also includes advanced hydrodynamic (ELCOM) and ecosystem components (CAEDYM).

Spatial and temporal discretization varies considerable by researchers, as does the complexity of the eutrophication or biological component. However, many researchers are still using simpler models, due to the ability to run long-term and hypothetical simulations quickly. Table 2.1 summarizes many of the studies outlined above, comparing the complexities.

The more advanced models are useful for investigating linkages between nutrient pools for the entire system, and are ever increasing in biological complexity as the understanding of the biogeochemistry improves. However, they required substantial inputs that are rarely determined locally (e.g., rate processes, loading time-series for all state variables, etc.) Alternatively, the simpler models can be more easily applied, and used to understand changes or responses in the system over long periods of time.

The models developed in this dissertation expand on some of the classical approaches for estimated oxygen dynamics in the Great Lakes. Chapter 3 demonstrates the development of a very simple 1st order dissolved oxygen depletion rate model, similar to Burns et al. (2005) and Rosa and Burns (1987). However, the approach is advanced by applying the depletion rate concept to a vertically segmented grid that incorporates temporal changes in thermocline depth based on observed meteorology. The previous investigations of dissolved oxygen depletion rate (Burns et al. 2005; Rosa and Burns 1987) simply calculated the values based on linear regressions between observed DO values. Their approach therefore could not differentiate between water column and sediment oxygen demand. Additionally, their approach assumed a constant thermocline depth during stratification. The biological component to the model in Chapter 4 is similar to Di Toro and Connolly (1980), however the hydrodynamics again allow for temporally changing mixing. Additionally, due to the fine scale vertical discretization of the mixing regime, the model can be used to simulate the effect of altering meteorological conditions, such as a warming climate that results in a longer stratified period or a smaller hypolimnion. These advances can help better define the roles that loading and meteorology have in defining hypoxia. The eutrophication model developed here also incorporated an innovative approach to adjust sediment oxygen demand under forecasting conditions, as described in Chapter 4. Additionally, the output from the 1-dimensional model domain was converted to hypoxic area using the formulation from Zhou et al. (2013) to provide, for the first time, model predicted, long term estimates of the areal extent of hypoxia. Finally, the period of record of meteorological and loading conditions that drive this model provide a robust dataset. Therefore, it is possible to simulate many hypothetical scenarios, while also representing conditions both pre- and post-dreissenid invasion in the system.

Table 2.1 Summary of Existing Water Quality Models in the Great Lakes and Lake Erie.

Citation	System(s)	Hydrodyanmic Model Type	Eutrophication Model Type	Time Period	Spatial Complexity	Spatial Scale	Biological Complexity
Di Toro et al. 1973	Western Basin Lake Erie	none	NPZ	1967-1968	2D	7 water column segments	Average, Nutrient, Phytoplankton, Zooplankton
Thomann et al. 1975, Thomann et al. 1976	Lake Ontario	none	NPZ	1966-1969	1D	2 vertical layers	Average, Nutrient, Phytoplankton, Zooplankton
Chapra 1977	All Great Lakes	none	Linked-Mixed Batch Reactor	1950-2010	1D	10 Segments	Simple, TP
Di Toro and Connelly, 1980	Lake Erie	none	NPZ	1970; 1975	3D	7 water column segments, 3 sediment	Average, Nutrient, Phytoplankton, Zooplankton
Bierman et al. 1980	Saginaw Bay	none	Phytoplankton	1974-1975	-	single segment	Simple-Average; used internal nutrient pools
Scavia 1980	Lake Ontario	none	NPZ	1972	1D	3 vertical layers	Average, Nutrient, Phytoplankton, Zooplankton
Di Toro, et. al. 1987	Lake Erie	none	NPZ	1970-1980	3D	7 water column segments, 3 sediment	Average, Nutrient, Phytoplankton, Zooplankton
Rosa and Burns 1987	Lake Erie	none	Emperical/ Regression	1929-1980	-	-	Very Simple, Regression of DO values

Bierman et al. 2005	Saginaw Bay	none	NPZ + Dreissinids	1991	2D	7 segments	Advanced-Nutrient, Phytoplankton, Zooplankton, Sediments, Dreissenids
Burns et al. 2005	Lake Erie	none	Emperical/ Regression	1983-2002	-	-	Very Simple, Regression of DO values
Zhang et al. 2008	Lake Erie	CE-QUAL-W2 (1 year)	CE-QUAL-W2	1994 Hydrodyanmics, 1997-1999 Biology	2D	222 longitudinal segments x 1 m layers	Advanced-Nutrient, Phytoplankton, Zooplankton, Sediments, Dreissenids
LimnoTech 2010	Maumee Bay	EFDC	A2EM	2004-2005	3D	4613 horizontal cells x 1m layers	Advanced-Nutrient, Phytoplankton, Zooplankton, Sediments, Dreissenids
Rucinski et al. 2010	Lake Erie	POM-GL	DO Depletion Model	1987-2005	1D	48 segments	Simple, DO
Leon et al. 2011	Lake Erie	ELCOM	CAEDYM	2002	3D	2km x 40 layers	Advanced-Nutrient, Phytoplankton, Sediments
Chapra and Dolan 2012	All Great Lakes	none	Linked-Mixed Batch Reactor	1950-2010	1D	10 Segments	Simple, TP
Bocaniov et al. 2013	Lake Erie	ELCOM	CAEDYM	2002	3D	2km x 40 layers	Advanced-Nutrient, Phytoplankton, Sediments, Dreissenids

CHAPTER 3: A Simple 1-Dimensional, Climate Based Dissolved Oxygen Model for the Central Basin of Lake Erie

3.1 Introduction

Historically, Lake Erie has been subject to significant cultural eutrophication. Excess phosphorus (P) entering the lake primarily from agricultural runoff and point source discharges (Dolan 1993) have resulted in hazardous and nuisance algal blooms, poor water clarity, and summer hypoxia in the hypolimnion of the central basin. In response to concern about the consequences of eutrophication, the governments of the U.S. and Canada, largely through the auspices of the Great Lakes Water Quality Agreement (GLWQA 1978), implemented a program of P load reduction that was unprecedented for any region of the world (DePinto et al. 1986). A combination of point and non-point phosphorus load reductions achieved the target load of 11,000 metric tonnes per year and the response of the lake was rapid, profound, and close to that predicted by models (Bertram 1993; Di Toro et al. 1987; Makarewicz 1993). Despite this apparent success at reversing eutrophication, periodic hypoxia (dissolved oxygen < 2mgĀL^{-1}) in the hypolimnion of the central basin of Lake Erie persisted, and more recently enlarged and reemerged as a potential hazard to ecosystem health (Burns et al. 2005). Several natural and anthropogenic factors are at least jointly responsible for causing this resurgence. These include changes in climate and hydrology (Blumberg and Di Toro 1990; Diaz 2001; Atkinson, et al., 1999; Lam et al. 1987), invasion of benthic filter feeders (e.g., zebra and quagga mussels; Hecky et al. 2004), and increased agricultural loading (Richards 2006).

Climate change is expected to result in warmer temperatures, loss of ice cover, and decreased lake levels in many areas (Bates et al. 2008). The warming climate could have considerable implications on the Lake Erieôs stratification, and modeling studies have suggested this can impact dissolved oxygen (Blumberg and Di Toro 1990; Fang and Stefan 1997; Lehman 2002). The timing and strength of stratification is a function of climate (i.e., atmospheric heating, wind mixing). Early and hot summers can lead to longer stratified periods and a deeper thermocline, resulting in a smaller reservoir of bottom-water oxygen and prolonged isolation from surface mixing. Additionally, shorter term meteorological conditions have been shown to have an impact on the rate of oxygen depletion via enhanced mixing from storms (Lam et al. 1987). Hydrology is also a function of climate, and increasing wetter periods with more intense and frequent winter and spring storms (Croley 1990; Lofgren et al. 2002) can lead to increased runoff and the associated nutrient loads that stimulate phytoplankton growth and thus significantly impact dissolved oxygen conditions (Edwards et al. 2005; El-Shaarawi 1987). Because these processes can vary considerably from year to year, the extent to which they contribute to hypoxia is also variable. The primary purpose of this paper is to describe a modeling analysis performed to quantify the relative effects climate has had on inter-annual variability in dissolved oxygen dynamics in the central basin of Lake Erie. This is accomplished by isolating climate effects on thermal structure and exploring the resulting ability of the model to reproduce observations in hypoxia structure and formation between 1987 and 2005, a period capturing dramatic changes in the ecosystem of Lake Erie.

3.2 Study Area

Lake Erie is the smallest and shallowest of the Laurentian Great Lakes and it has the highest ratio of drainage area to surface area. Its drainage basin is the most populated and it contains the highest proportion of agricultural lands and several major urban areas. These physical characteristics and land use can lead to excessive nutrients entering the lake (Richards 2006; Richards and Baker 2002).

The morphology of Lake Erie is also conducive to eutrophication and has been shown to influence oxygen depletion (Charlton 1980b). The lake has three distinct basins (Figure 3.1). The western basin is the shallowest, and rarely stratifies thermally, preventing low oxygen conditions from developing in bottom waters. Conversely, the eastern basin is very deep, and does experience strong stratification. However, its hypolimnion is large enough that oxygen resources are rarely depleted. The central basin, however, is transitional with an intermediate depth, allowing it to stratify annually, but with a relatively thin hypolimnion. It also receives a significant load of nutrients from the western basin. Thermal stratification inhibits oxygen transfer to bottom waters, and decomposition of organic matter decreases oxygen conditions. As a result, the central basin is generally the only part of Lake Erie to experience hypoxia (Bertram 1993).

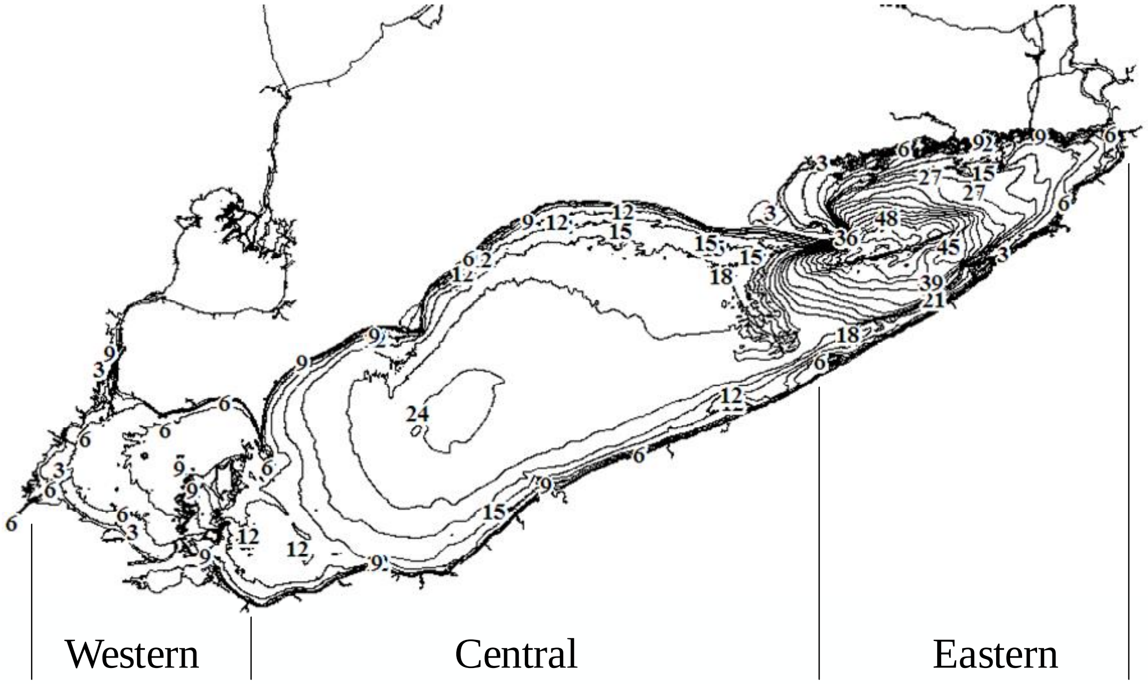

Figure 3.1: Basins and bathymetry of Lake Erie

3.3 Modeling

3.3.1 Modeling Objective and Approach

The objective was to investigate the inter-annual variability in dissolved oxygen dynamics in central basin of Lake Erie, and to assess the extent to which that variability is caused by variability of climate-driven mixing and temperature regimes. To accomplish this, a one-dimensional, linked thermal budget and dissolved oxygen model was developed. The dissolved oxygen model is a considerable simplification of the biological processes in the lake because the model was intended to focus on the effects of vertical stratification and mixing dynamics.

3.3.2 Thermal Model

Previously, a 1D model with a Richardson number dependent vertical diffusivity coefficient was developed to simulate thermal structure of Lake Erie in 1967-82 (Lam and Schertzer, 1987). The physical model used in this study is based on a 1D version of the Princeton Ocean Model (Blumberg and Mellor, 1987) developed for Lake Michigan applications (Chen et al. 2002). The 1D model uses a two-equation Mellor-Yamada turbulence model for vertical diffusivity (Mellor and Yamada, 1982) and is fully described in Mellor (2001). Model depth is 24 m with 48 layers of 0.5 m each.

Meteorological forcing (momentum and heat fluxes) was calculated using bulk methods described in Beletsky and Schwab (2001) and was based on hourly surface observations from the Cleveland, Ohio airport during 1988-2005. Archived data for wind speed, dew point, and cloud cover were obtained from the NOAA National Climatic Data Center. The airport data were adjusted to be more representative of overlake conditions using the empirical relationships used operationally in the Great Lakes Coastal Forecasting System (Schwab and Bedford 1999).

The model was calibrated with 1994 temperature observations in central Lake Erie (Figure 3.2). Adjustments to increase mixed layer depth consisted of increase of a coefficient B in the surface wave breaking parameterization (Mellor and Blumberg 2004), to a value of 8×10^{-5}, and addition of internal wave breaking parameterization ~ $C \times N^2$ (where N ï is Brunt-Vaisala frequency). The latter process was shown to be important for accurate mixed layer depth simulation (Kantha and Clayson, 1994). Without including this process, the model produced too shallow a mixed layer. A value of 2.8 for coefficient C provided the best match of modeled temperature with 1994 observations. Decreasing the internal time step to 1 min led to slight improvement in model results as well. The short wave radiation model used in POM (after

Paulson and Simpson 1977) was modified in accordance with results of McCormick and Meadows (1988) obtained for Lake Erie. The incoming short wave radiation is split 55/45 between infra-red and visual bands with extinction coefficients of 2.85 m^{-1} and 0.28 m^{-1}, respectively. Overall, model errors (RMSE) were between 0.5 and 1.7 ^{o}C with maximum errors occurring in the thermocline, below 17 m (Figure 3.3).

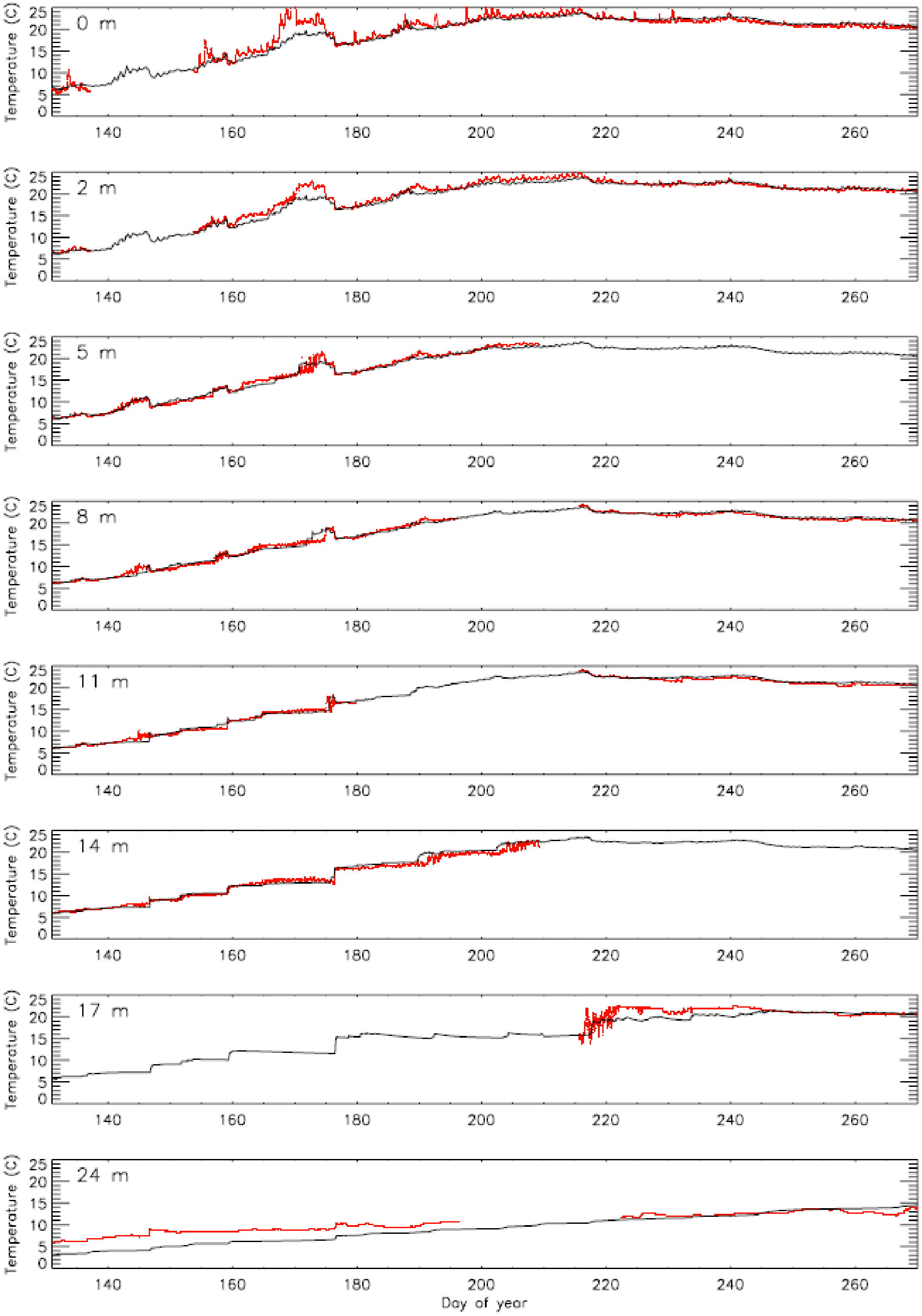

Figure 3.2: Time-series of modeled (black) versus observed (red) temperature at various depths in central Lake Erie in 1994

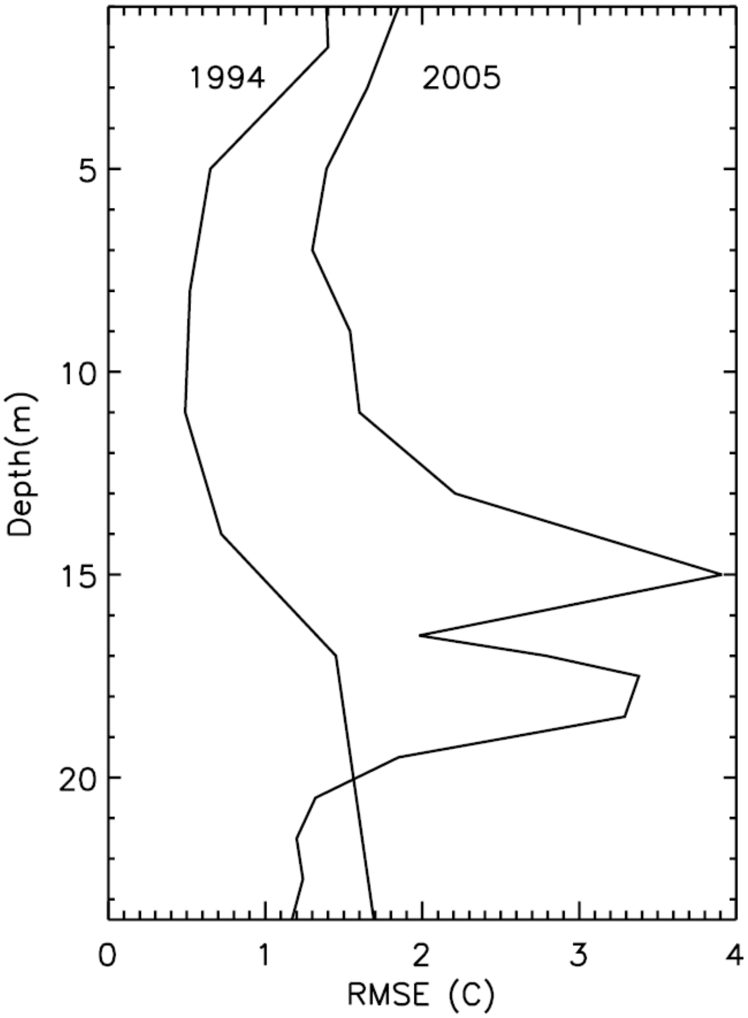

Figure 3.3: Comparison of thermal model error (RMSE) with depth.

3.3.3 Dissolved Oxygen Model

The dissolved oxygen sub-model consists of a coupled set of differential mass balance equations, one for each of the 48 model segments. This system of equations was solved numerically using an Euler integration scheme. The mass balance equation for the n^{th} segment is shown in Equation 1.

$$\frac{\partial DO_n}{\partial t} = -WCOD_n + \frac{E_{n-1,n}}{z}\frac{A_n}{V_n}\left(DO_{n-1} - DO_n\right) + \frac{E_{n+1,n}}{z}\frac{A_n}{V_n}\left(DO_{n+1} - DO_n\right) + SOD_n \qquad (1)$$

Where: DO_n = Dissolved oxygen (mgĀL^{-1}) in model segment n

$WCOD_n$ = Water column oxygen demand (mgĀL^{-1}Ād^{-1}) in model segment n

SOD_n = Sediment oxygen demand (gĀm^{-2}Ād^{-1}) in bottom layer (0 in other layers)

$E_{n-1,n}$ = Turbulent dispersion coefficient (m^{2}Ās^{-1}) across the interface between segment n$_{-1}$ and segment n

A_n = Interfacial area (m^2) of model segment n

V_n = Volume (m^2) of model segment n

z = model segment thickness (m)

The model computes vertical profiles of dissolved oxygen on an hourly basis, and operates at the same vertical scale as the thermal model. Mixing rates between layers and temperature profiles were transferred from the thermal model each time-step. A first-order, temperature-corrected deoxygenation rate, termed water column oxygen demand (WCOD), was applied to each layer to represent bulk oxygen dynamics (i.e., a combination of photosynthesis, respiration, decomposition, etc.). This rate can vary among layers depending on the light, temperature, nutrient, and other conditions that can affect the oxygen dynamics. The well-mixed epilimnion is strongly impacted by the boundary condition at the surface (described below), thus the WCOD was only applied below the thermocline, where respiration > photosynthesis. Additionally, a temporally constant areal flux is applied to the bottom segment, representing sediment oxygen demand (SOD). Table 3.1 shows model input and output variables and their source. Figure 3.4

shows a conceptual diagram of the model framework. The temperature correction to the WCOD term is illustrated below.

$$WCOD(T) = WCOD(20^o C) \cdot \theta^{T-20}$$

Where: $WCOD(T) =$ Water column oxygen demand at temperature T

$WCOD(20^o C) =$ Water column oxygen demand at temperature T=20^{o}C

$\theta =$ Temperature correction coefficient (1.04)

T = Temperature (^{o}C)

Table 3.1 Description and source of dissolved oxygen model input and output parameters.

Parameter	Description	Spatial Resolution	Source	Input/Output
E	Bulk verical dispersion coefficient ($m^2 \cdot s^{-1}$)	Segment Specific	Thermal Model	Input
T	Temperature (^{o}C)	Segment Specific	Thermal Model	Input
WCOD	Water Column Oxygen Demand ($mgO_2 \cdot L^{-1} \cdot d^{-1}$)	Segment Specific	Calibration	Input
SOD	Sediment Oxygen Demand ($gO_2 \cdot m^{-2} \cdot d^{-1}$)	Bottom Segment	Literature	Input
DO_{BC}	Dissolved Oxygen Boundary Condition ($mgO_2 \cdot L^{-1}$)	Top Segment	Field Data	Input
DO	Dissolved Oxygen ($mgO_2 \cdot L^{-1}$)	Segment Specific	Calculated	Output

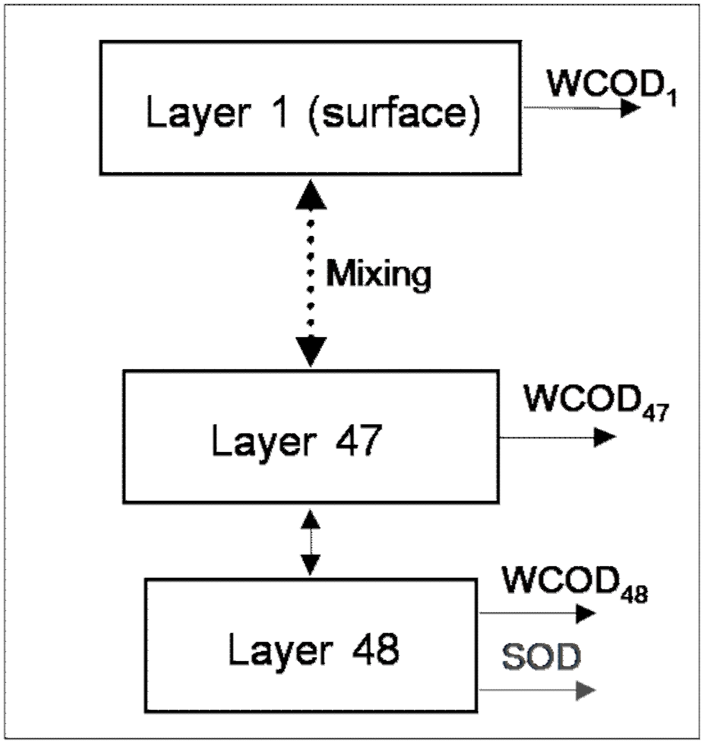

Figure 3.4: Conceptual diagram of dissolved oxygen model

3.3.4 Observations

Long-term (1987-2005) observations of dissolved oxygen depth profiles were compiled from several stations in the Central Basin of Lake Erie. These data were obtained from several sources, including Great Lakes National Program Office (GLNPO), National Water Research Institute of Environment Canada (NWRI), and the International Field Years on Lake Erie Program (IFYLE 2006).

Boundary conditions were set at the water surface based on observations and linear interpolation across sampling times. The data provide roughly distinct profiles from six to ten stations during each cruise throughout each year. Reported SOD values have not varied significantly over the time period of the model , so a value of 0.7 $gO_2 \cdot m^{-2} \cdot d^{-1}$ was used (Matisoff and Neeson 2005; Schloesser et al. 2005; Snodgrass 1987; Snodgrass and Fay 1987), corrected for differences from a base temperature (20 ^{o}C) using an Arrhenius function similar to that of the WCOD described previously.

Charlton (1980a) found that hypolimnetic oxygen concentrations in Lake Erie generally decreased linearly with time during the 1950s ï 1970s, resulting in a constant depletion rate for each year. More recent studies of the depletion rates (Burns et al. 2005; Rosa and Burns 1987) report single annual values, based on calculated differences between seasonally averaged observations; however, they note that seasonal production, especially at the thermocline, can significantly affect the oxygen dynamics. While the dynamic model allows for within year variation in WCOD values, the variability in oxygen depletion is most likely a result of nutrient cycling and biological processes, and because these dynamics are not explicitly modeled, varying the WCOD on a daily basis would result in essentially a curve-fitting exercise. Instead, by using a constant hypolimnetic WCOD rate throughout the year, one can assess how well the model captures the oxygen dynamics as a function of seasonal changes in the hydrodynamic effects only. That is, if the model can capture the dissolved oxygen profiles without varying the annual-average WCOD across years, then the mixing and thermal regime would be much more significant in determining the extent of hypoxia, compared to biological process.

3.4 Results

3.4.1 Thermal Model Results

For model validation two periods with observations were selected, 2004 and 2005. During these and other modeled years (1988-2005) the same coefficient values obtained in the 1994 calibration were used. The 2005 dataset was considerably more complete (see Rao et al. 2008 for details of observation campaign), therefore model validation discussion is restricted primarily to

2005 (Figure 3.5). Overall, the 1D model accurately described the onset of stratification and thermocline development in summer. Most problems occurred in late August and early September, when the model underestimated the sudden increase in mixed layer depth caused by storms on days 242 and 272. There was also a mixing event during days 205-215, where the warmer waters from the metalimnion were pushed down to the bottom of the model domain. A potential cause for this disturbance could be a result of Ekman suction caused by anti-cyclonic circulation. The latter storm almost totally eliminated thermocline which did not occur in the model run until around day 298. A similar problem occurred in the model in 2004, and this is attributed to 3D effects not represented in the 1D model, such as horizontal advection and internal wave propagation.

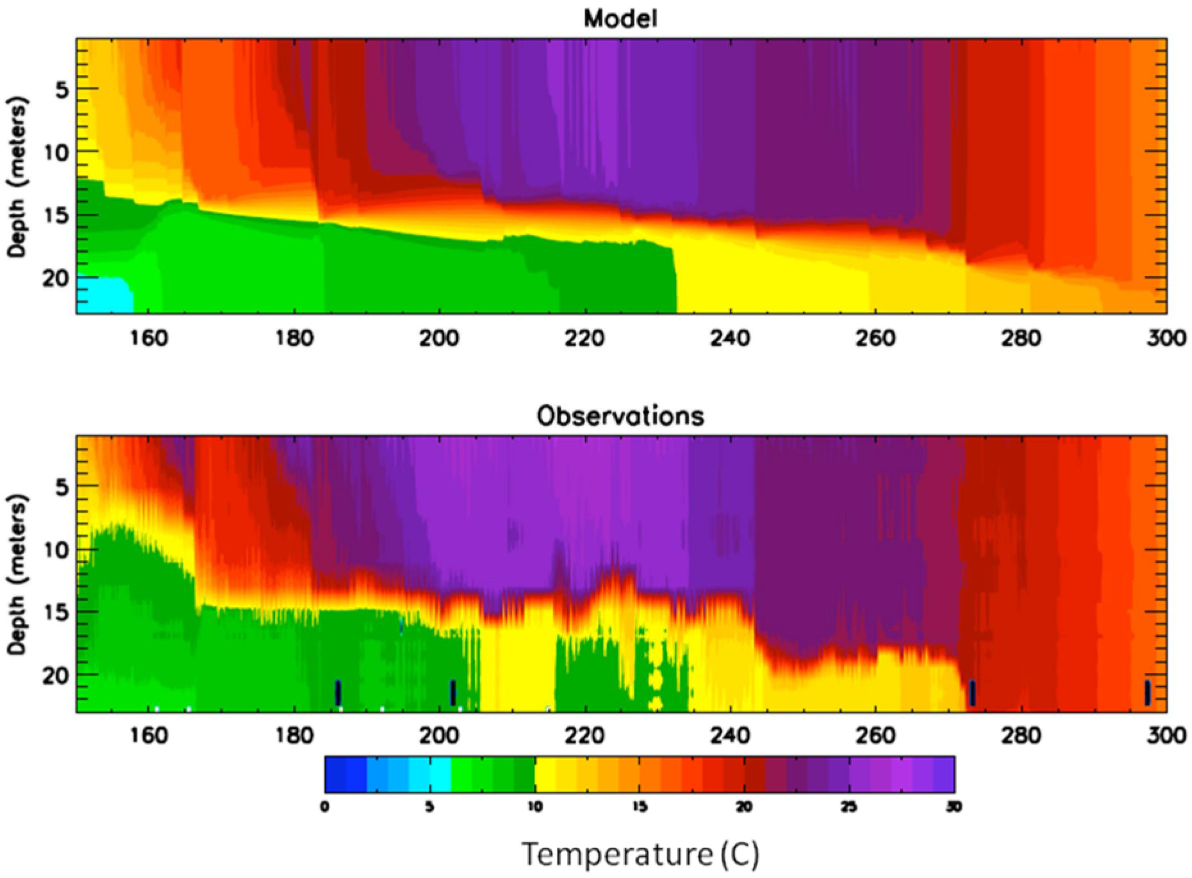

Figure 3.5: Modeled (upper panel) versus observed (lower panel) temperature in central Lake Erie in 2005.

As in the 1994 calibration, maximum model errors (RMSE) in 2005 occurred in the thermocline, at and below 15 m (Figure 3.3). Model errors were higher in 2005 than in 1994 (between 1.2 and 3.9 ^{o}C), most probably due to the more complete thermocline observations in 2005. The magnitude of errors is comparable but somewhat higher than found in other recent (although 3D) modeling studies of Lake Michigan (Beletsky and Schwab 2001) and Lake Ontario (Huang et al, in press) which reported RMSE up to 2.5 ^{o}C. In addition to the 3D effects, higher errors can be also attributed to a particularly sharp thermocline developing in Lake Erie by the end of summer (Schertzer et al. 1987).

Additional model validation is presented in Figure 3.6 which shows comparison of modeled and observed hypolimnion depth in 2005. To identify the mixed layer, thermocline, and hypolimnion depths more objectively, each vertical temperature profile (both modeled and observed) was approximated (in a least squares sense) with a 3-layer structure with uniform temperature in the top and bottom layers, and a linear temperature decrease between the top and bottom layers. The model generated a deeper than observed thermocline during July and August but (as mentioned above) underestimated the 5 m decrease in hypolimnion thickness due to storm on day 242. In the model results, this decrease is less than 1 m (seen in Figure 3.5). The hypolimnion recovered somewhat by day 260 when the model started matching observations until another storm on day 272. The model did simulate a deeper hypolimnion (by about 2 m) in 2004 versus 2005 observed by Rao et al. (2008).

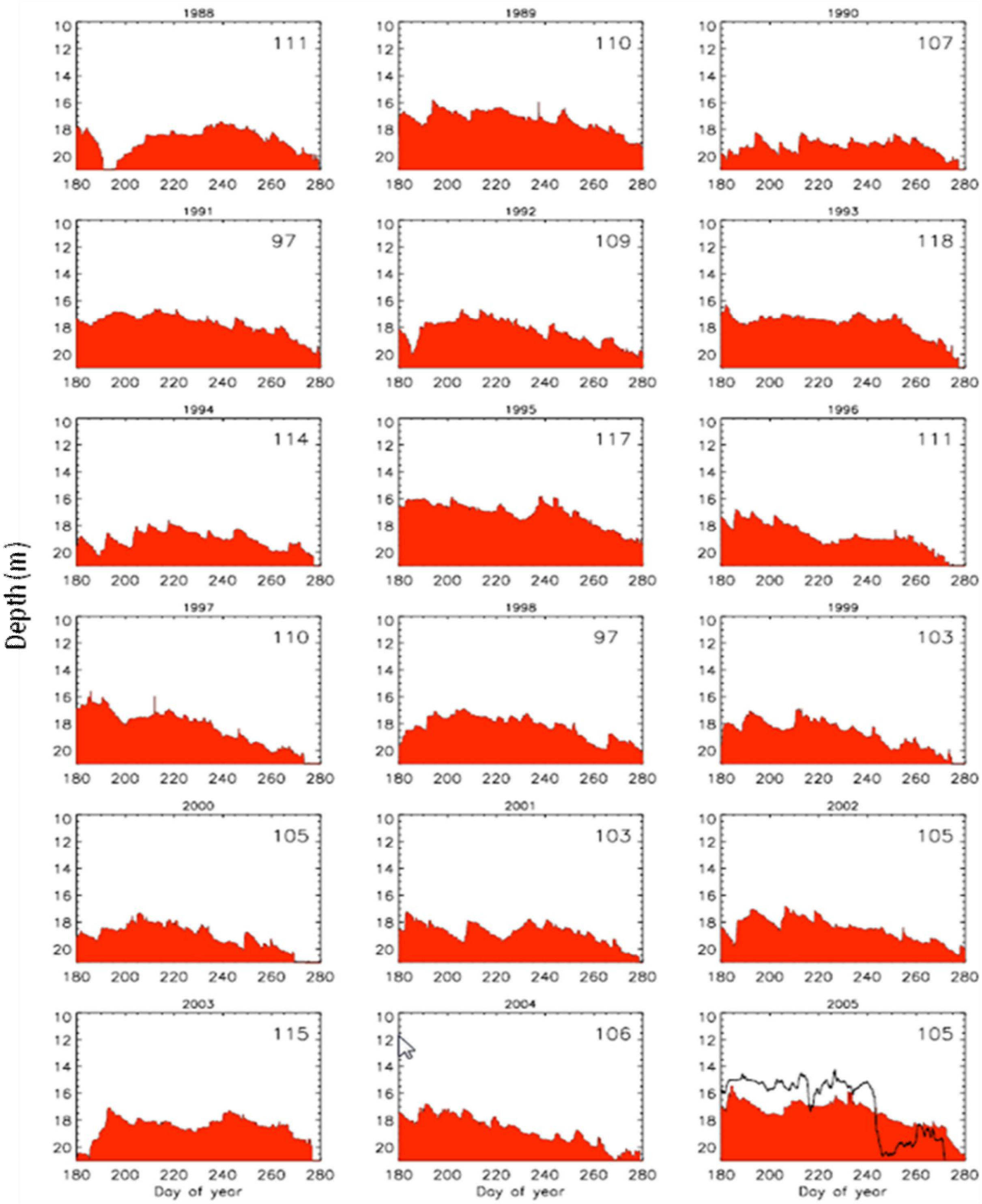

Figure 3.6: Modeled hypolimnion thickness in 1988-2005 (bottom 3 meters are not shown). The number in the upper right corner is the day of stratification onset. The 2005 panel also shows observed (18-hr smoothed) hypolimnion thickness (black line).

Figure 3.6 also shows inter-annual variability of hypolimnion depth for other modeled spring-summer-fall periods in 1988-2005. Since ice cover was not simulated, the model was initialized with vertically uniform temperature based on cruise observations made between April 1 and April 25 each year. Initial water temperature in early spring varied substantially between years, i.e. it was about 1 °C in 1994 after the cold 1993-1994 winter to slightly over 4 °C in 1998 after the exceptionally warm winter of 1997-1998. This affects the onset of stratification (day when lake surface temperature becomes higher than 4 °C), which varied by about 3 weeks, from day 97 to day 118 (Figure 3.6).

Inter-annual variability of mean hypolimnion depth (which varied between 17.2 and 19.3 m depths) is clearly pronounced in model results (Figure 3.6) with years 1989, 1995 and 2005 exhibiting thick hypolimnia, while 1990 and 1994 showed thin hypolimnia. This is mostly related to inter-annual variability of wind stress (which varied between 0.53 and 0.71 dynes·cm^{-2}) because higher wind stress leads to more mixing and hence a deeper (i.e., thinner) hypolimnion (Figure 3.7). The dependence of hypolimnion depth on the net heat flux (which varied between 17 and 52 W·m^{-2}) less revealing since the latter itself correlates with wind speed (via latent and sensible heat flux components). No significant correlations between temperature gradient in the thermocline (between 1.6 and 2.6 °C per meter) and either wind stress or heat flux were found. At the same time, there is a clear link between air temperature and lake surface temperature, both changing with similar amplitude (between 20.0 and 21.4 °C and between 21.3 and 22.9 °C respectively).

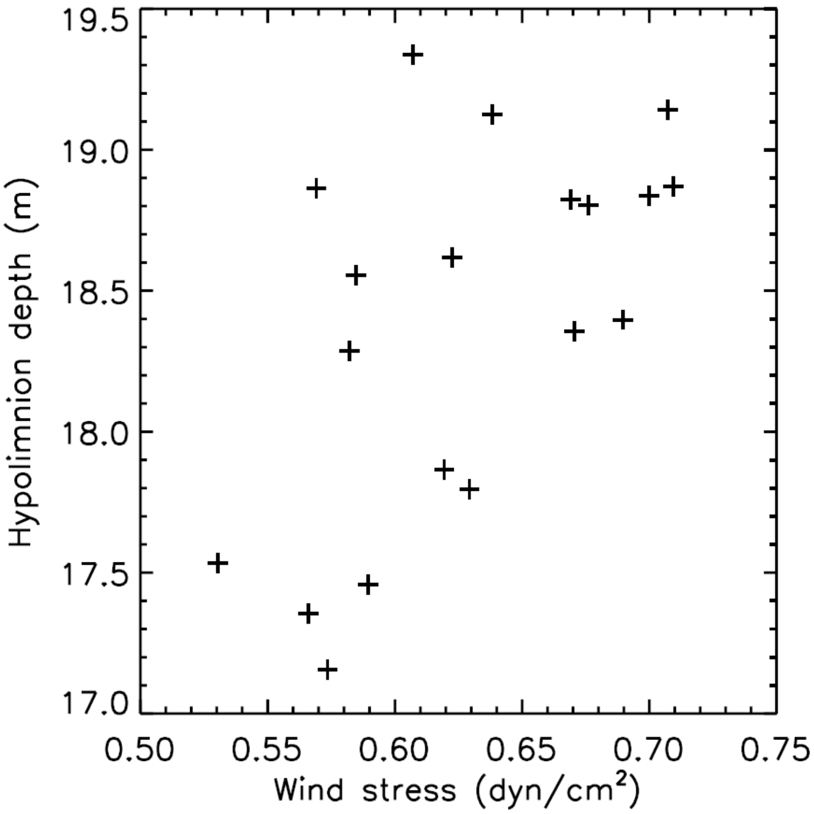

Figure 3.7: Scatter plot of average hypolimnion depth (m) versus average wind stress (dyne·cm^{-2}) in 1987-2005

3.4.2 Dissolved Oxygen Model Results

The model was calibrated for 1987-2005 by varying the hypolimnetic WCOD values to match the observed timing of the onset of hypoxia. WCOD values were held constant throughout the year, but varied across years to provide the best match to intra-annual variations in dissolved oxygen concentrations , and then to explore if and how WCOD varied among years. Observed oxygen vertical profiles were also used to guide the calibration. An example of model output is shown in Figure 3.8. The magnitude and timing of the oxygen minima are also captured well. There are small scale changes in observations (e.g., in mid-July) that the model does not capture, and these coincide with the limitations of the thermal model in capturing fluctuations at the thermocline (Figure 3.5). These fluctuations in the oxygen conditions are consistent with the storm episode disruptions detailed by Lam et al. (1987) and demonstrate a limitation of the 1D model framework.

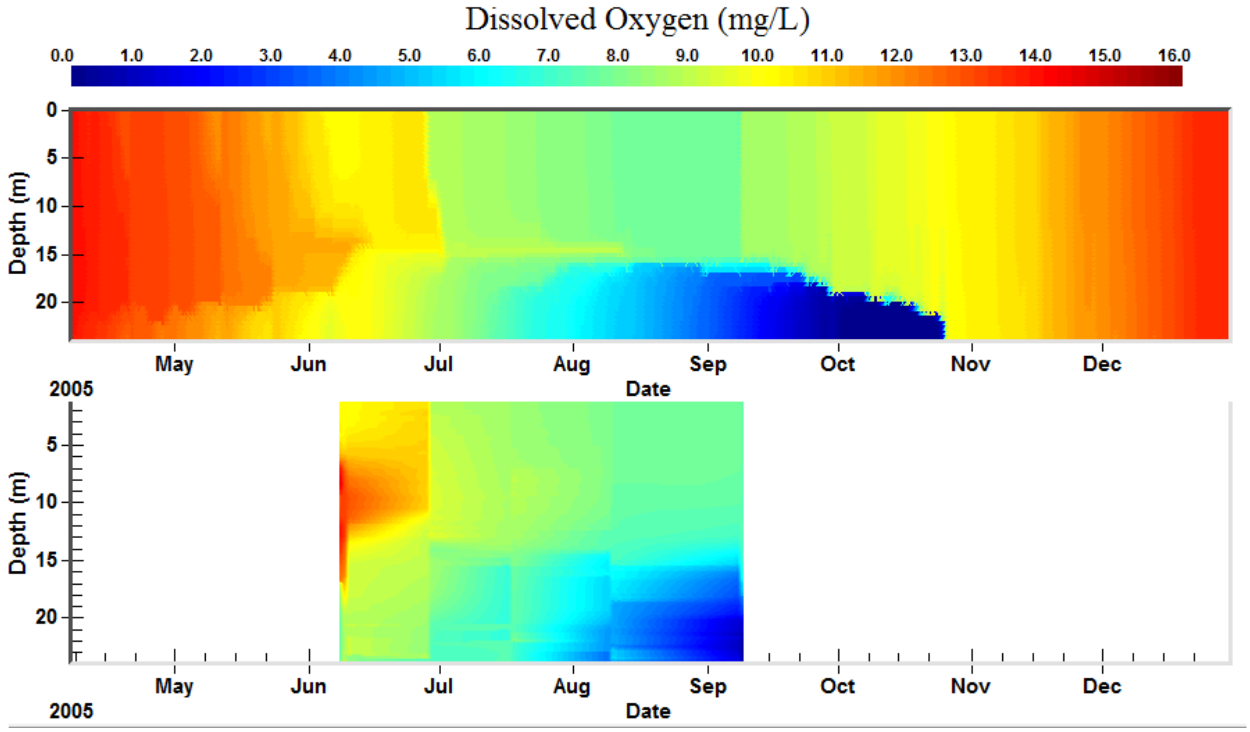

Figure 3.8: Calibrated dissolved oxygen model results for 2005. Model output shown in upper panel, observations in bottom panel, when data are present.

To illustrate long-term model performance, average modeled hypolimnetic DO concentration is compared to average observations below the thermocline (Figures 3.9-3.11). Because the model boundary condition is specified at the surface, the epilimnion model averages match the observations very well. Overall, the model performs well in capturing the temporal profiles for most years. Again, small scale fluctuations in the observed dissolved oxygen concentration are not captured well, as the model assumes a constant loss rate throughout a given year. To demonstrate the sensitivity to the calibrated WCOD term, model results are shown using upper and lower bounds corresponding to the range of calibrated annual-average WCOD values (1 and 0.001 $\text{mg}\cdot\text{L}^{-1}\cdot\text{d}^{-1}$, respectively).

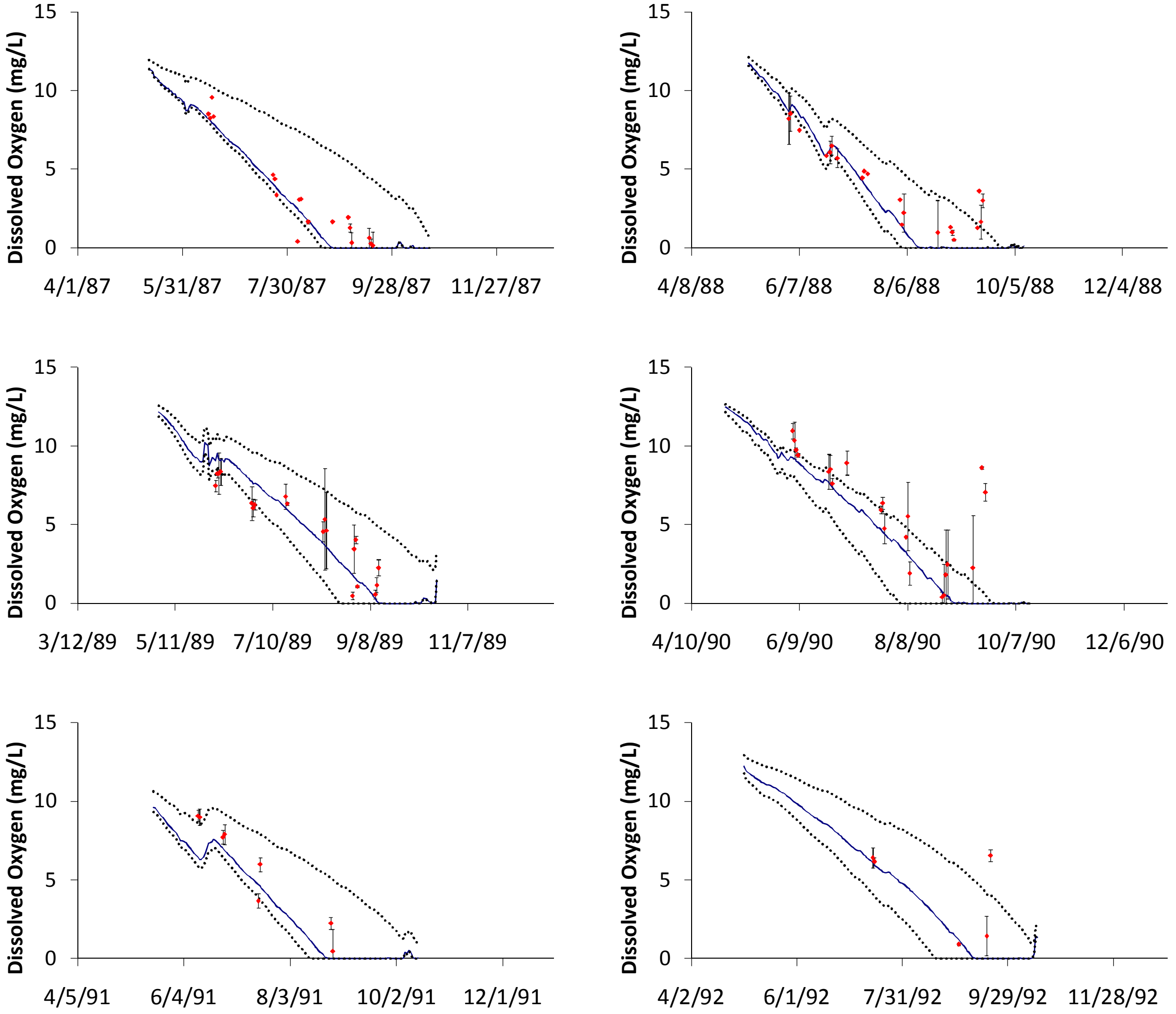

Figure 3.9: Calibrated dissolved oxygen model results averaged over hypolimnion (1987-1992). Model shown as blue line, data (+/- 1 s.d.) shown as red dots, and results using upper and lower bounds of WCOD shown as black dotted lines.

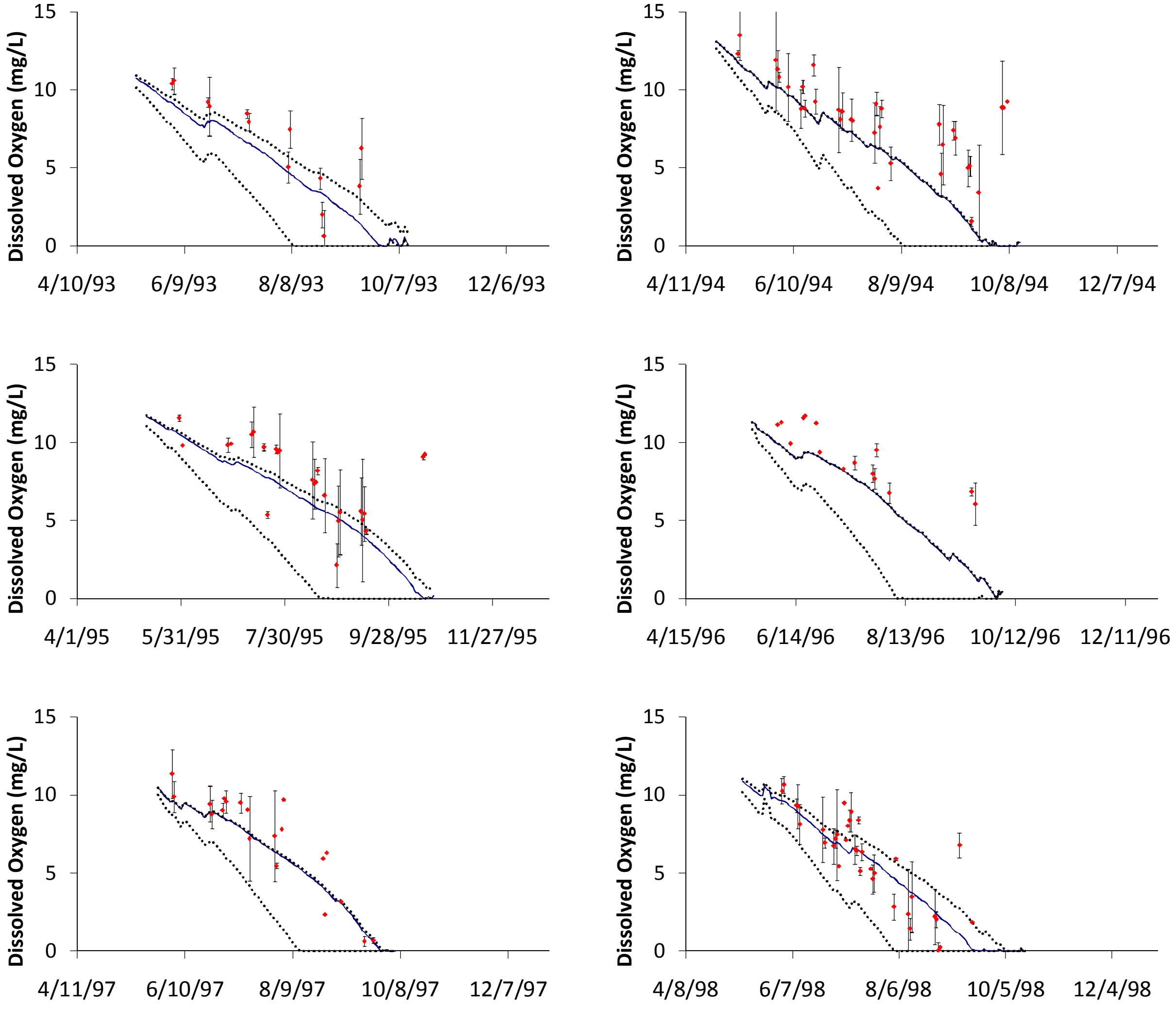

Figure 3.10: Calibrated dissolved oxygen model results averaged over hypolimnion (1993-1998). Model shown as blue line, data (+/- 1 s.d.) shown as red dots, and results using upper and lower bounds of WCOD shown as black dotted lines.

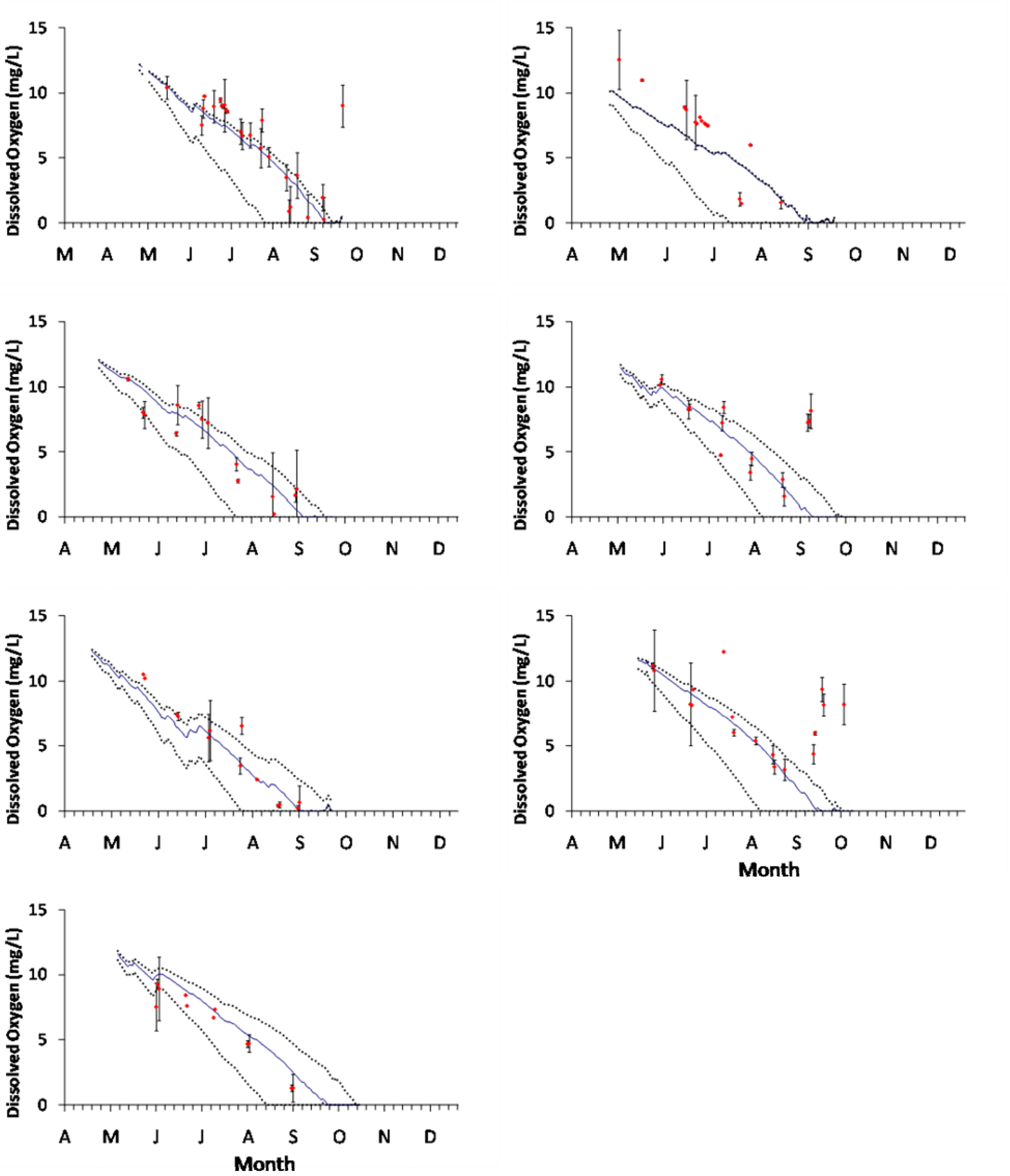

Figure 3.11: Calibrated dissolved oxygen model results averaged over hypolimnion (1999-2005). Model shown as blue line, data (+/- 1 s.d.) shown as red dots, and results using upper and lower bounds of WCOD shown as black dotted lines

3.5 Discussion

The primary objective was to test the hypothesis that climate-driven variability in thermal structure and mixing alone could explain the inter-annual variability and trend in hypolimnetic oxygen depletion rates. For this to be the case there would be no need to vary WCOD across years. However, to reproduce those depletion rates WCOD would vary (Figure 3.12), and therefore reject the hypothesis that variation in thermal structure alone controlled changes in hypoxia.

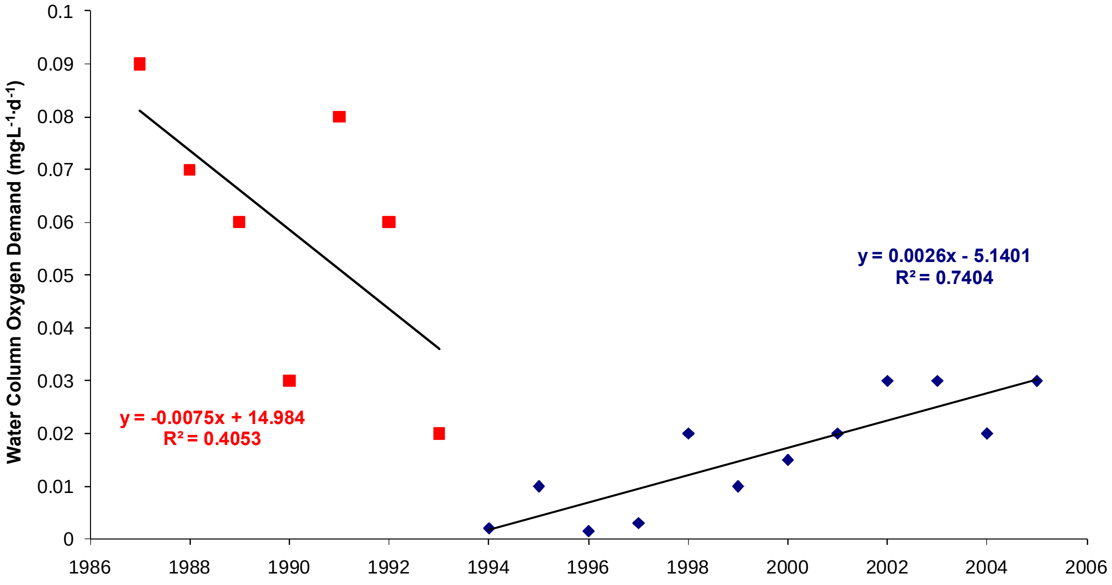

Figure 3.12: Calibrated WCOD rate term (1987-2005)

The sediment oxygen demand and water column demand (WCOD) were combined, resulting from the calibration to compare the model-derived total hypolimnetic volumetric oxygen demand (HVOD) with observed rates that were estimated by slopes of linear regressions through hypolimnetic oxygen time-series. The model-estimated rates compare well with those based on observations (Figure 3.13). Figure 3.13 also includes the HVOD rates that would result by using the minimum and maximum hypolimnetic WCOD rates as constants (dotted lines), and further demonstrates the variability required to match observations.

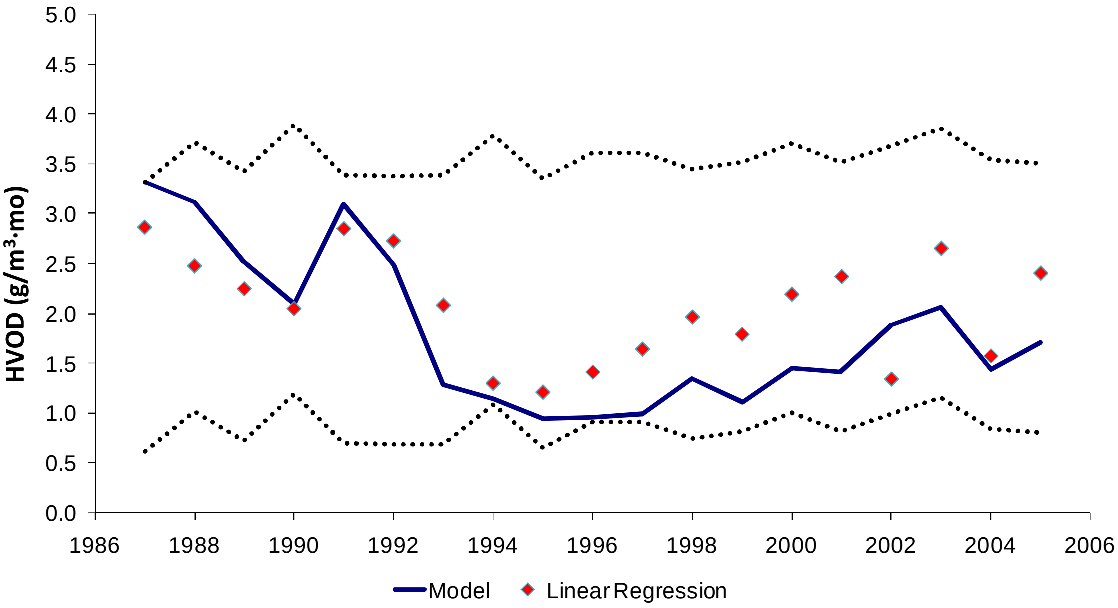

Figure 3.13: Comparison of model estimated HVOD from linked thermal-dissolved oxygen model (blue line) and estimated from linear regression of data (red points). Model estimated HVOD rates using the upper and lower bound WCOD values are shown in dotted lines.

To test this more explicitly relationships were developed between the oxygen depletion rate and initial thermocline depth and between the oxygen depletion rate and date of onset of thermal stratification and found little correlation (r=0.17 and 0.46, respectively). So, while these factors can contribute to the magnitude of hypoxia, the relative influence on inter-annual variability appears to be small compared to differences in biological productivity.

The calibrated WCOD values decreased significantly between 1987 and 1996, and then increased through 2005. This implies that eutrophication processes contributing to hypoxia (i.e., generation of organic matter in the water column) had declined up to 1994, but are increasing in recent years. Soluble reactive phosphorus loading to the western and central basins (Richards 2006) followed a similar trend (Figure 3.14) post 1993; however total phosphorus does not follow the same trend. A regression of WCOD versus the corresponding annual SRP load in the post-1993 period resulted in a correlation coefficient of 0.70, while a regression with annual total phosphorus load (Dolan 1993, Dolan and McGunagle 2005) yielded only a correlation coefficient of 0.11(using the load from the previous year resulted in a slightly better correlation of 0.20). Further supporting the notion that oxygen demand is correlated with biological productivity, a regression between the WCOD and average in lake chlorophyll-a concentration yielded a correlation coefficient of 0.41.

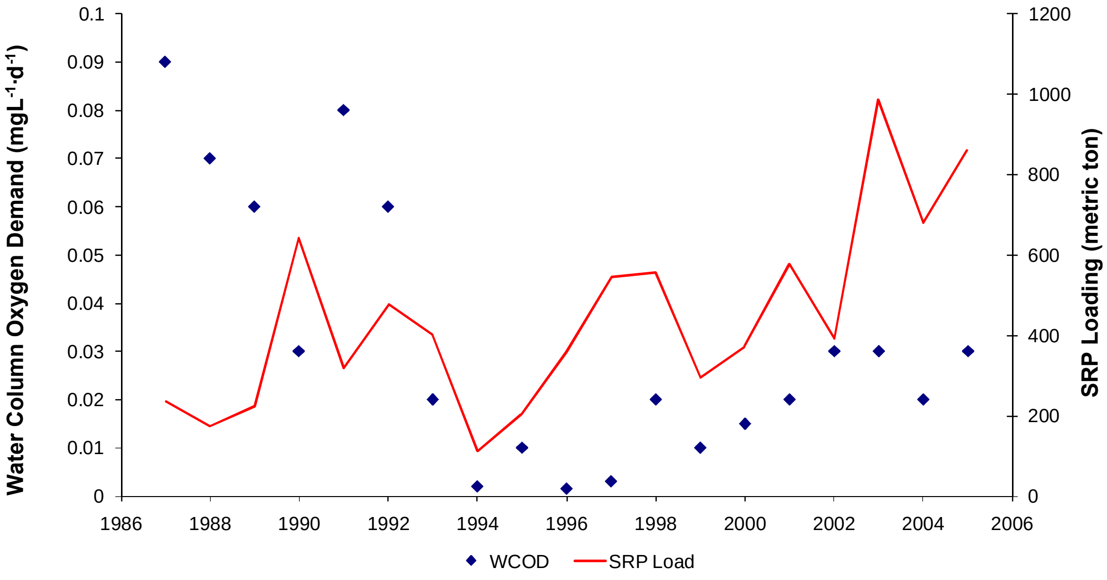

Figure 3.14: Correlation between calibrated WCOD rate term (points) and annual soluble reactive phosphorus loading (red line).

Rosa and Burns (1987), Burns et al. (2005), and Chartlon (1980a) estimated a similar HVOD term for Lake Erie in previous works based on the rate of change in observed data. Those works did not account for vertical variations in dissolved oxygen data, were not as temporally resolved, and did not explicitly incorporate the physical mixing of the system. Despite the different methodologies, the estimates when combined with SOD are similar to theirs. The previous studies used data dating back to the 1929 (sporadic years from 1948 ï 1979; 1980-2002), and the HVOD values obtained were in the 2 to 4 gÂm^{-3}Âmo^{-1} range, however, the values are in the 1 to 2 gÂm^{-3}Âmo^{-1} range, post-1993.

The HVOD term incorporates the oxygen demand associated with the deposition of organic matter to the sediments, which represents a significant portion of the total oxygen depletion. Because the SOD is large and does not change dramatically over the period of analysis, it masks annual variability in HVOD. SOD represents 63% of the HVOD on average in the analysis. The relative contribution is much lower in earlier years because WCOD values are higher before 1994. The modeling analysis isolates the water column oxygen demand, and better represents the seasonal oxygen dynamics. By isolating the water column depletion from the bulk hypolimnetic depletion, one can better distinguish changes in the oxygen dynamics, as the biologic processes in the water column vary more rapidly than in the sediments.

It should be noted, however, that there are other important characteristics of hypoxia other than the depletion rate (including spatial extent, volume, and duration) that are not examined here. These factors may be more significantly linked to the physical and morphologic conditions in the lake; however, one cannot appropriately quantify this with a 1-dimensional model of this complexity.

3.6 Conclusions

A one-dimensional, coupled, thermal dynamics-dissolved oxygen model was driven by realistic, climate-driven physics and calibrated and applied for 1987-2005. The dissolved oxygen component was calibrated to seasonal oxygen concentrations by adjusting only the water column oxygen demand (WCOD) term for each year, with the goal of focusing on the impact of the lake's thermal structure on oxygen resources. If it were possible to match observations in all years using a single value for WCOD, the role of the thermal structure could be considered to be the dominant forcing. However, using reasonable upper and lower bounds for WCOD in sensitivity runs demonstrated that the model did not perform well unless WCOD was adjusted year by year; in fact, WCOD shifted from one extreme to the other (Figures 3.9-3.11).

The analysis indicates that water column oxygen demand in the Central Basin of Lake Erie changed significantly between 1987 and 2005, with higher depletion rates early, declining to a minimum in 1993, followed by an increase from 1994 to 2005 (Figure 3.13). The initial thermocline depth at the onset of stratification varied between 17 and 20m, but did not follow a similar trend and was not significantly correlated with the depletion rate. Similarly, WCOD was not significantly correlated with average hypolimnetic volume. Most of the relationship between the thermal structure and oxygen depletion rate is related to the depth over which water exposed to the sediment oxygen demand is mixed. However, because the depth of the thermocline varies only approximately 2 m from year to year, this difference doesn't appear to account for the differences in total hypolimnetic oxygen demand.

In contrast, soluble reactive phosphorus loads followed a similar trend, increasing from 1994-2005. Richards (2006) documented the change in phosphorus loads to Lake Erie from 1980-2005 and showed for the four major tributaries studied, an increasing SRP loading trend since the mid-1990s, while total phosphorus load did not significantly increase in the Maumee sub-basin and increased much less than SRP, overall. Potential causes for this shift include: demographic changes, increased agricultural practices and animal density, and a possible SRP surface enrichment due to conservation tillage practices (Richards 2006). The SRP load is more likely to directly stimulate primary production than is total phosphorus, and it was correlated with the calibrated water column oxygen demand. This suggests that changes in the characteristics of the phosphorus load and its influence on primary production, as opposed to changes in climate, are the dominant driver of changes in hypoxia since the mid-1990s. Chapter 4 provides a more sophisticated modeling approach, which directly incorporates the impact of the phosphorus load on the autochthonous production of decomposable organic carbon (i.e., phytoplankton).

CHAPTER 4: Modeling Lake Erie’s hypoxia response to nutrient loads and physical variability

4.1 Introduction

Over recent decades, Lake Erie has experienced cultural eutrophication (Beeton 1963), recovery in response to load reductions (DePinto et al. 1986), and a recent return to eutrophic conditions of the past (Burns et al. 2005; Zhou et al. 2013; Bridgeman et al. 2013). Among symptoms of eutrophication, hypoxia (dissolved oxygen concentration below 2 mgĀL^{-1}) has been a key indicator for Lake Erieôs central basin (El-Shaarawi 1987; Rosa and Burns 1987) and excess phosphorus loading from point and agricultural non-point sources (Dolan 1993; Dolan and Chapra 2012) has been the key driver in both its growth and recovery phases.

In response to concern about the consequences of eutrophication in the 1960 and 1970s, the governments of the U.S. and Canada, largely through the auspices of the Great Lakes Water Quality Agreement (GLWQA 1978), implemented a program of P load reduction that was globally unprecedented (DePinto et al. 1986). A combination of point and non-point phosphorus load reductions achieved the Lake Erie target load of 11,000 metric tonnes per year, and the response of the lake was rapid, profound, and close to that predicted by models. However, despite this apparent success in reducing central basin hypoxia, it reemerged in the mid-1990s and is now approaching the extent seen in early decades (Zhou et al. 2013).

Among the several natural and anthropogenic factors potentially responsible for altering hypoxic conditions, changes in climate and hydrology (Diaz 2001; Blumberg and Di Toro 1990) and changes in phosphorus loading are key, and thus the subject of this analysis.

4.2 Modeling Approach

Several linked or coupled hydrodynamic-eutrophication models have been developed for Lake Erie. The spatial sophistication of these works has varied from a 1D approach as demonstrated here, to 2D domains (Zhang et al. 2008), or even 3D domains (DiToro and Connelly 1980; DiToro, et. al. 1987; Leon et al. 2011). The complexity of the biological portion of the models has varied greatly, ranging from simple statistical relationships (Burns et al. 2005; Rosa and Burns 1987; Rucinski et al. 2010) to models using dozens of state variables in both the water column and sediments (Leon et al. 2011). All of these approaches have merit for investigating specific forcings of hypoxia in Lake Erie, such as near shore nutrient cycling, or cross lake nutrient transport. However, they also are limited in their ability to provide forecast management scenarios, either due to exorbitant computation time or lack of input data at the spatial and temporal scales needed. The 1D approach allows for quick simulation of several dozen hypothetical scenarios related to reductions in nutrient loads, inter-annual variability in physical drivers, and long-term change in sediment oxygen demand (SOD) associated with such loads.

Rucinski et al. (2010) and Chapter 3 demonstrated, with a 1D hydrodynamic model linked to a very simple oxygen demand model that, after accounting for interannual variability in temperature and mixing regimes driven by historical meteorological conditions, there remains significant inter-annual variability in the water column oxygen demand. This oxygen demand is driven by in situ decomposition of autochthonous production of organic matter, which is in turn driven by the availability of phosphorus, the limiting nutrient. To explore those relationships, a separate eutrophication model was developed, driven by 19 years (1987-2005) of observed nutrient loads and meteorology, to simulate the phosphorus driven production of organic matter and the contribution of its decay to the evolution of hypolimnion hypoxia in the Central Basin. This 1-dimensional linked hydrodynamic and eutrophication model was developed and corroborated with 1987-2005 observations, and then confirmed with observations from the 1960s and 1970s, and compared to observed process rates where available. It should also be noted that this period includes both the decline and the re-emergence of hypoxia through the 1990s (Zhou et al. 2013).

The one-dimensional hydrodynamic model described in section 3.3.2, representing the offshore waters of the central basin (24 m in depth, Figure 4.1), provided the thermal structure and associated vertical mixing input to the eutrophication model. The same meteorological data and model output developed in the analysis described in Chapter 3 were used in this analysis. Both the hydrodynamic and eutrophication models operate on the same spatial scale of 48 half-meter thick layers. The 1-D hydrodynamic model is based on the Princeton Ocean Model (Blumberg and Mellor, 1987) and was applied previously for Lake Michigan (Chen et al. 2002) and Lake Erie (Rucinski et al. 2010). It uses the Mellor-Yamada turbulence closure scheme to parameterize vertical mixing (Mellor and Yamada, 1982). The hydrodynamic model is driven by hourly meteorological observations from the Cleveland, Ohio airport with overland-overlake correction described in Beletsky and Schwab (2001).

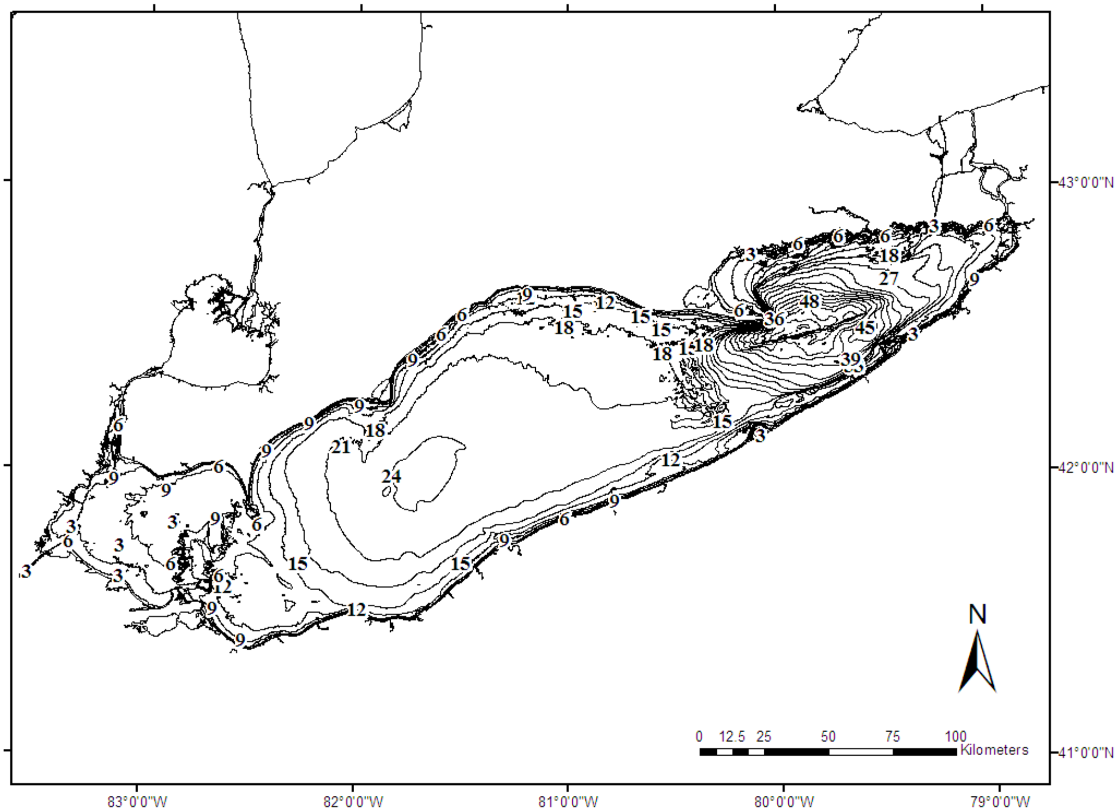

Figure 4.1: Morphology of Lake Erie.

Calibration and confirmation of the hydrodynamic model is fully described in Rucinski et al. (2010). Briefly, calibration was accomplished using temperature data from 1994, representative of central basin open water conditions, and confirmed with data collected in 2005. Maximum model error (represented as RMSE) varied with depth, and found to be 1.9 ^{o}C and 3.4 ^{o}C for 1994 and 2005, respectively. Both years exhibited maximum errors near thermocline depth. While some model errors can be attributed to either inaccuracies in forcing functions or model physics (e.g. vertical mixing parameterization), others can be attributed to 3D effects that are not represented in a 1D model, such as internal wave propagation, horizontal and vertical advection and diffusion. In particular, mid-lake thermocline conditions can be impacted by vertical velocities (upwelling or downwelling) generated by wind stress curl (Beletsky et. al. 2012). The hydrodynamic and eutrophication models are linked by first simulating the thermal structure of the model domain, and then passing the hourly outputs from the hydrodynamic model (i.e., temperature and vertical mixing coefficients) to the eutrophication model.

The eutrophication model incorporates external phosphorus and carbon loading; internal phosphorus and carbon cycling; algal growth, death, and sinking; zooplankton grazing, oxygen consumption and production; and sediment interactions (Figure 4.2). Stoichiometry among the state variables follows Redfield (1934). Algal growth rate is based on uptake of available (dissolved reactive) phosphorus following the Michaelis-Menton relationship, light limitation as a function of a constant extinction coefficient with self-shading from algal biomass, and water temperature. Algal photosynthesis and respiration are temperature-dependent 1st order rates, as are settling terms and mineralization of unavailable (organic) to available phosphorus. Sediment oxygen demand is a 0th order areal flux. These differential equations (Table 4.1) are solved using an Euler integration scheme; the details on the kinetic processes are outlined in the Appendix.

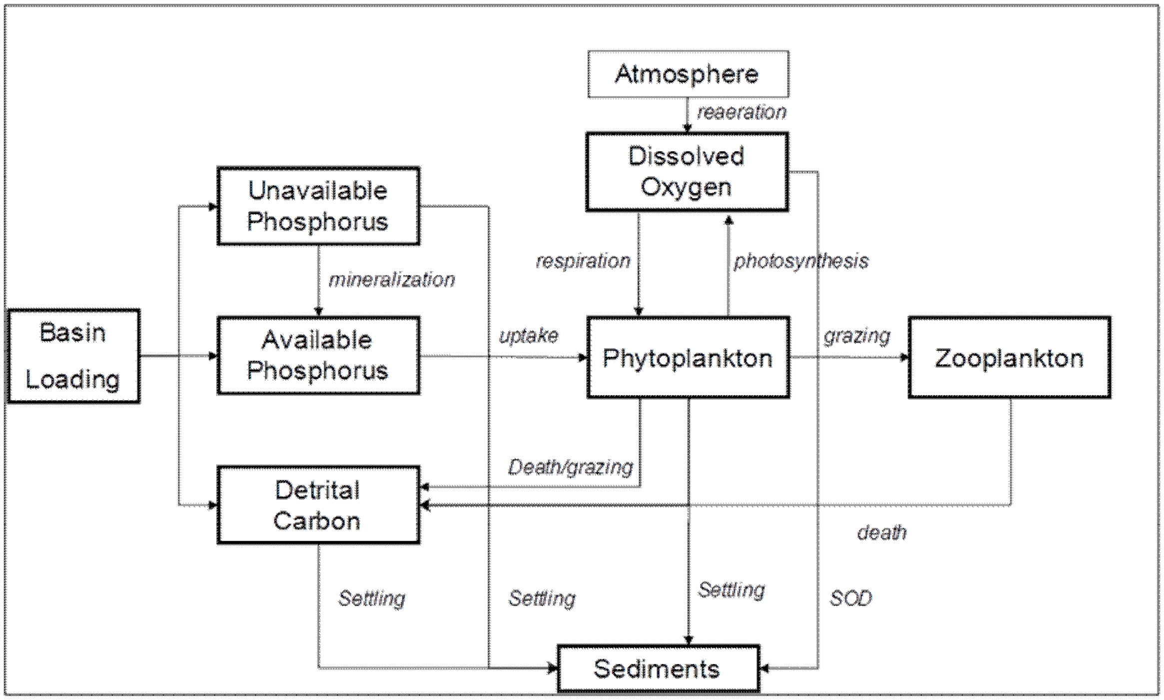

Figure 4.2: Conceptual diagram of simple eutrophication model.

Table 4.1 Eutrophication Model.

Phytoplankton

$$\frac{\partial Pc_n}{\partial t} = Pg_n - \mathrm{Pr}_n - Pvs_n + Pvs2_n + Diff_u + Diff_L - Out$$

Where: Pc_n = Phytoplankton carbon in model segment n
Pg_n = phytoplankton growth in model segment n
Pr_n = phytoplankton respiration in model segment n
Pvs_n = settling across the interface between segment n_{+1} and segment n
$Pvs2_n$ = settling across the interface between segment n_{-1} and segment n
$Diff_u$ = Turbulent dispersion across the interface between segment n_{-1} and segment n
$Diff_L$ = Turbulent dispersion across the interface between segment n_{+1} and segment n
Out = advection from model segment n to eastern basin

Available Phosphorus

$$\frac{\partial AP_n}{\partial t} = Wap_n - Pvs_n + Pvs2_n + Diff_u + Diff_L + AP_{rec,n} + MinP_n - Out$$

Where: UP_n = Available phosphorus in model segment n
Wap_n = Available phosphorus load in model segment n
$UP_{rec,n}$ = Recycled available phosphorus via zooplankton grazing and phytoplankton and zooplankton death in segment n
$MinP_n$ Mineralization of unavailable to available P in segment n

Unavailable Phosphorus

$$\frac{\partial UP_n}{\partial t} = Wup_n - Pvs_n + Pvs2_n + Diff_u + Diff_L + UP_{rec,n} - MinP_n - Out$$

Where: UP_n = Unavailable phosphorus in model segment n
Wup_n = Unavailable phosphorus load in model segment n
$UP_{rec,n}$ = Recycled unavailable phosphorus via zooplankton grazing and phytoplankton and zooplankton death in segment n
$MinP_n$ Mineralization of unavailable to available P in segment n

Zooplankton

$$\frac{\partial Zoo_n}{\partial t} = Zg_n - Zd_n - Zr_n - Out$$

Where: Zoo_n = Zooplankton carbon in model segment n
Zg_n = Zooplankton growth in model segment n
Zr_n = Zooplankton respiration in model segment n
Zd_n = Zooplankton death in model segment n

Organic Carbon

$$\frac{\partial OC_n}{\partial t} = Woc_n - Pvs_n + Pvs2_n + Diff_u + Diff_L - Oxid_n + \mathrm{Pr}_n + Zd_n + Zr_n - Out$$

Where: OC_n = Organic carbon in model segment n
Woc_n = Organic carbon load in model segment n
$Oxid_n$ = oxidation of organic carbon in segment n

Dissolved Oxygen

$$\frac{\partial DO_n}{\partial t} = \mathrm{Re}\,ar_n + Pg_n - \mathrm{Pr}_n + Diff_u + Diff_L - Oxid_n - SOD - Out$$

Where: DO_n = Dissolved oxygen in model segment n
$\mathrm{Re}\,ar$ = reparation at the surface
SOD = Sediment oxygen demand in the bottom layer

4.3 Observations

Long-term (1987-2005) observations of dissolved oxygen (DO), total phosphorus (TP), dissolved reactive phosphorus (DRP), and chlorophyll-a (CHL) were compiled from several stations in the central basin of Lake Erie. Zooplankton data were far less abundant, with only 2005 data used in this analysis. Data were obtained from multiple sources, including Great Lakes National Program Office (GLNPO), Environment Canada, Water Science & Technology Branch (ECWSTB), and the International Field Years on Lake Erie Program (IFYLE 2006) for central basin stations with an average depth of 20 m.

TP loads are from Dolan (1993) and Dolan and McGunagle (2005), and DRP loads (available P in the model) are from Richards (2006) and Richards and Baker (2002). Significant manipulation was required to convert these data into model inputs. First, loads to the western basin were routed to the central basin after accounting for a constant net apparent settling loss of 10 mĀyr^{-1} based on an estimate of basin specific net apparent settling rates for phosphorus via a post-audit of The Great Lakes Total Phosphorus Model (Lesht et al. 1991).

These TP loads were then apportioned, as well as those entering the central basin, into available and unavailable portions on a daily basis in the following manner. Dolan (1993) and Dolan and McGunagle (2005) provide western and central basin annual water year (Oct - Sept) loads. Richards (2006) and Richards and Baker (2002) provide daily loads of both TP and DRP for the Maumee and Raisin rivers that flow into the western basin and the Sandusky, Vermillion, Cuyahoga, and Grand (Ohio) rivers that flow into the central basin. To apportion the TP loads, the daily loads were summed into water year totals and used to establishe a ratio of this subset of daily-derived annual loads to the total basin loads. This ratio was then used to decompose the

Dolan-computed total basin loads to daily loads by applying the ratio to the daily load time-series (Richards 2006; Richards and Baker 2002). For example, if the total measured water-year Maumee plus Raisin TP loads were 2500 metric tonnes, and the total western basin load from all tributaries in that water year was 7500 metric tonnes, a scaling factor of 3.0 would be applied to the daily Maumee plus Raisin loads to provide daily total western basin loads.

A slightly modified approach was used to estimate daily DRP loads. The daily DRP:TP ratio from Richards (2006) and Richards and Baker (2002) was applied to the daily TP loads derived as described above. Finally, the DRP load from the Detroit River was based on estimates by Dolan (1993) and an average DRP:TP ratio from Richards (2006). Due to lack of available daily Detroit River loading estimates over the study period, it was assumed this portion of the load was constant. Particulate P load was estimated as the difference between TP and DRP. Note that the eastern basin loading is ignored in this analysis.

The base light extinction coefficient (0.3 m^{-1}) was estimated from extensive data on photosynthetic active radiation at varying depths in the central basin (GLNPO). Measured sediment oxygen demand (SOD) has not varied significantly over the analysis period, so for model testing an average value of 0.75 gO2Ām^{-2}Ād^{-1} (Matisoff and Neeson 2005; Schloesser et al. 2005; Snodgrass 1987; Snodgrass and Fay 1987) was used, corrected for temperature deviations from 20 ^{o}C. Other rate coefficients were adjusted within the bounds of literature values during calibration (Table 4.2).

Table 4.2 1D Model Parameter Set.

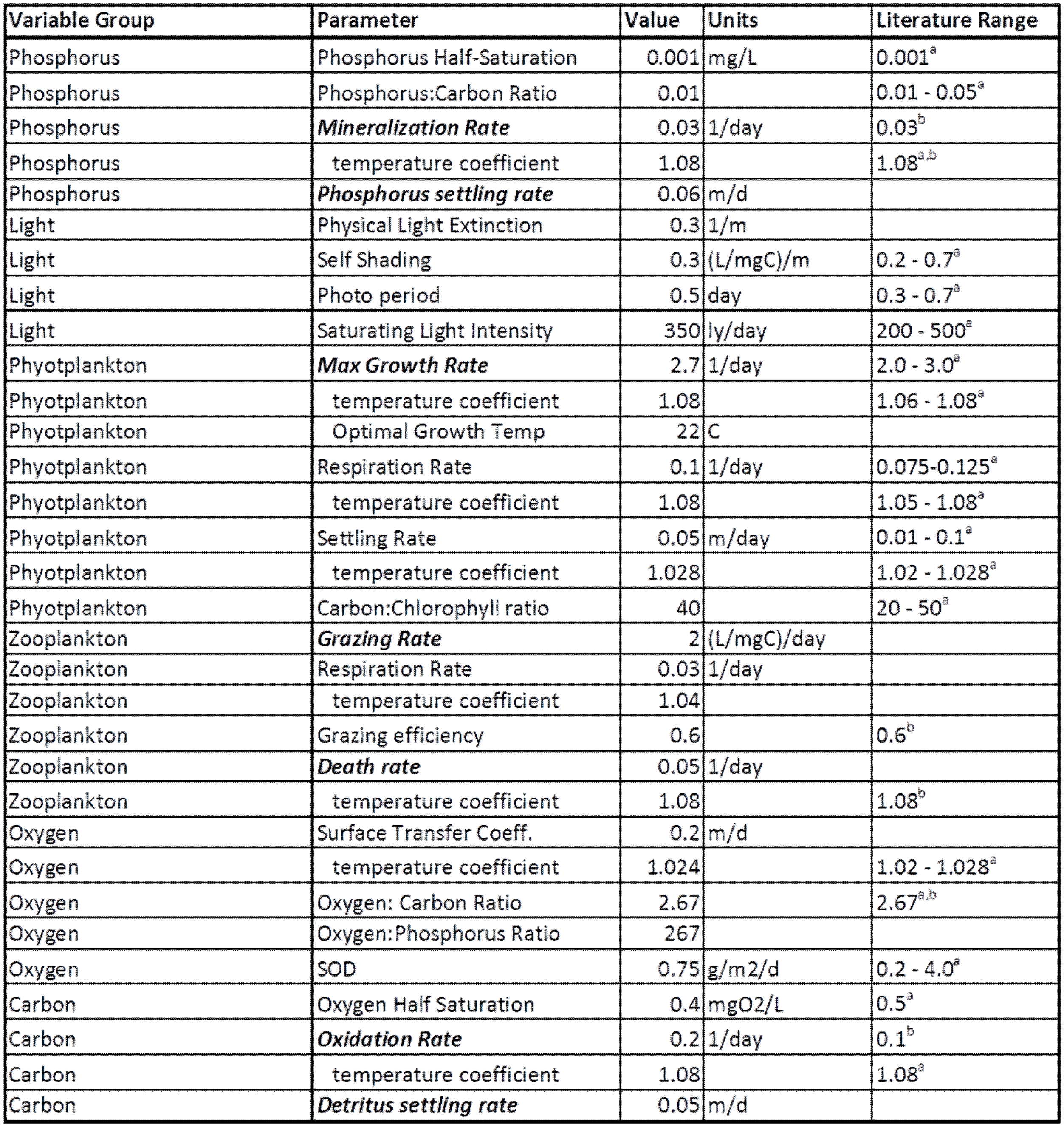

Variable Group	**Parameter**	**Value**	**Units**	**Literature Range**
Phosphorus	Phosphorus Half-Saturation	0.001	mg/L	0.001[a]
Phosphorus	Phosphorus:Carbon Ratio	0.01		0.01 - 0.05[a]
Phosphorus	***Mineralization Rate***	0.03	1/day	0.03[b]
Phosphorus	temperature coefficient	1.08		1.08[a,b]
Phosphorus	***Phosphorus settling rate***	0.06	m/d	
Light	Physical Light Extinction	0.3	1/m	
Light	Self Shading	0.3	(L/mgC)/m	0.2 - 0.7[a]
Light	Photo period	0.5	day	0.3 - 0.7[a]
Light	Saturating Light Intensity	350	ly/day	200 - 500[a]
Phyotplankton	***Max Growth Rate***	2.7	1/day	2.0 - 3.0[a]
Phyotplankton	temperature coefficient	1.08		1.06 - 1.08[a]
Phyotplankton	Optimal Growth Temp	22	C	
Phyotplankton	Respiration Rate	0.1	1/day	0.075-0.125[a]
Phyotplankton	temperature coefficient	1.08		1.05 - 1.08[a]
Phyotplankton	Settling Rate	0.05	m/day	0.01 - 0.1[a]
Phyotplankton	temperature coefficient	1.028		1.02 - 1.028[a]
Phyotplankton	Carbon:Chlorophyll ratio	40		20 - 50[a]
Zooplankton	***Grazing Rate***	2	(L/mgC)/day	
Zooplankton	Respiration Rate	0.03	1/day	
Zooplankton	temperature coefficient	1.04		
Zooplankton	Grazing efficiency	0.6		0.6[b]
Zooplankton	***Death rate***	0.05	1/day	
Zooplankton	temperature coefficient	1.08		1.08[b]
Oxygen	Surface Transfer Coeff.	0.2	m/d	
Oxygen	temperature coefficient	1.024		1.02 - 1.028[a]
Oxygen	Oxygen: Carbon Ratio	2.67		2.67[a,b]
Oxygen	Oxygen:Phosphorus Ratio	267		
Oxygen	SOD	0.75	g/m2/d	0.2 - 4.0[a]
Carbon	Oxygen Half Saturation	0.4	mgO2/L	0.5[a]
Carbon	***Oxidation Rate***	0.2	1/day	0.1[b]
Carbon	temperature coefficient	1.08		1.08[a]
Carbon	***Detritus settling rate***	0.05	m/d	

[a]Wool et al. 2002; [b]DiToro and Connely 1980

4.4 Model Parameterization and Evaluation

Model performance was assessed by comparing output to state variable observations while ultimately applying the same parameter values to the entire 19 year data set (1987-2005). Model coefficients were determined via an iterative calibration/corroboration process, focusing on DO and CHL observations, and to a lesser extent on DRP and zooplankton biomass because data for those constituents were less available. While particular emphasis was placed on calibrating to the 1994 and 2005 observations because those years had the most observations, additional modest adjustments were used in the corroboration with other years in the 1987-2005 dataset. While data were collected much less frequently in some years, the length of the record serves as an adequate corroboration dataset.

For comparisons, both model output and observations were aggregated into mixed layer averages, representing the epilimnion, metalimnion, and hypolimnion based on the temperature profiles from the hydrodynamic model. The metalimnion was estimated as the zone where the temperature gradient was at least 2°C per meter. Because stratification in the hydrodynamic model varies, the depth of the bottom of the metalimnion (i.e., top of the hypolimnion) changes both seasonally and annually as a consequence of meteorological inputs. Table 4.2 lists the coefficient values, as well as calculated rates based on data (SOD, light extinction). Parameters in bold italics are ones that were adjusted.

Results for DO (Figure 4.3), DRP (Figure 4.4), and CHL (Figure 4.5) show best correspondence in years where the calibration was most focused (1994, 2005). The model-data comparison for DO agrees quite well in the full corroboration data set. The model captures the expected temporal trends in DO and CHL (where data are available), however, CHL data are only available during spring and fall cruises for the vast majority of years, and therefore the data fail to capture phytoplankton dynamics during the summer. The temporal trends in DRP are difficult to delineate because those data were only available for the late summer in most years. However, as expected the values reach very low concentrations coinciding with increased phytoplankton and zooplankton abundance. Comparison with vertically averaged zooplankton (Figure 4.6) was only possible for 2005, and the model estimates captured the temporal trend reasonably well during the stratified period. The vertical trends in DO are also captured well.

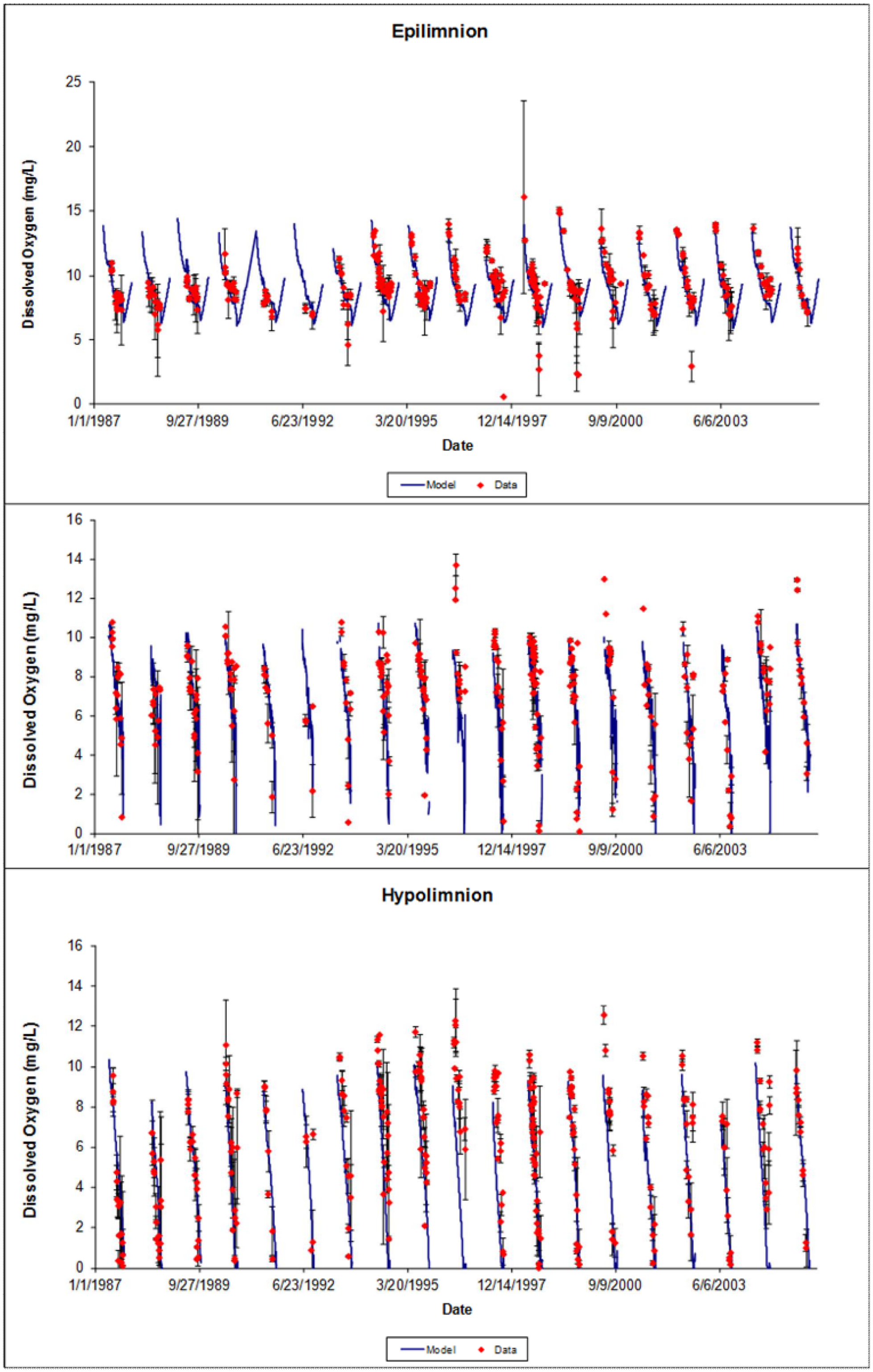

Figure 4.3: Comparison of model (line) and data (points) for mixed-layer averages of dissolved oxygen 1987-2005.

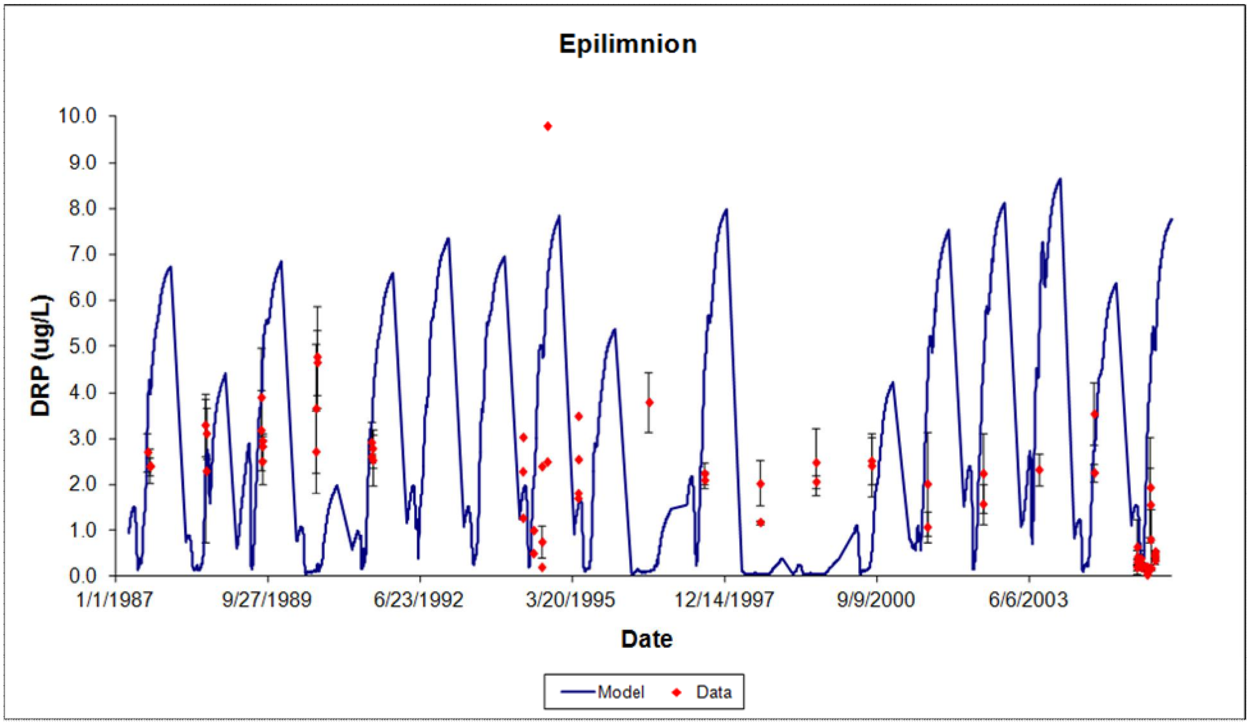

Figure 4.4: Comparison of model (line) and data (points) for epilimnion mixed-layer average of dissolved reactive phosphorus 1987-2005.

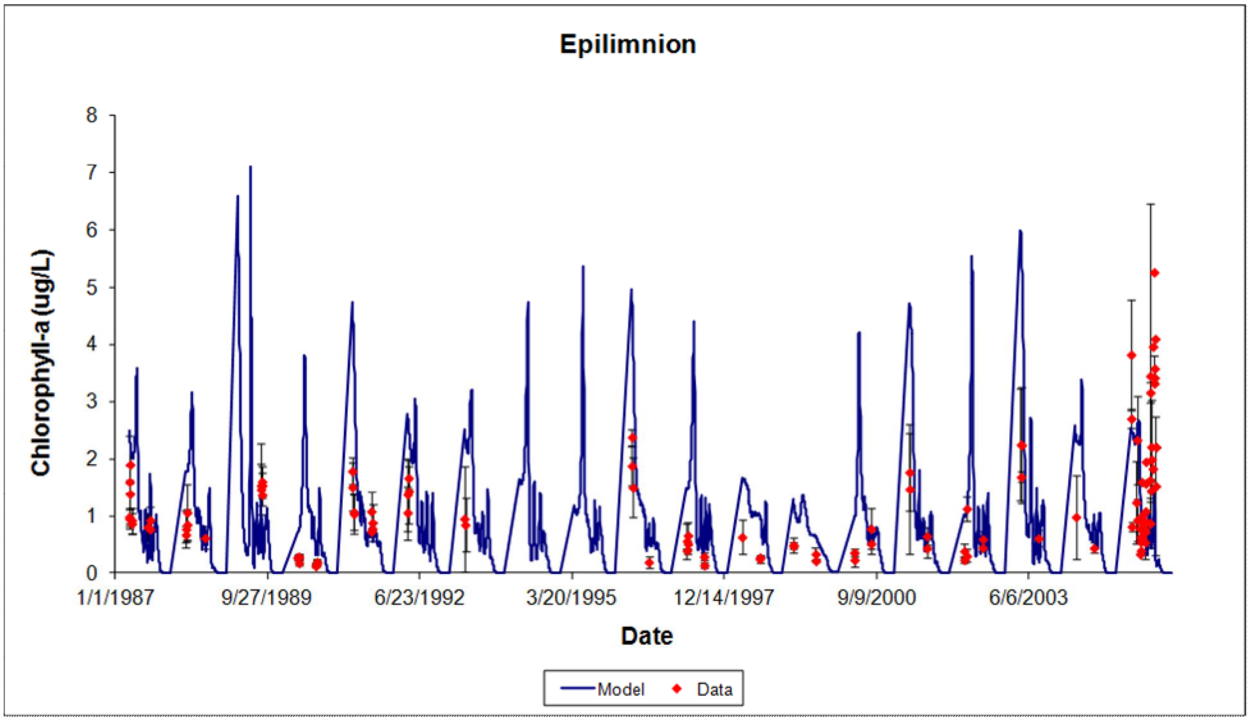

Figure 4.5: Comparison of model (line) and data (points) for epilimnion mixed-layer average of chlorophyll-a 1987-2005.

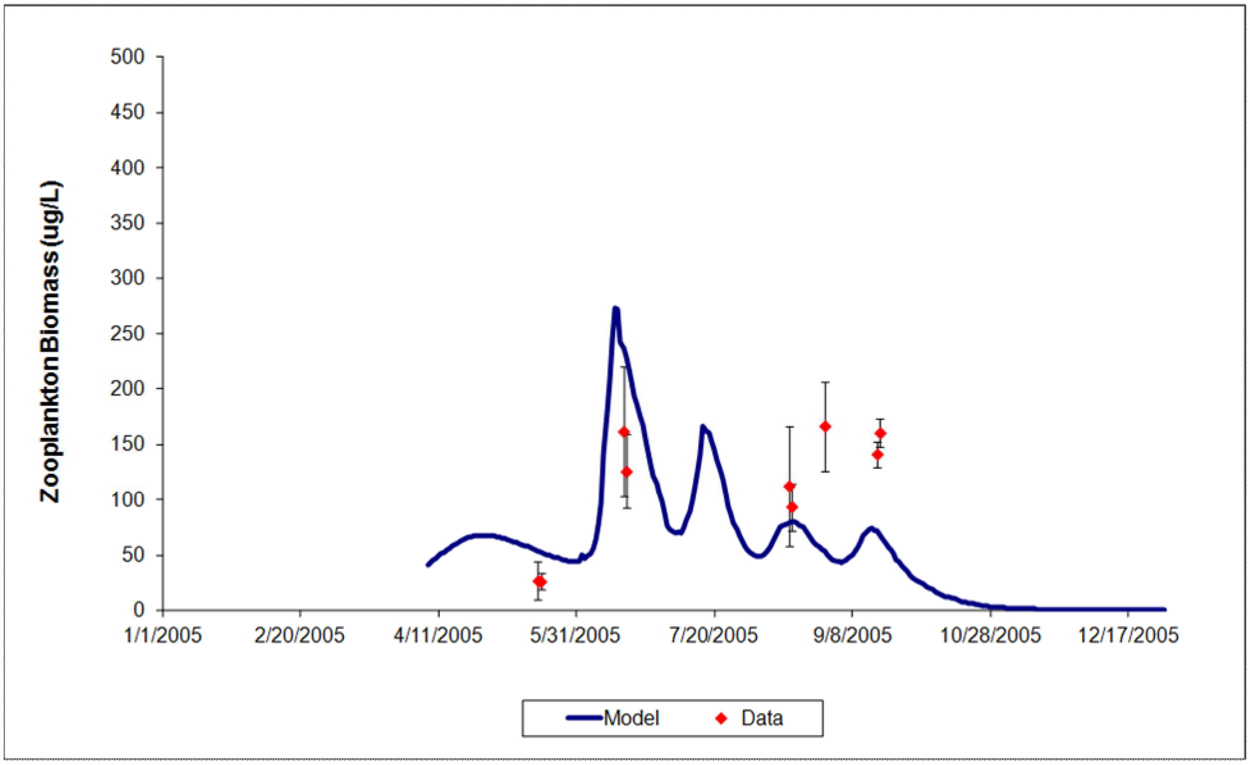

Figure 4.6: Comparison of model (line) and data (points) for epilimnion mixed-layer average of zooplankton 2005

As a another corroboration test, model output was used from the layers located within the daily evolving hypolimnion, and a relationship between bottom water dissolved DO and hypoxic area ($A= 9.3\exp(-DO^2/7.09)$) developed by Zhou et al. (2013) was used to compare modeled areal extent to those estimated from a geostatistical analysis of the observations (Zhou et al. 2013). It is important to note that hypoxic area derived from geostatistical analysis of observations from individual cruises (Zhou et al. 2013) varies considerably within a year, even when cruises were only a few weeks apart (Figure 4.7). Yet, the model captures that intra-annual variability, expressed as the minimum and maximum 7-day average for each summer, and a comparison between modeled and observed summer hypoxic area, averaged over the timeframe of the observations in each year, shows the model also captures the inter-annual dynamics of this key management-focused metric.

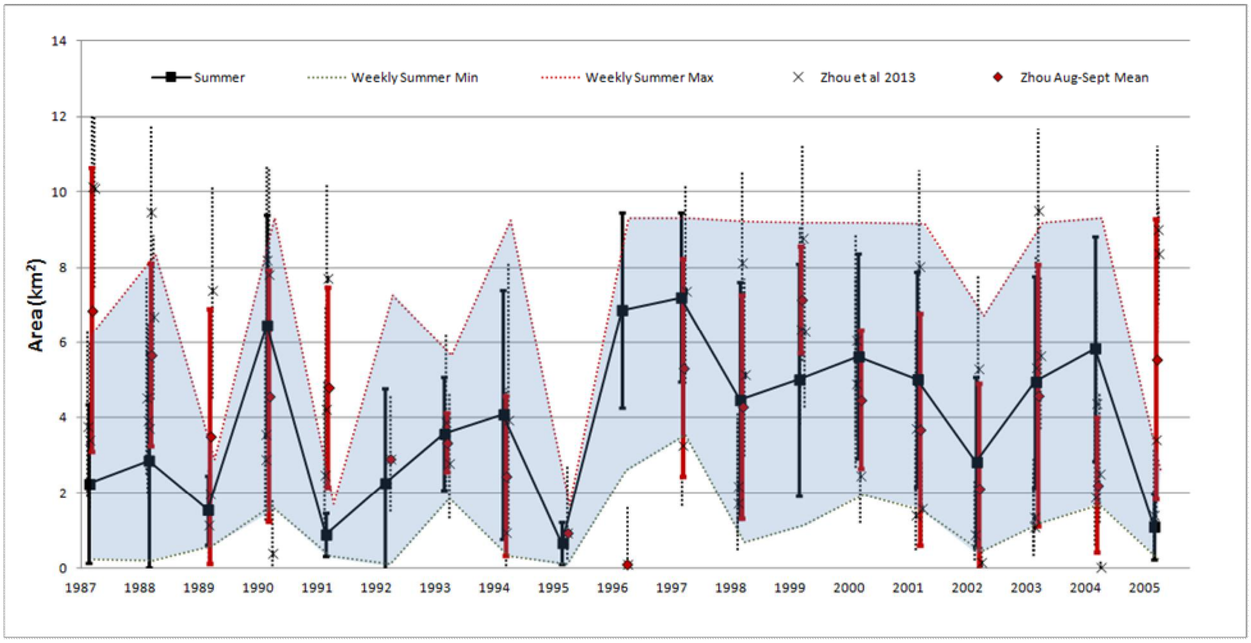

Figure 4.7: Light symbols with dotted error bars are 95% confidence intervals for individual cruises (Zhou et al. 2013). The shaded region represents modeled 7-day minimum and maximum for Aug-Sept. Red symbols and error bars are monthly means and standard deviation of the individual cruise estimates. Dark black line and bars represent model Aug-Sept means and standard deviation.

While the model is relatively simple, containing only six state variables, there are over thirty parameters that can be adjusted during calibration. The vast majority of these parameters values are within ranges used in similar models of large lakes, from the literature, and from EPA model guidelines (Table 4.2). However, in such under-determined models (Anderson 2005; Friedrichs et al. 2006), it is possible to match state variable observations with more than one set of rate coefficients, such that over-estimation of one rate process is compensated by under-estimation of another. For this reason and to further confirm model performance, the calibrated model results were also compared to sedimentation, primary production, and oxygen depletion rates. The June-September mean primary production rates calculated by the model (18.7 - 92.7 mgCĀm^{-3}Ād^{-1}) are within the range of values measured during the growing season (Table 4.3). There are fewer published measurements of sedimentation rates in Lake Erie, particularly in recent decades. However, the model average of 1.59 g(dw)Ām^{-2}Ād^{-1} is consistent within the 0.2-71.2 g(dw)Ām^{-2}Ād^{-1} range measured in Lake Erie by Charlton and Lean (1987) and the 1.47- 2.2 g(dw)Ām^{-2}Ād^{-1} range measured in offshore Lake Ontario by Rosa (1985). Modeled hypolimnetic dissolved oxygen depletion rates are also comparable to those estimated by the much simpler models (Rucinski et al. 2010) and by regression of hypolimnetic averaged concentrations (Figure 4.8). Depletion rates were also comparable to those found by Burns et al. (2005) and Rosa and Burns (1987).

Table 4.3 Published Primary Production Rates in Lake Erie.

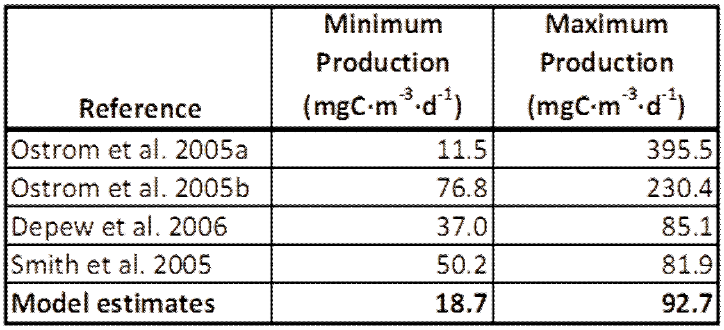

Reference	Minimum Production (mgC·m^{-3}·d^{-1})	Maximum Production (mgC·m^{-3}·d^{-1})
Ostrom et al. 2005a	11.5	395.5
Ostrom et al. 2005b	76.8	230.4
Depew et al. 2006	37.0	85.1
Smith et al. 2005	50.2	81.9
Model estimates	**18.7**	**92.7**

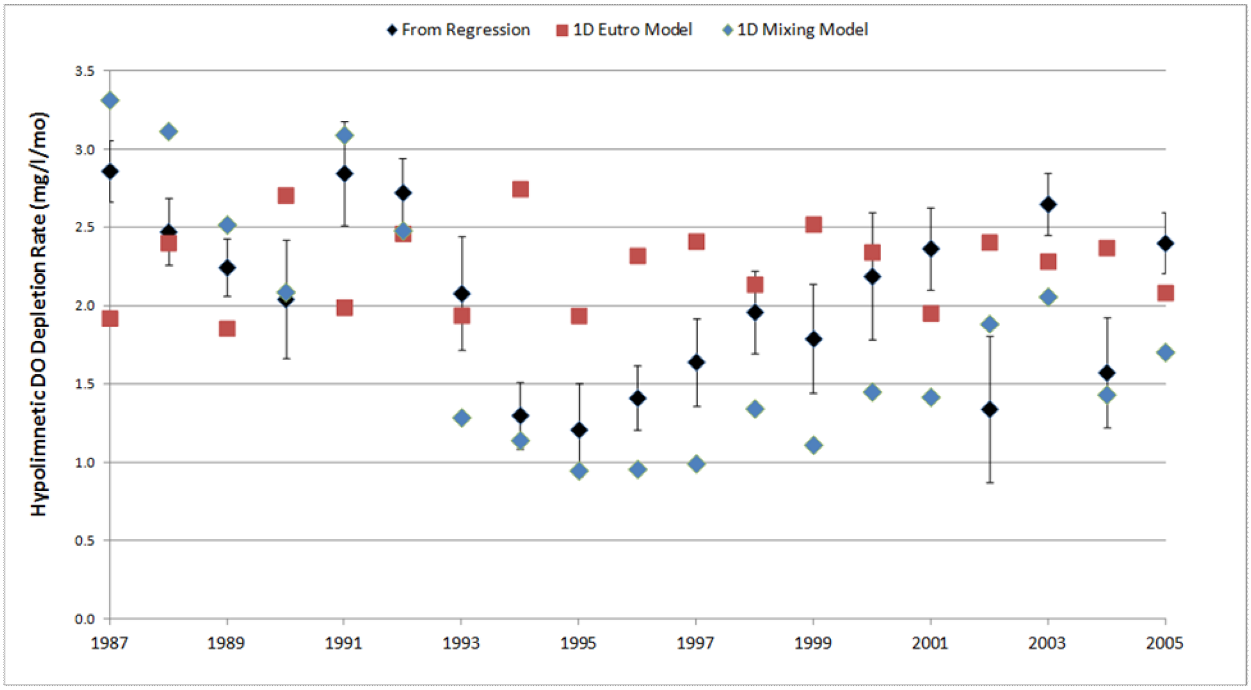

Figure 4.8: Comparison of water column depletion rates from Rucinski et al. 2010 (blue diamonds), linear regression (black diamonds; standard error shown in vertical error bars), and the model described here (red squares).

Overall, the calibration, corroboration, and confirmation tests outlined above (as well as the additional tests to data outside the calibration set described below) provide sufficient confidence in the modelộs ability to reproduce hypoxia dynamics on seasonal and interannual scales.

4.5 Application and Discussion

In an earlier analysis that aggregated all oxygen consumption into water column and sediment demands, Rucinski et al. (2010) and Chapter 3 found that SOD represented on average 63% of the total hypolimnetic oxygen demand. In the present model, SOD also represents a substantial fraction of the overall demand. For example, in a simple model test, after removing all external phosphorus load, a 67% reduction of SOD is still required to eliminate hypoxia.

Because SOD is dependent upon settled organic matter, primarily from phytoplankton production driven by nutrient loads, it is logical to assume that reduced loads would eventually lead to reduced SOD. So, it was necessary to developed estimates of SOD changes in response to projected changes in phosphorus loads. To account for this, a relationship developed by Borsuk et al. (2001) between SOD and carbon deposition was used:

$$SOD = a\left(\frac{L_c}{1 + kL_c h}\right)^b$$

where L_c is deposited organic carbon, h is the thickness of hypolimnion, and a, b, and k are model coefficients. Although their study focused mostly on large estuaries, it was possible to calculate values for a, b, and k via a least-squares regression such that the equation reproduced the average observed SOD for rates of organic carbon deposition simulated by the eutrophication model across the range of loads from the 19-year data set (Figure 4.9). This provides a reasonable representation of the relationship between carbon sedimentation and SOD; however to adjust SOD in the load-reduction scenarios, it is required to know how SOD would vary with nutrient load. To address this, current model was run with a wide range of loads to generate a relationship between load and carbon deposition and then, by way of the modified Borsuk equation, created a TP-SOD relationship (Figure 4.10):

$$SOD = \left(\frac{SOD_{\max} \; TP_{load}}{K_{SOD} + TP_{load}}\right)$$

where $SOD_{\max}$ is Maximum sediment oxygen demand , TP_{load} is the annual total phosphorus load, and K_{SOD} represents a half-saturation constant. This approximation assumes that SOD reaches a new steady state with nutrient loading. The values for SODmax and KSOD, obtained by regression, are 0.98 gĀm^{-2}Ād^{-1} and 3847 tonnesĀyear^{-1}, respectively. With this ability to adjust

SOD based on loads, the model was used to investigate the response of several water quality metrics as a function of load and inter-annual variability in physical drivers.

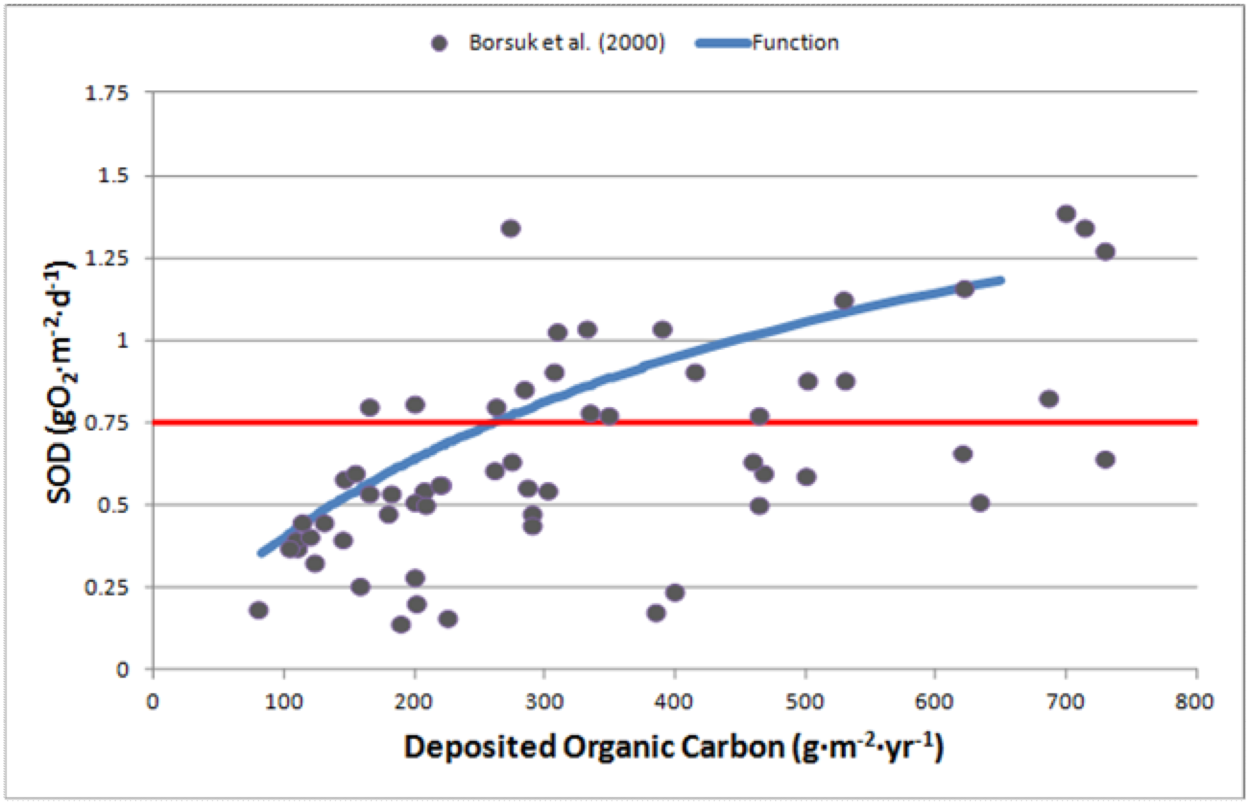

Figure 4.9: Comparison of model calculated SOD and sampled estuaries in Borsuk et al. 2001. Average of published Lake Erie SOD values is shown as solid red line. Solid blue line shows the obtained function relating SOD to deposited carbon. Black circles show the values published in Borsuk et al. 2001 for other systems.

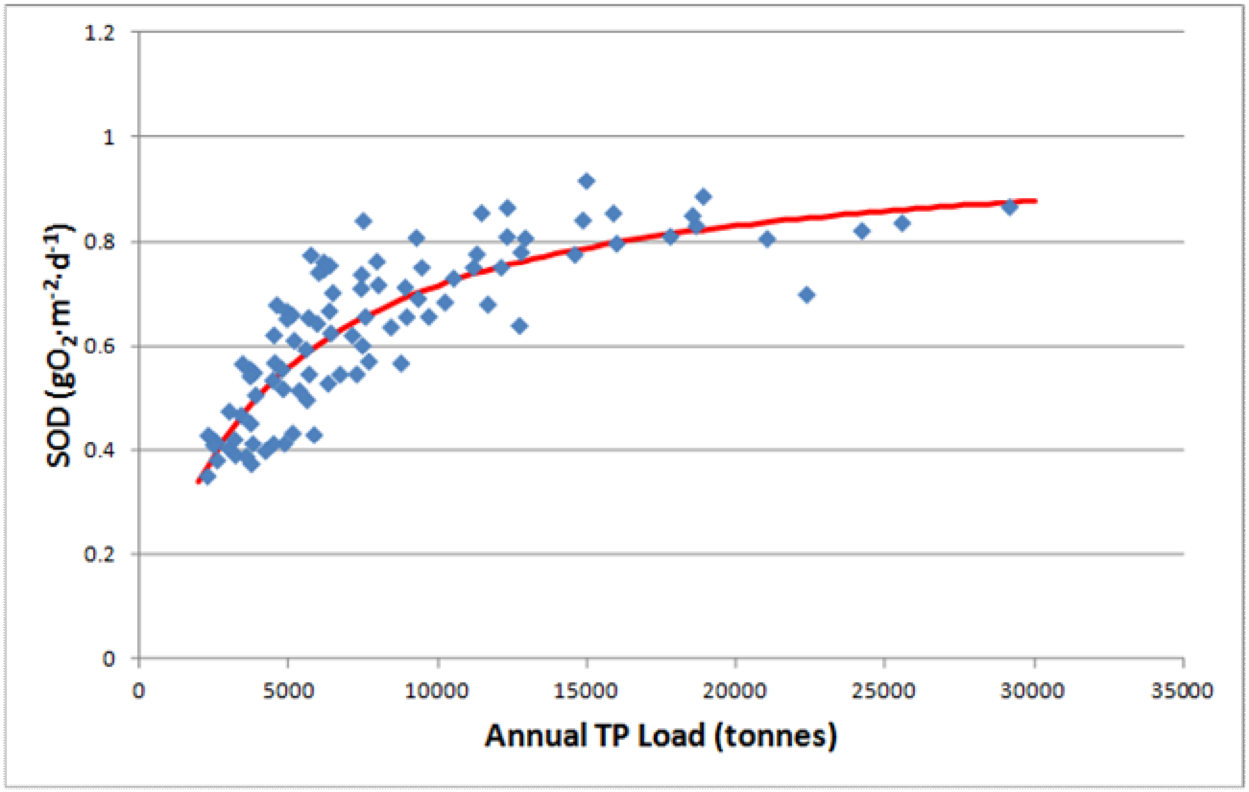

Figure 4.10: Relationship between annual total phosphorus load and model calculated SOD. Model estimated values shown as blue diamonds. Regression curve shown as red line.

To explore the systemôs response to altered loads and inter-annual variability in physical drivers, response curves were generated by scaling the 1997 load time-series by factors ranging between 0.1 and 2.0 and running the model with temperature and mixing patterns from each of the 19 years to generate response envelopes represented by the mean and standard deviation of the 19 cases. This approach allows development of response curves for the central tendency in hypoxic response, but also emphasize that the meteorological conditions in a given year can produce substantial deviation from that mean. That is, while one can estimate the projected impact of a load reduction on average, the actual hypoxia metric might deviate substantially in any given year. The 1997 loading time series was used as the base case because it resulted in a steady state SOD equal to the observed rates and it represented loads and hypoxic extent typical of the recent era.

Response curves were generated for hypoxic area, hypoxic days, oxygen depletion rate, and bottom DO concentration as a function of annual TP load (Figure 4.11) and DRP load (Figure 4.12). It should be noted that the loads used in these curves represent total western and central basin loads. Eastern basin loads are assumed to not influence the central basin significantly. Observed means and standard deviations of these metrics, where available, are also plotted along with the model response to illustrate the modelôs ability to represent the general relationships, given the inherent variability in the observations, as well as capture the variability associated with inter-annual meteorological variability.

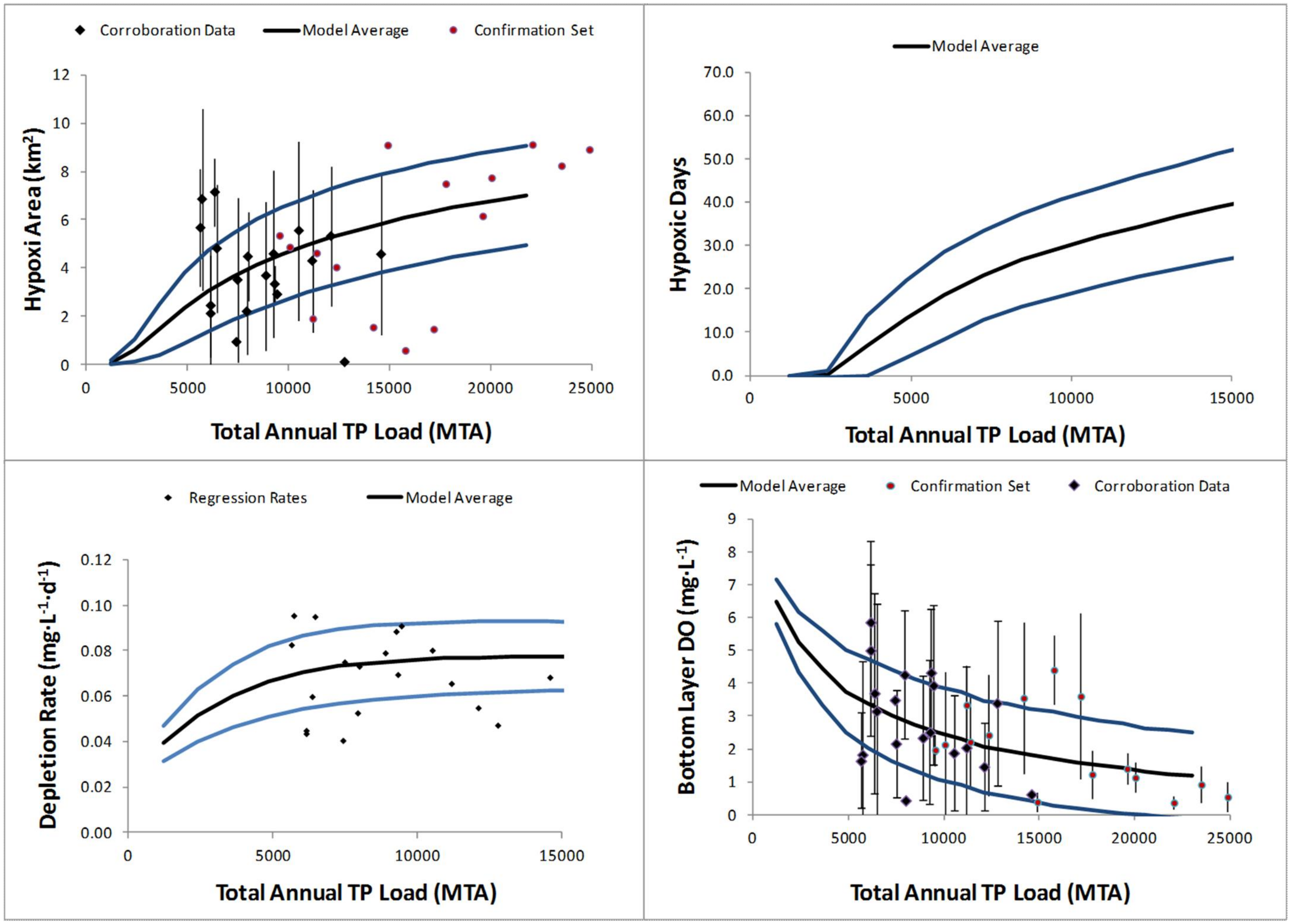

Figure 4.11: Response of hypoxia area, hypoxic days, oxygen depletion rate, and bottom layer dissolved oxygen as a function of western and central basin TP load. Curves represent the mean +/- std of cases representing hydrometeorology from the 19 years 1987-2005. Symbols and error bars are means and stdev of observations. Black symbols represent the 1987 - 2005 data sets. Red symbols are for years outside the 1987-2005 series.

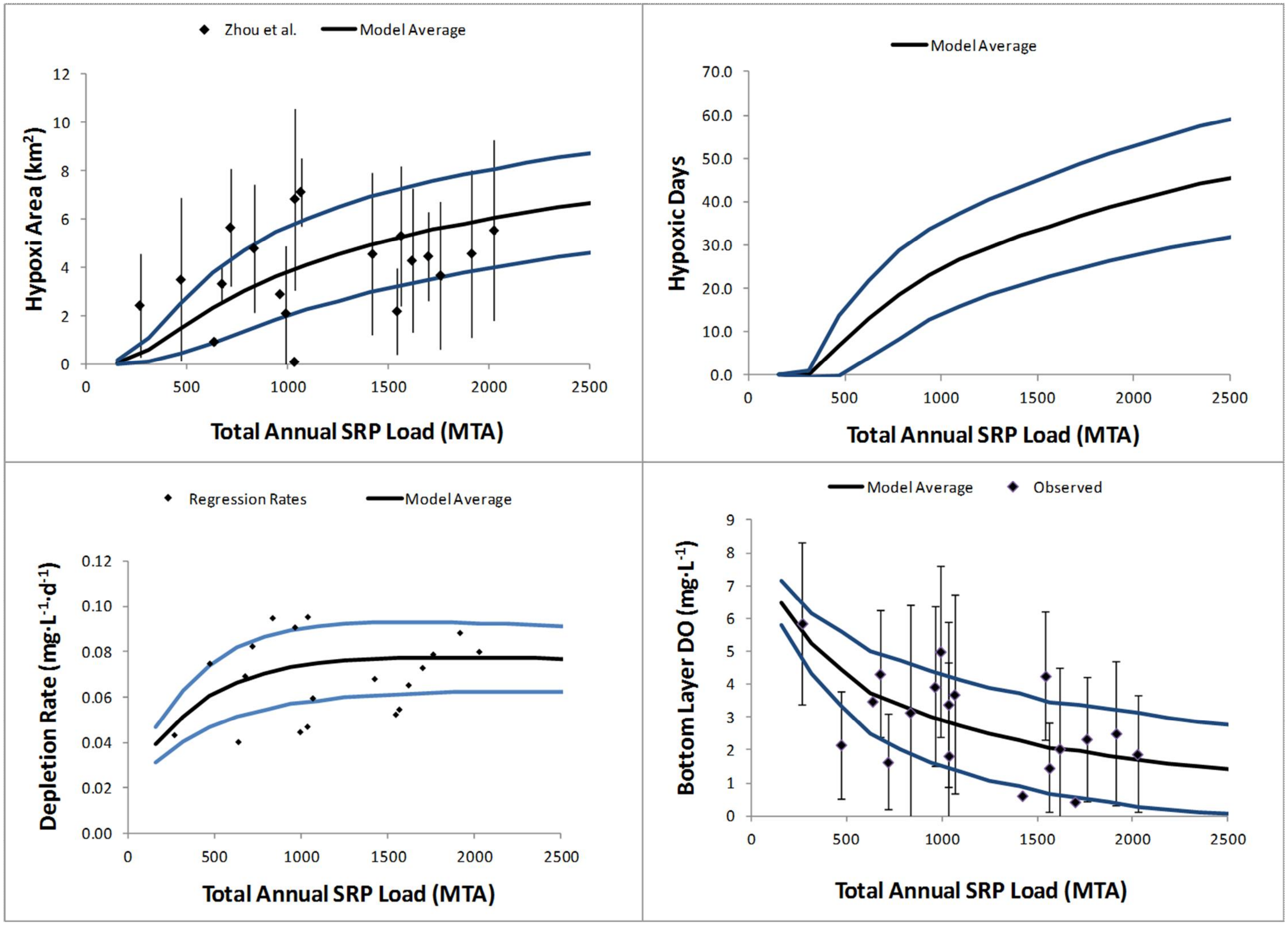

Figure 4.12: Response of hypoxia area, hypoxic days, oxygen depletion rate, and bottom layer dissolved oxygen as a function of western and central basin DRP load. Curves represent the mean +/- std of cases representing hydrometeorology from the 19 years 1987-2005. Symbols and error bars are means and stdev of observations. Black symbols represent 1987 - 2005 data sets.

In a final model evaluation test, Figure 4.11 includes observations from years considerably outside of the loading range in the 1987-2005 calibration/corroboration dataset. It shows the modelôs ability to capture most of those observations, including those with much higher loads from the 1960s and 1970s. This evaluation represents a more rigorous confirmation of the model beyond the corroboration using the 1987-2005, when P loads did not vary as much.

4.6 Conclusions

This 1-dimensional linked hydrodynamic and eutrophication model was developed and corroborated to 1987-2005 observations, and then verified with observations from the 1960s and 1970s. The model effectively captures both vertical and temporal trends in DO, and generally reproduces the temporal trends in CHL, phosphorus, and zooplankton biomass although sufficient data capturing the summer trends are often not available. Additionally, the model estimates of several key internal process rates matched observations. By incorporating a relationship between external load and SOD, the load-response curves envelopes, accounting for inter-annual variability in meteorological conditions, provide a valuable tool to reassess loading targets to Lake Erie with the goal of reducing hypoxia.

This analysis can be used to draw some management implications. By inspection of Figure 4.11, it is clear that the western basin (WB) and central basin (CB) TP load would have to be approximately 4300 MTÄyear^{-1} (4804 MTÄyear^{-1} total load because the WB+CB load is roughly 90% of the total load) to even reduce the hypoxic area to 2,000 km^{2} (approximately the area of hypoxia in the early 1990s when fish communities were generally thriving). This load is substantially lower than the current total load target of 11,000 MT, a 46% reduction from the 2003-2011 average loads, and 56% below the current target. If a new target were developed for DRP (Figure 4.12), achieving that hypoxic area would require a DRP load reduction to 550

MTĀyear^{-1} (equivalent total load of 598 MTĀyear^{-1} because WB+CB is 92% of total DRP), a value roughly equivalent to values in the early 1990s. Because there has been such a significant increase in the DRP load since then, this represents a very substantial 78% reduction from the 2005-2011 average DRP load. These projections provide the central tendency in hypoxic response, but also include projection envelopes that represent variation due to changes in meteorological conditions. That is, while it provides the projected impact of a load reduction that would be expected on average, the actual hypoxia metric might deviate substantially in any given year, based on the observed meteorology in that year.

It is also interesting to note that recent recommendations to reduce the occurrence of western basin cyanobacteria blooms would not be sufficient to significantly reduce central basin hypoxia. For example, the Ohio Lake Erie Phosphorus Task Force recommended that to keep blooms to acceptable levels, the March-June Maumee River TP loads (as a surrogate for all WB tributaries) should be less than 800 MT (Ohio EPA 2013), which is a 31% reduction from the 2005-2011 average of 1160 MT (Richards, pers. com). If all western and central basin non-point sources were reduced by the same 31% and applied across the full year, the resulting annual TP load would be reduced to 6273 MTĀyear^{-1}, still considerably higher than the 4300 MTĀyear^{-1} target identified above. So, in setting targets, it is important to recognize that western basin cyanobacteria and central basin hypoxia endpoints likely require separate considerations.

The analysis has limitations, including a rather simplified lower food web kinetics and a 1D model domain that only is applied to the Central Basin. While Occamôs razor was used here, additional model components may be worth exploring if the response curves are altered by adding more complexity. For example, one could add multiple phytoplankton classes, nitrogen cycles, nutrient speciation, and sediment diagenesis. Extending the model domain to 3D could allow for a more direct estimate of hypoxic area and the ability to explore near-shore effects of dreissenids and benthic algae. Also, it would be valuable to explore the effect of decreases in phosphorus loading to the Western Basin production of decomposable organic carbon that can be then transported to the Central Basin. This particular model refinement may bring the cyanobacteria load reduction target more in line with the Central Basin load reduction target. In addition, it is worth noting that this analysis focused only on the effects of variability in historical meteorological conditions. Thus, the response curves might not necessarily apply under climate conditions not represented within the range of 1987-2005 conditions. A subsequent analysis will include application of the model under hypothetically warming climate scenarios.

CHAPTER 5: Modeling the relative impacts of potential climate-induced changes – phosphorus load seasonality and thermal regime – on hypoxia in Lake Erie

5.1 Introduction

Lake Erie has historically been subject to significant cultural eutrophication (Beeton 1963). This resulted in nuisance algal blooms, poor clarity, and little to no dissolved oxygen in the hypolimnion of the Central Basin. In the 1970s and 1980s, legislation, such as the Great Lakes Water Quality Agreement (GLWQA 1978), set limits on the total annual load of phosphorus that can enter the lake. Initially the trophic status of the lake responded positively (DePinto et al. 1986). However, data from the past two decades have shown that the harmful effects of eutrophication have reemerged, most notably hypoxia (dissolved oxygen concentration below 2 $\text{mg}\cdot\text{L}^{-1}$; Burns et al. 2005; Zhou et al. 2013). Excess phosphorus loading from point and agricultural non-point sources (Dolan 1993) has been a key driver in both the lake's hypoxia growth and recovery phases.

Chapter 4 investigated the lake's hypoxic response to varying loading magnitudes under recent climate conditions. That analysis is expanded here to incorporate changes in load and hydrologic timing and seasonality, as well as the potential impacts of hypothetical climate change conditions.

In Chapter 4, a 1-dimensional, linked hydrodynamic and eutrophication model was developed and calibrated to 19 years of water quality observations (dissolved oxygen, chlorophyll-a, phosphorus species, and total zooplankton biomass) for the summer stratification period in the central basin of Lake Erie (Figure 5.1). This model was further corroborated with observed process rates (primary production and sedimentation) and areal hypoxic extents (Zhou et al. 2013), and confirmed with observations from the 1960s and 1970s.

In that analysis, it was suggested that the TP load to Lake Erie would have to be reduced to approximately 4800 MTĀyear^{-1} to reduce hypoxic area to 2000 km^{2} (as opposed to the current load target of 11,000 MTĀyear^{-1}). Here, the relative influence of meteorology and load seasonality in the hypoxia predictions was explored. The chapter describes the modeling approach and provides a comparison of several hypoxic metrics for a suite of 6 hypothetical scenarios.

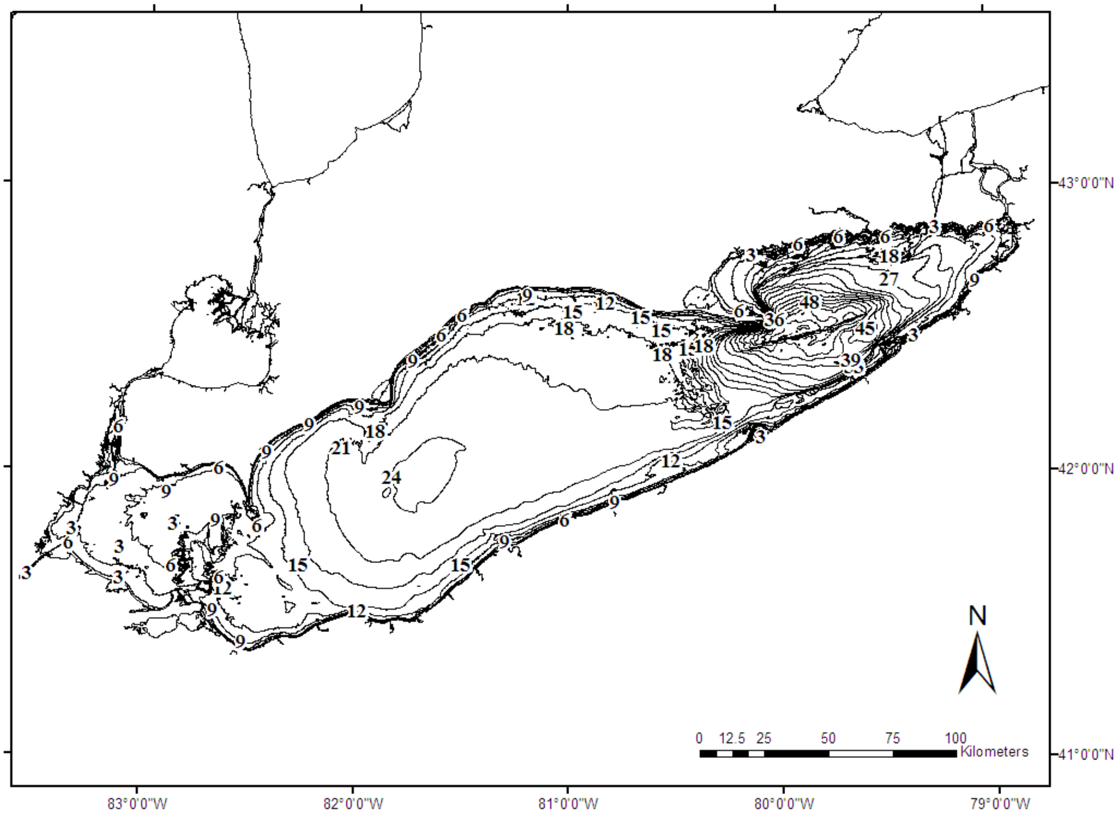

Figure 5.1: Morphology of Lake Erie.

5.2 Modeling Approach

Extending the previous model application, the relative impacts of load seasonality and meteorological conditions were compared. Table 5.1 summarizes the scenarios that were applied in this study.

Scenario A is the ñcontrolò scenario using the 1997 loading time-series and meteorology, a typical meteorology and loading year as described below. Scenario B explores the impact of variation in loading seasonality, Scenario C explores the impact of meteorological variability, and Scenario D explores the combination of both seasonality in loading and meteorological variability.

The low and high warming scenarios (E and F) are described in more detail subsequently. Briefly, the low warming scenario (E) corresponds to a 2 ^{o}C increase in air temperature in the winter and a 4 ^{o}C increase in the summer. The high warming scenario (F) corresponds to a 5 ^{o}C increase in winter and a 7 ^{o}C increase in summer.

Table 5.1 Summary of Model Scenarios

Scenario	Annual Loading Magnitude	Loading Seasonality	Meteorological Conditions	No. of Runs
A	Equal to 1997 Annual Load	1997 seasonality	1997 meteorology	1
B	Equal to 1997 Annual Load	1987 - 2005 seasonality	1997 meteorology	19
C	Equal to 1997 Annual Load	1997 seasonality	1987 - 2005 meteorology	19
D	Equal to 1997 Annual Load	1987 - 2005 seasonality	1987 - 2005 meteorology	19 x 19
E	Equal to 1997 Annual Load	1997 seasonality	Low warming (scaled 1987-2005 meteorology)	19
F	Equal to 1997 Annual Load	1997 seasonality	High warming (scaled 1987-2005 meteorology)	19

5.3 Model Description

The model framework used in this study is a 1-dimensional, linked hydrodynamic-eutrophication model as described in Chapter 4. Both sub-models operate on the same temporal and spatial scale. The model spatially represents a vertical profile of the offshore waters of the Central Basin of Lake Erie (Figure 5.1); resulting in a total depth of 24 m. The model is discretized vertically into 48 layers of 0.5 m thickness.

Calibration and confirmation of the hydrodynamic portion of this model is fully described in Rucinski et al. (2010) and Chapter 3. The hydrodynamic model is run first, and then the outputs (i.e., temperature and mixing between layers) are used as inputs to the eutrophication model.

The eutrophication portion of the model incorporates external phosphorus and carbon loading; internal phosphorus and carbon cycling; algal growth, death, and sinking; zooplankton grazing, oxygen consumption and production; and sediment interactions (Figure 5.2). Model parameters and differential equations were described in Chapter 4. The model effectively captures both vertical and temporal trends in dissolved oxygen; and generally reproduces temporal trends for chlorophyll-a, phosphorus, and zooplankton biomass, despite limited data availability in most years. Additionally, a novel addition to this model was the incorporation of a relationship between external load and sediment oxygen demand (SOD), allowing for investigation of hypothetical loading regimes and the resultant steady state SOD.

Because hypoxic extent is a key management metric for Lake Erie, we converted model output (bottom-layer DO concentration) to hypoxic area using a relationship developed by Zhou et al. (2013).

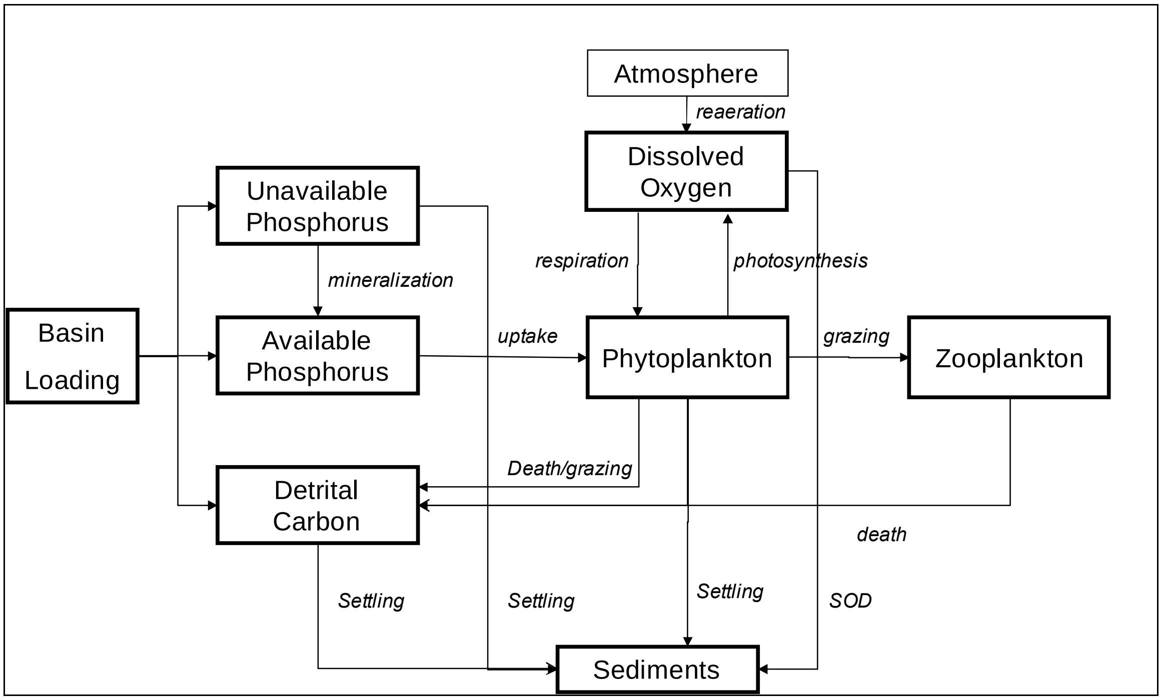

Figure 5.2: Conceptual diagram of simple eutrophication model.

5.4 Results and Discussion

Six scenarios were developed:

Scenario A

This base-year scenario represents the observed loads and meteorology of 1997. The year 1997 was chosen as a base year because its annual load corresponds to the average SOD when the loading-SOD relationship is applied, as described in Chapter 4. The 1997 annual load was used for all other scenarios, so that the impact of a time variable SOD would not interfere in the analysis of the results. Scenario A is considered the baseline case against which the others are compared.

Scenario B

In this scenario, we scaled each of the 1987-2005 loading time-series to match the total annual load of 1997, while maintaining the load seasonality of each individual year. Because total annual load is constant among these runs and we used the 1997 meteorology for all runs, the error bars from this scenario are a measure of sensitivity of load timing.

Scenario C

In this scenario, the observed 1997 loading time series was applied to each of the individual hydrodynamic regimes from 1987-2005. The error bars from this scenario represent sensitivity to meteorological forcing (e.g., wind speed and direction, air temperature, cloud cover).

Scenario D

Scenario D incorporates both sources of variability; applying the 19 scaled load time series to each of the 19 hydrodynamic regimes. .

Scenario E

In this scenario, we altered the hydrodynamic regimes to correspond to a low warming condition (2ºC increase in air temperature in the winter, and a 4ºC increase in the summer), while running the same loading time-series as Scenario C. For the input to the hydrodynamic model, the observed air temperature time-series was scaled upward using a polynomial spline that intersected with the winter and summer air temperature increases (e.g., Figure 5.3). As in Scenario C, the error bars from this scenario represent sensitivity to meteorological forcing (e.g., wind speed and direction, air temperature, cloud cover), but in a warmer climate.

Scenario F

Scenario F is analogous to Scenario E, however, the winter and summer air temperatures are increased by 5 ^{o}C in winter and 7 ^{o}C in summer).

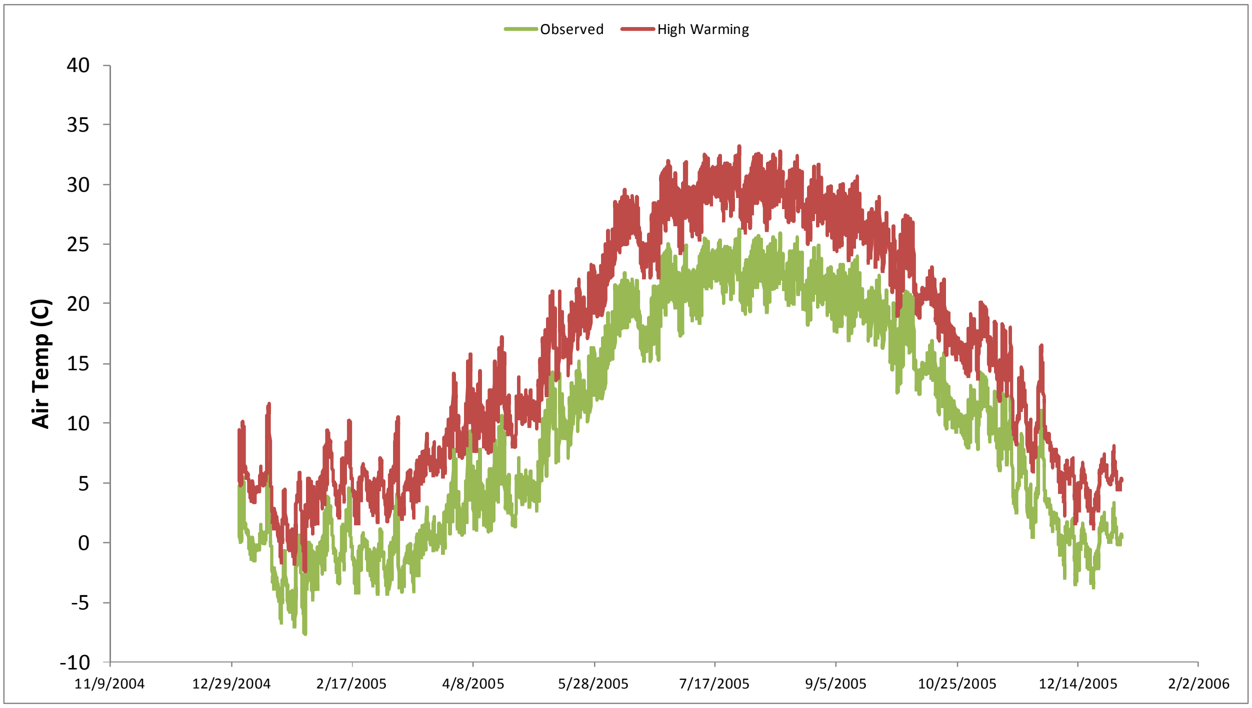

Figure 5.3: Example air temperature time-series in hypothetical warming scenario.

For comparison among scenarios, we use the means and standard deviations of August-September model output, the most frequent time period of hypoxia in the Central Basin. The output metrics consist of hypoxic area, hypoxic days, DO depletion rate, and bottom water DO (Table 5.2, Figure 5.4). It is worth noting that comparing the scenario means via analysis of variance tests (ANOVA) resulted in no statistically significant difference in any of the four metrics among scenarios.

Table 5.2 Model Output Hypoxia Metrics for Each Scenario.

Scenario	Hypoxic Area (10^3 km^2)		Hypoxic Days		DO Depletion Rate (mg/L/mo)		Bottom DO (mg/L)	
	Aug/Sept Mean	Aug/Sept St. Dev	Aug/Sept Mean	Aug/Sept St. Dev	Aug/Sept Mean	Aug/Sept St. Dev	Aug/Sept Mean	Aug/Sept St. Dev
A	6.07	-	36.0	-	2.65	-	1.59	-
B	6.00	0.66	35.8	4.5	2.67	0.08	1.64	0.32
C	4.90	1.13	26.7	10.9	2.18	0.45	2.18	0.45
D	5.38	1.77	35.7	10.0	2.38	0.24	1.99	0.92
E	5.74	1.70	38.4	9.4	2.22	0.15	1.78	0.84
F	5.90	1.65	39.5	10.1	2.10	0.14	1.70	0.81

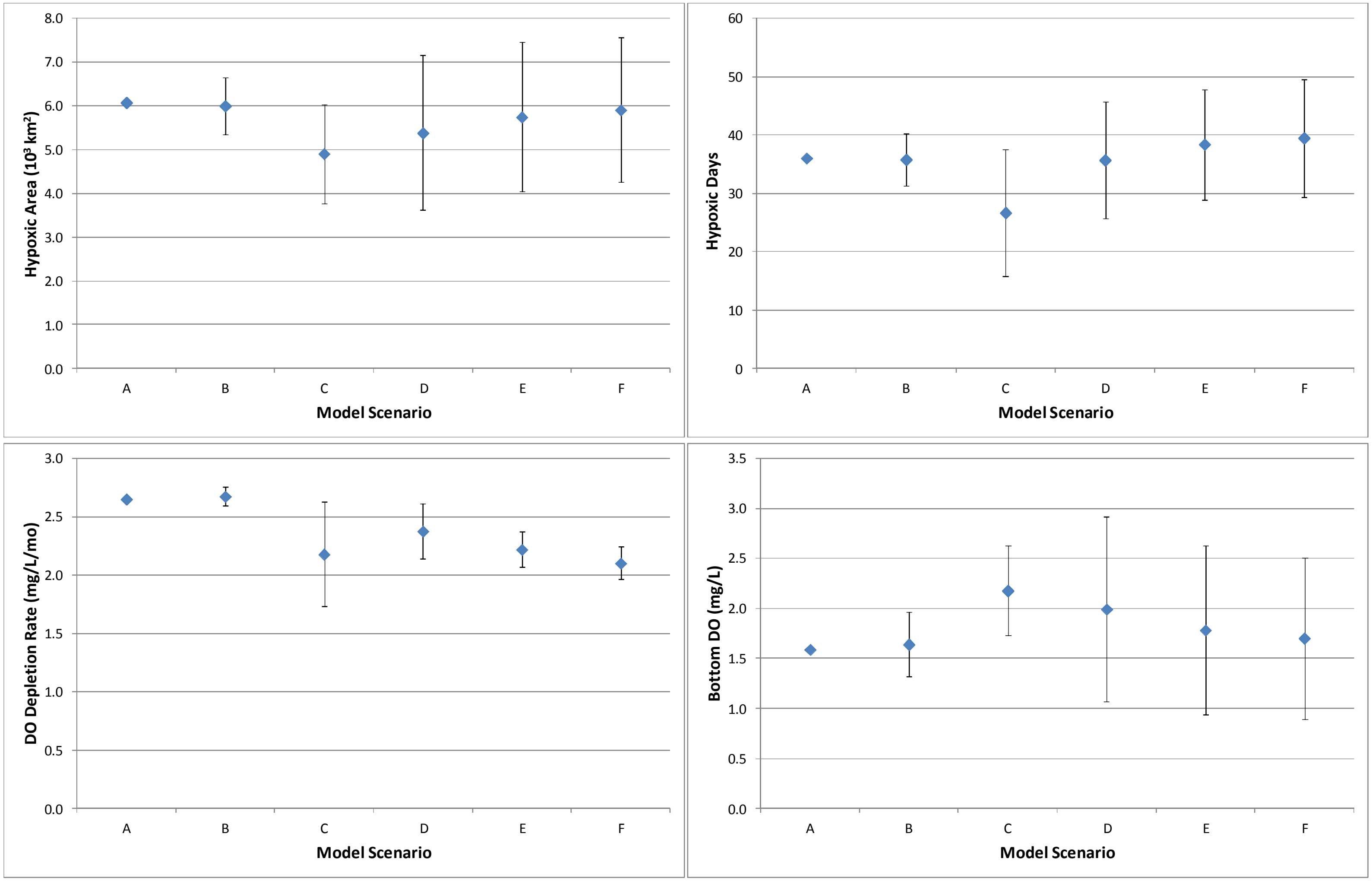

Figure 5.4: Model scenario output for four hypoxia metrics. The blue diamonds represent the Aug-Sept means, while error bars represent of the standard deviation for runs within each scenario.

Figure 5.5 shows the hypoxic area response to a metric of load seasonality: the percent of the annual TP load that is delivered in spring (Mar - Jun). Scenario B (shown in red diamonds) incorporates only the variability of only load seasonality, while Scenario D (shown in blue triangles) incorporates both load seasonality and meteorological variability. The slope of the trend line in Scenario B shows a slight positive correlation between the spring TP load, and the predicted hypoxic area. However, the trend line for Scenario D is essentially flat, and the values deviate from the trend line more than for Scenario B.

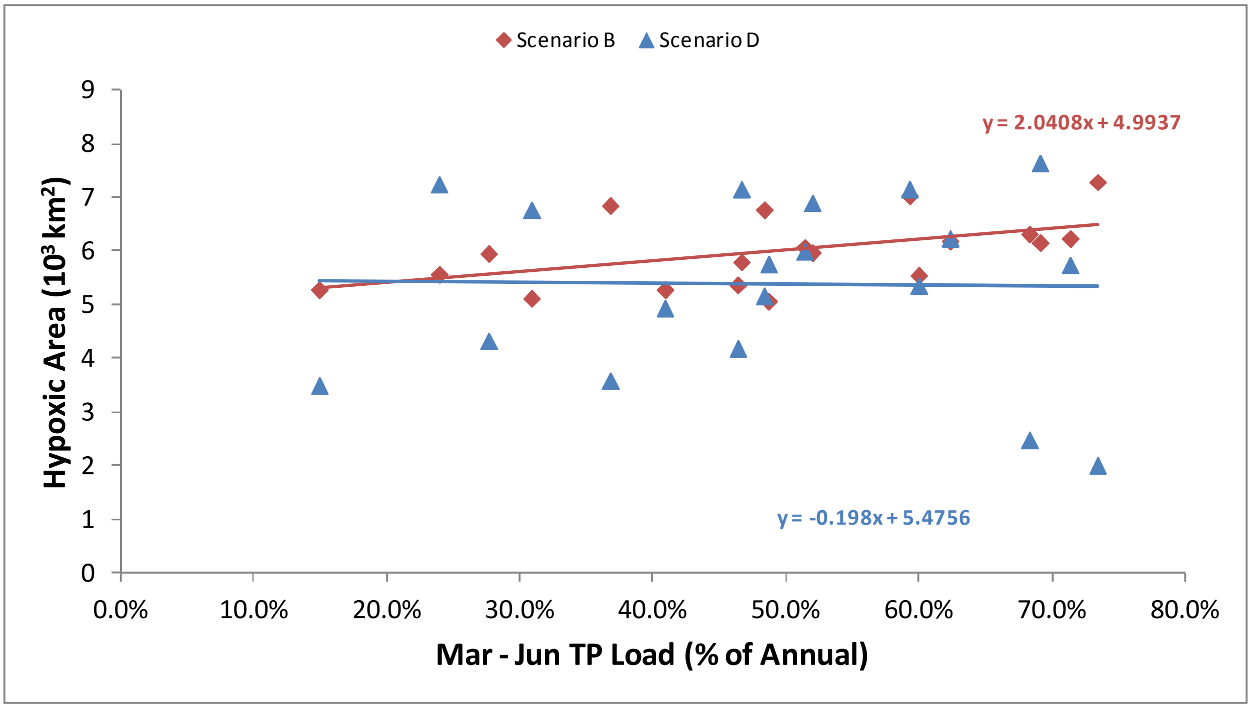

Figure 5.5: Comparison of the spring TP load percentage in Scenarios B and D.

The hypoxic area metric was compared to a measure of thermal stratification: the summer-average depth to the bottom of the thermocline as a surrogate for hypolimnetic volume (Figure 5.6) for Scenarios C (incorporation of only meteorological variability) and D (incorporation of both load seasonality and meteorological variability). The relationship shows that deeper thermoclines (representing a smaller hypolimnetic volume) result in larger hypoxic areas. This is likely because the smaller hypolimnion starts with less oxygen and depleting processes can drive concentrations below 2 mgĀL^{-1} more readily. Both Scenarios C and D show a positive relationship between hypoxic area and hypolimnion depth. Comparing the hypoxic area relationships between spring load (Figure 5.4) and average hypolimnion depth (Figure 5.5) suggests that meteorological variability may have a stronger influence on hypoxia in Lake Erie.

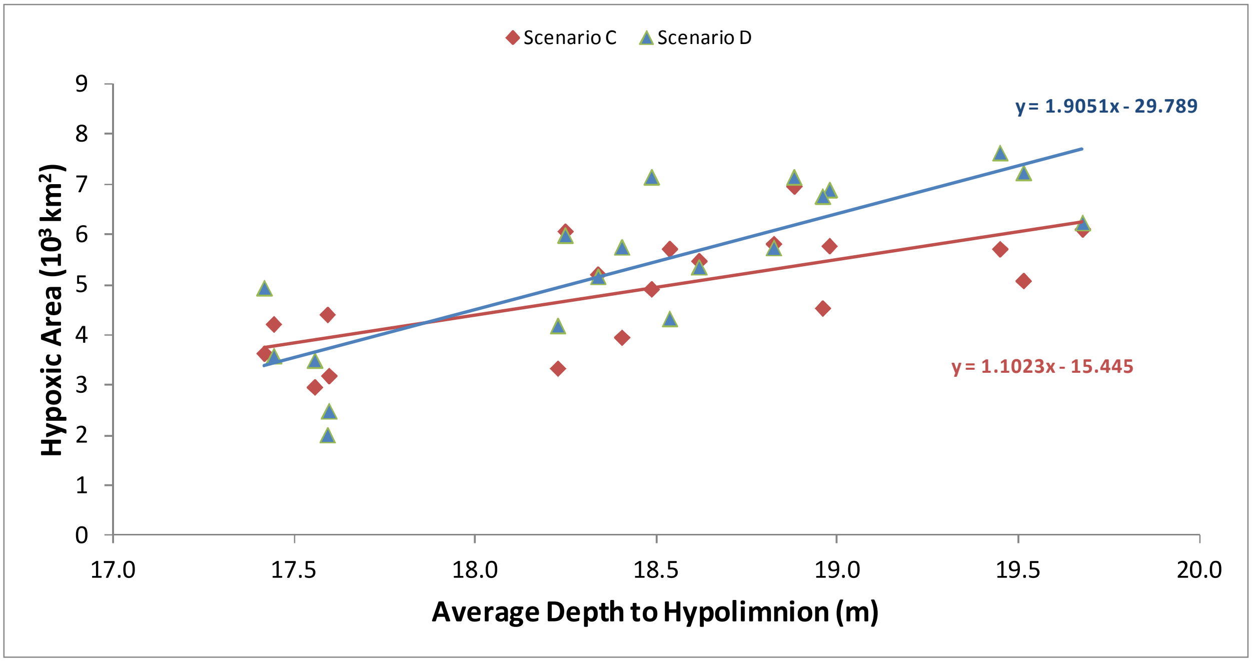

Figure 5.6: Comparison of the summer average hypolimnion depth for Scenarios C and D.

The climate warming runs (E and F) are analogous to Scenario C; i.e., the 1997 loading time-series was applied to 19 different years of hydrodynamic output (Table 5.1). The hydrodynamic regimes used in Scenario E and F both have longer periods of stratification (Figure 5.7) compared to those of Scenario C; however, the hypolimnion is often thicker in the climate warming scenarios. This is a result of less mixing in the epilimnion due to reduced wind-stress and a more stable atmosphere above the air-water interface. In both climate warming scenarios, the effect on the severity of the hypoxia metrics is a combination of the duration of stratification (increased hypoxic severity) and a thicker hypolimnion (decreased hypoxic severity). For the conditions simulated in this analysis, the duration of stratification appears to outweigh the effect of a slightly thicker hypolimnion (Figure 5.4). In fact, the duration of stratification increases on average by 20% in the lower warming scenario, and 35% in the higher warming scenario, while the average increase in hypolimnion thickness is 2% in the lower warming scenario, and 3% in the higher warming scenario. It should also be noted that fall turnover date in the climate warming scenarios is significantly later than under current climate conditions. The hypoxic area maxima typically occur just prior to fall turnover, as the decomposition of organic matter has depleted most of the available dissolved oxygen in the hypolimnion.

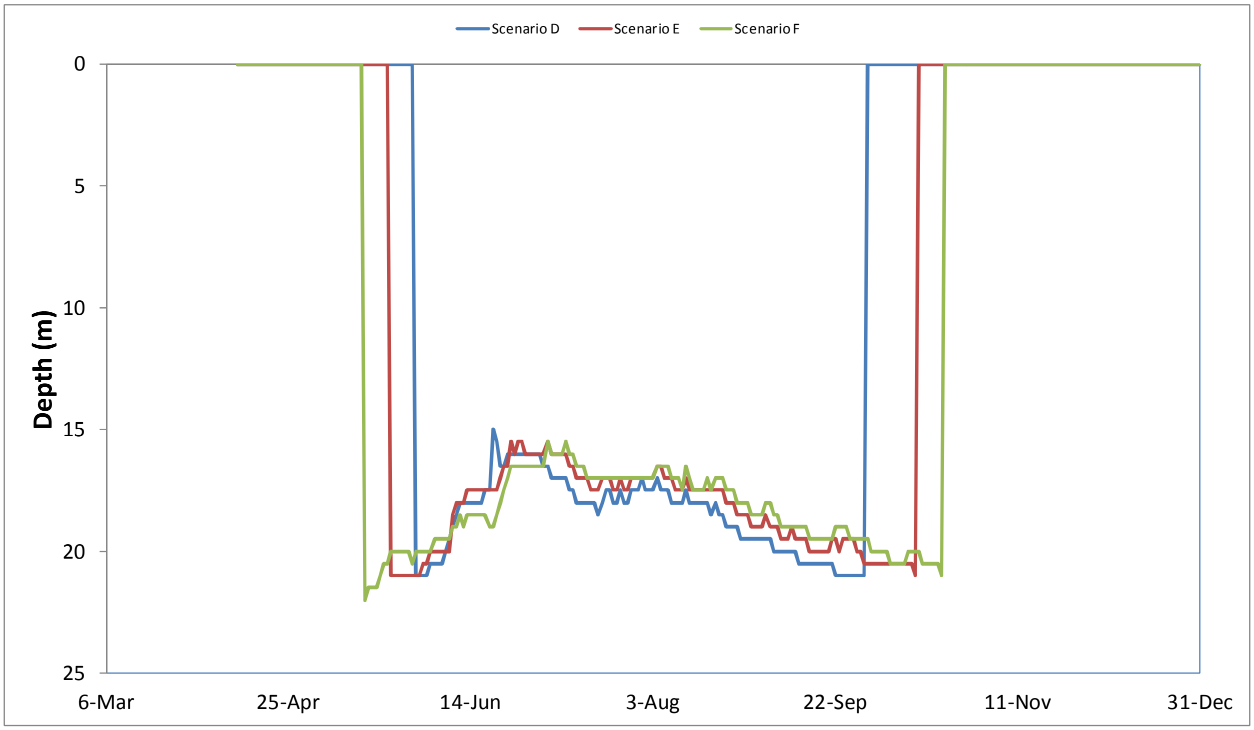

Figure 5.7: Comparison of stratification development between Scenario C and the two warming scenarios (E and F).

The DO depletion rate shows a downward slope in the climate warming scenarios (Table 5.2), suggesting that the increasing trend in hypoxia is a result of a prolonged stratification period, not necessarily the decomposition of more autochthonous carbon production. The duration of limited oxygen transfer across the thermocline enhances the relative effect of the SOD. Additionally, because Scenario F has a more prolonged stratified period than Scenario E, the model predicts an increasing trend for all four of the hypoxic metrics.

5.5 Conclusions

In Chapter 4, a management-oriented model was developed and tested, and used to project Lake Erieĝs Central Basin hypoxic response to nominal loads under a range of meteorological conditions. Herein, the analysis was expanded to explore the influence of annual variations in meteorological conditions, seasonality of loads, and climate.

The variability assessed for four hypoxia metrics (i.e., the error bars in Figure 5.4) demonstrates that Lake Erieôs hydrodynamic regime, driven by interannual variability in meteorology (Scenario C), contributes more to the overall uncertainty (Scenario D) than load seasonality (Scenario B). Figure 5.5 and 5.6 also demonstrate the relationship between hypoxia and meteorology is stronger than with load seasonality. The model also suggests that a warmer climate can potentially result in more extensive hypoxia, if the duration of thermal stratification increases enough to outweigh the effect of a thicker hypolimnion. Although the model did predict small increases in mean hypoxia in these scenarios, the uncertainties in the predictions are large enough that the means are not significantly different. However, due to the increased duration of stratification (Figure 5.7), the effects of SOD are increased in the hypolimnion in these scenarios. Additional model runs with more pronounced warming may be warranted to better define an expected level of hypoxia increase in relation to air temperature increase, and better define the balance between extended duration of stratification and a thicker hypolimnion. It should be noted that the climate scenarios only considered changes in air temperature and not changes in runoff, storms, wind, or cloud cover.

Comparisons of Scenarios B and C with Scenario D demonstrated that mixing drives more of the variability than changes in load seasonality. This suggests that while controlling the amount of phosphorus entering the system will likely reduce hypoxia; predictions on its severity will necessarily have uncertainties due to the relationship with the thermal regime (i.e., interannual variability). However, this analysis along with that presented in Chapter 4, demonstrates that the model can be used to estimate expected hypoxic conditions, but forecasting these expectations for a given year must be done within the ranges of uncertainty shown in Figures 5.4 - 5.6.

CHAPTER 6: Synthesis, Limitations and Future Direction

This chapter summarizes the results from the three modeling chapters, and presents a discussion of the study limitations and potential future work to address those. This chapter also summarizes some efforts that have already been initiated to further this research.

6.1 Multi-complexity Modeling Approach

This dissertation focused on using a series of models with varying complexity, from a simple vertically stratified dissolved oxygen model, to a more complex lower food web and nutrient cycling model. This approach allowed a focus on which parameters and model dynamics are important in simulating and forecasting hypoxia, while also allowing for long-term forecasts under a range of hypothetical conditions.

The simplest model, described in Chapter 3 (Rucinski et al. 2010), aggregated all biological processes into a single term (water column oxygen demand, WCOD), while the spatial and hydrodynamic complexity was an improvement on previous studies (Rosa and Burns 1987; Burns et al. 2005). While it was possible to draw conclusions on the importance of physical conditions, SRP:TP loading ratios, and also confirming a system wide shift in nutrient load response in the mid-1990s, this model did not independently simulate the known forcing of primary production via nutrient loading. Additionally, because the model requires observed DO data to obtain WCOD values, it cannot be used in a forecasting framework.

Therefore, a more complex lower food web model was developed (Chapter 4). This more complex model was calibrated and applied under several management scenarios in both Chapters

4 and 5. The model allowed for testing the effects of phosphorus loading scenarios and hydrometeorological conditions on hypoxia in the Central Basin.

6.1.1 Simple Observation-Based Modeling

A linked 1-dimensional hydrodynamic-dissolved oxygen model was developed and applied in the central basin of Lake Erie over the period of 1987-2005. The model was used to quantify the relative contribution of meteorological forcings versus the decomposition of hypolimnetic organic carbon on dissolved oxygen concentrations. Other researchers have attempted to quantify total volumetric hypolimnetic dissolved oxygen depletion rate (HVOD; Burns et al. 2005; Rosa and Burns 1987), however the approach described here not only incorporated a fine scale vertical profile hydrodynamic model, it also allowed for differentiation between the water column portion of the oxygen demand (WCOD), and the sediment oxygen demand (SOD). This study found that existing sedimentary carbon apparently accounts for approximately 63% of the total HVOD. Consequently, by isolating the SOD component, which has been shown to be relatively constant over the past decade (Matisoff and Neeson 2005; Schloesser et al. 2005; Snodgrass 1987; Snodgrass and Fay 1987), from HVOD, the study demonstrated that a distinct change in trend of WCOD occurred in the mid 1990s, and that trend was driven by factors other than climate.

6.1.2 1-Dimensional Lower Food Web Model

The same 1-dimensional hydrodynamic model used for the empirical DO model described above was linked to a standard nutrient, phytoplankton, zooplankton (NPZ) eutrophication model. The eutrophication submodel was calibrated and corroborated to 1987-2005 observations, and then confirmed with observations from the 1960s and 1970s. By incorporating a relationship between external load and SOD, the model framework allows an investigation of the effects of a range of hypothetical loads. Additionally, the 1-dimensional vertical profile output was linked to an empirical relationship between bottom-water oxygen concentration and hypoxic area (Zhou et al. 2013) to estimate Lake Erie Central Basin hypoxia extent, a key management metric.

The application provided guidance on potential system load reductions called for in the new Great Lakes Water Quality Agreement (GLWQA, 2012). The model is also capable of differentiating between the response of the system to total phosphorus and dissolved reactive phosphorus loads.

Because of the ability to create dozens of combinations of load time-series and hydrodynamics, this application resulted in a series of load-response curves, which could potentially guide managers and stakeholders in the pursuit of new lake loading targets. For example, the analysis estimated that to reduce the annual hypoxic area to 2000 km^2, the TP loading target would need to be reduced by 56% of the current GLWQA target. The modeling analysis presented in Chapter 4 also suggested that a 78% reduction in DRP loading compared to current values would be required for the lake to reach this same hypoxic extent (2000 km^2). Richards (2006) and others have found significant changes in the DRP:TP loading ratio entering the lake via tributaries.

6.1.3 Sensitivity to Main Forcing Functions.

Much of Chapter 5 (and some of Chapter 4) was focused on understanding how sensitive the model was to the variations in the seasonality of nutrient loads and meteorological conditions. The 1-dmensional model was run under 6 hypothetical scenarios based on 1997 annual load, as well as for two hypothetical climate warming conditions. These analyses demonstrated that meteorological variability contributes more to overall model variability than seasonal load timing variability, with respect to affecting Central Basin hypoxia. Additionally, two hypothetical warming scenarios demonstrated that climate-driven prolonged thermal stratification affects hypoxia more than the potential increase in primary productivity.

6.2 Model Limitations

In Chapter 3, a simple dissolved oxygen model was developed, where all biological production and consumption processes were aggregated. It is clear that there are other important characteristics of hypoxia other than the depletion rate (including spatial extent, volume, and duration) that are not incorporated in that analysis. Even though subsequent analyses (Chapters 4 and 5) included nutrient loads and some in-lake dynamics, they also did not directly include important aspects of the Lake Erie ecosystem that can influence hypoxic severity, such as invasive benthic filter feeders (Hecky et al. 2004), benthic algae, the potential contribution of winter diatom growth to summer oxygen demand (Twiss et al. 2012), the autochthonous production of decomposable organic carbon in the Western Basin and subsequent transport to the Central Basin (LimnoTech, 2010), and the impact of 3-dimensional circulation patterns (Rao et al. 2008). These circulation patterns may be more significantly linked to the physical and morphologic conditions in the lake; however, they cannot be appropriately quantified with a 1-dimensional model of this complexity.

The modeling analyses presented here suggest that meteorological effects can have a significant impact on hypoxia, distinct from the impact created by nutrient loads, as described in Chapter 5. Chapter 3 also demonstrated that some relatively short-term disturbances in the thermocline (assumed to be caused by 3-dimensional circulation effects, such as internal waves or Ekman suction) can have a significant impact on dissolved oxygen transport into the hypolimnion (Figure 3.5 shows observed disruption of the thermocline with respect to temperature).

Three-dimensional modeling of Lake Erie is complicated for several reasons: a) substantial spatial and temporal temperature, loading, and in lake data are required, b) observed metrological conditions are required, and c) the run time required to calibrate and confirm the model parameters can be extraordinary, particularly for multi-year simulations.

To investigate these model limitations, substantial changes to the model framework are required. For example, to incorporate benthic filter feeders or benthic algae, the model needs to be converted into a 3-dimensional domain. More specifically, small scale differences in light penetration affecting benthic algae requires very fine horizontal grid discretization. Normally this is accomplished via grid ñnesting,ò where near shore grid areas have a much higher resolution than offshore areas. In addition to the computational complexity of this type of approach, it also requires very detailed bathymetry data, which is often extremely expensive or unavailable.

6.3 Initial Efforts to Address Limitations

The most obvious limitation on the model development is based on the spatial dimensions. While the majority of oxygen dynamics occur in the offshore waters of Lake Erie, much of the nutrient cycling occurs in the near shore area. Therefore, a 3-dimensional model of the lake could provide important insight into the near shore nutrient cycling and its potential impact on offshore waters.

While 3-dimensional ecosystem models in the Great Lakes are now being realized (Bocaniov et al. 2013), there exists no published 3-dimensional model that incorporates observed hydrodynamic properties, as well as the entire lower food web that has been incorporated into less spatially resolved models (e.g., multiple classes of phytoplankton and zooplankton, dissolved, refractory, and labile species of all significant nutrients, dreissenids, benthic algae, and sediment diagenesis process). While there are several efforts underway to tackle this goal, realistic computation and calibration time requires that some of the biogeochemical linkages be eliminated during model runs.

However, this research effort did result in initial development of a 3-dimensional model of the entire extent of Lake Erie. This 3-D model domain is shown in Figure 6.1. The domain consisted of 20 vertical layers and the horizontal discretization is 2km x 2km, while temporally it produces results on an hourly basis. The hydrodynamic portion of the linked model consists of a modified version of the Princeton Ocean Model, parameterized for the Great Lakes (POM-GL).

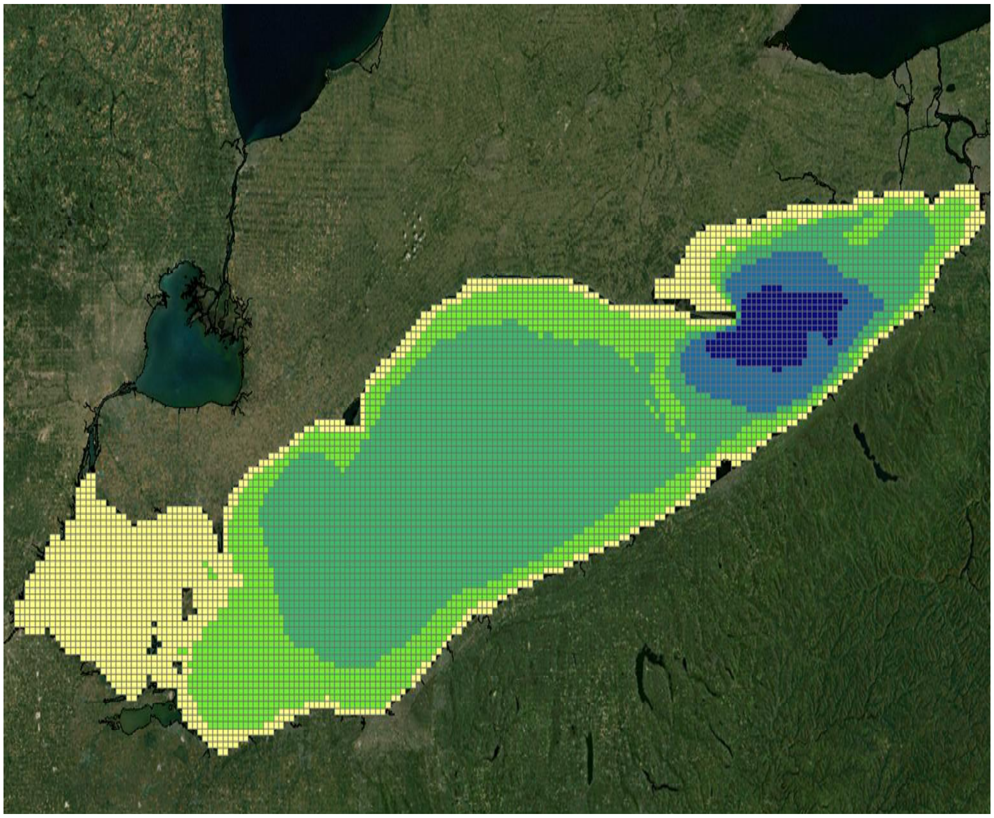

Figure 6.1: 3-dimensional grid of Lake Erie. Horizontally grid cells are 2 km x 2 km. Vertically there are 20 active water column layers.

As a result of the potential near shore nutrient dynamics, an initial attempt to calibrate the same eutrophication model presented in Chapter 4 was made, although applied in 3 dimensions. Figure 6.2 shows an initial attempt at calibration for dissolved oxygen, chloryohyll-a, and total phosphorus.

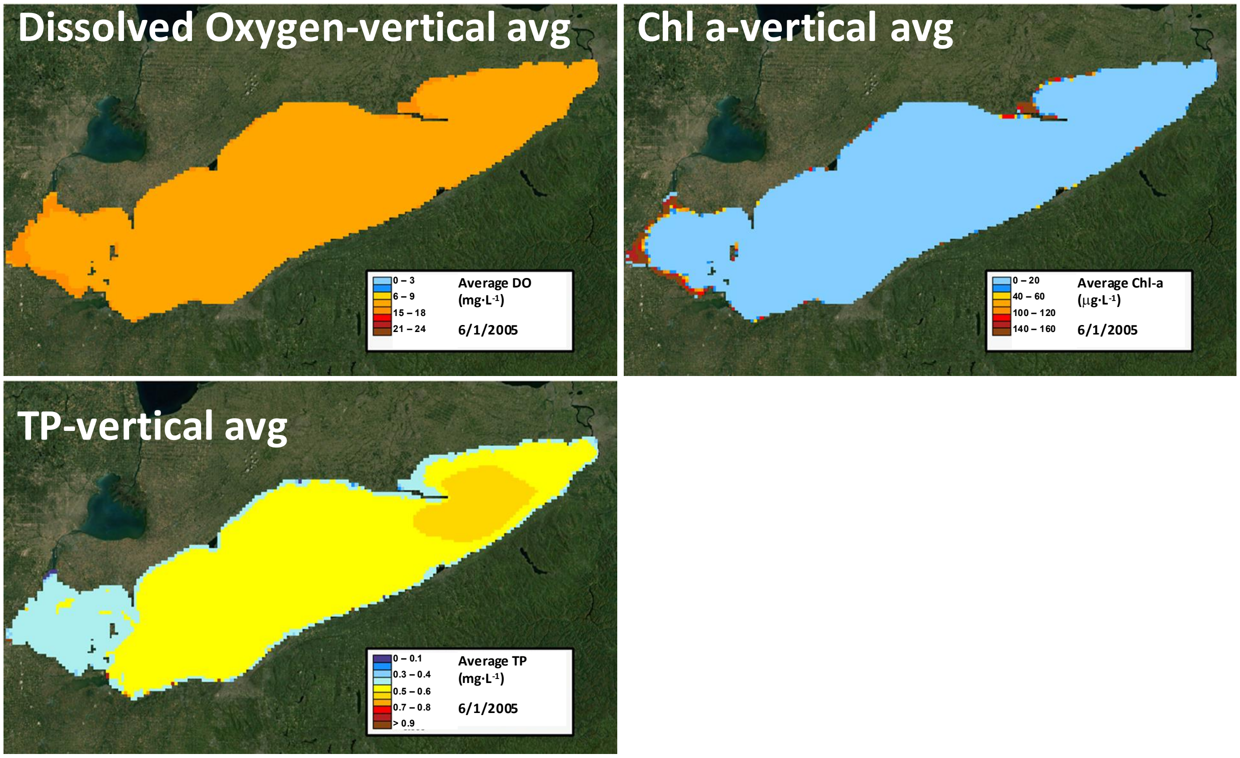

Figure 6.2: Initial model output for 3-dimensional eutrophication model.

The model output shown in Figure 6.2 is from an uncalibrated run investigating the 3-dimensional model. These results are a product of applying the calibrated 1-dimensional kinetic rate terms to the 3-dimensional model. This approach was also applied to the time sequence of the spatial dissolved oxygen concentrations (Figure 6.3).

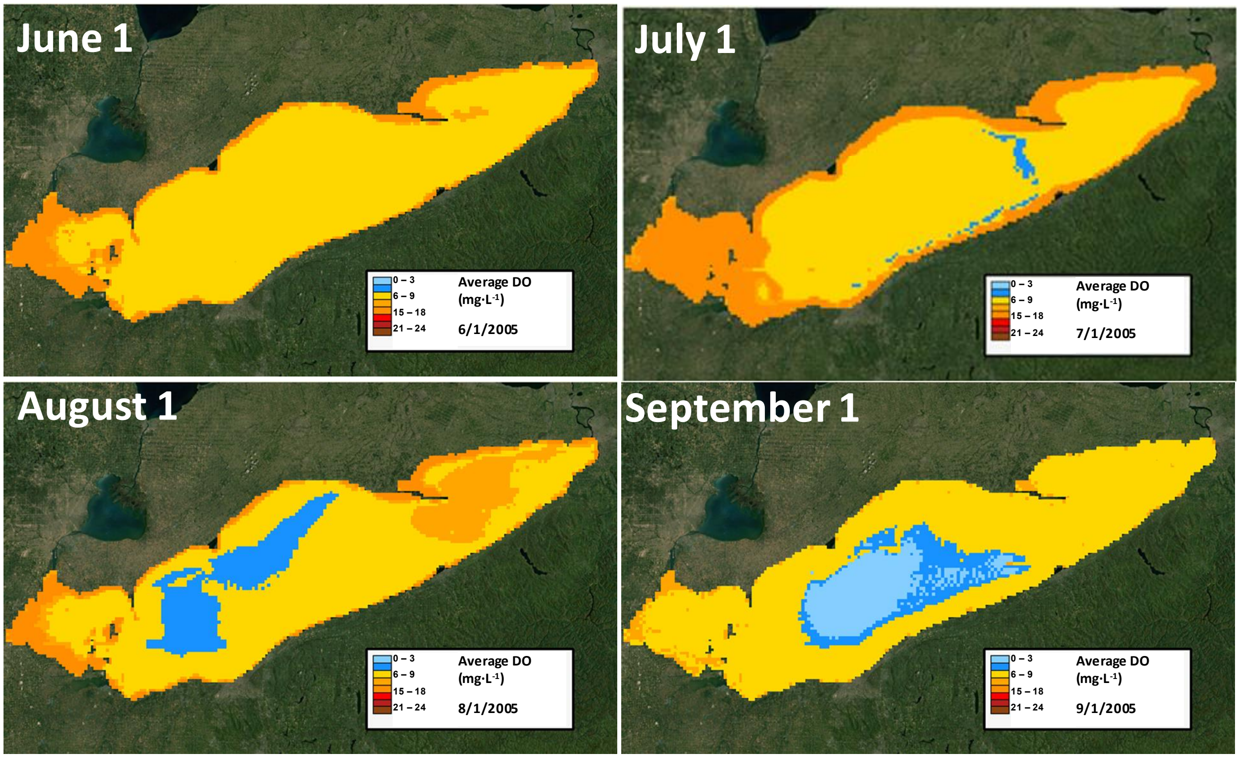

Figure 6.3: Initial dissolved oxygen simulation for 3-dimensional eutrophication model.

6.4 Further Efforts

Many studies have shown that benthic algae, such as *Cladophora* (Eastern Basin) and *Lyngbya* (Western Basin), have drastically impacted the waters of Lake Erie. There are currently advanced eutrophication models that can incorporate near shore benthic algal growth, and its subsequent decay. This type of model has been applied in Western Basin of the lake (the most productive region of Lake Erie; LimnoTech, 2010). Expanding this modeling approach to other near shore areas of Lake Erie may be able help determine the fate and transport of nutrients in other near shore areas of the lake. A simplification of the model's phosphorus cycle is shown in Figure 6.4, which demonstrates how both benthic filter feeders and benthic algae have a significant role in phosphorus cycling in near shore regions. Developing the capability to accurately model the processes seen in near shore regions of large lakes can ultimately help understand effective management approaches.

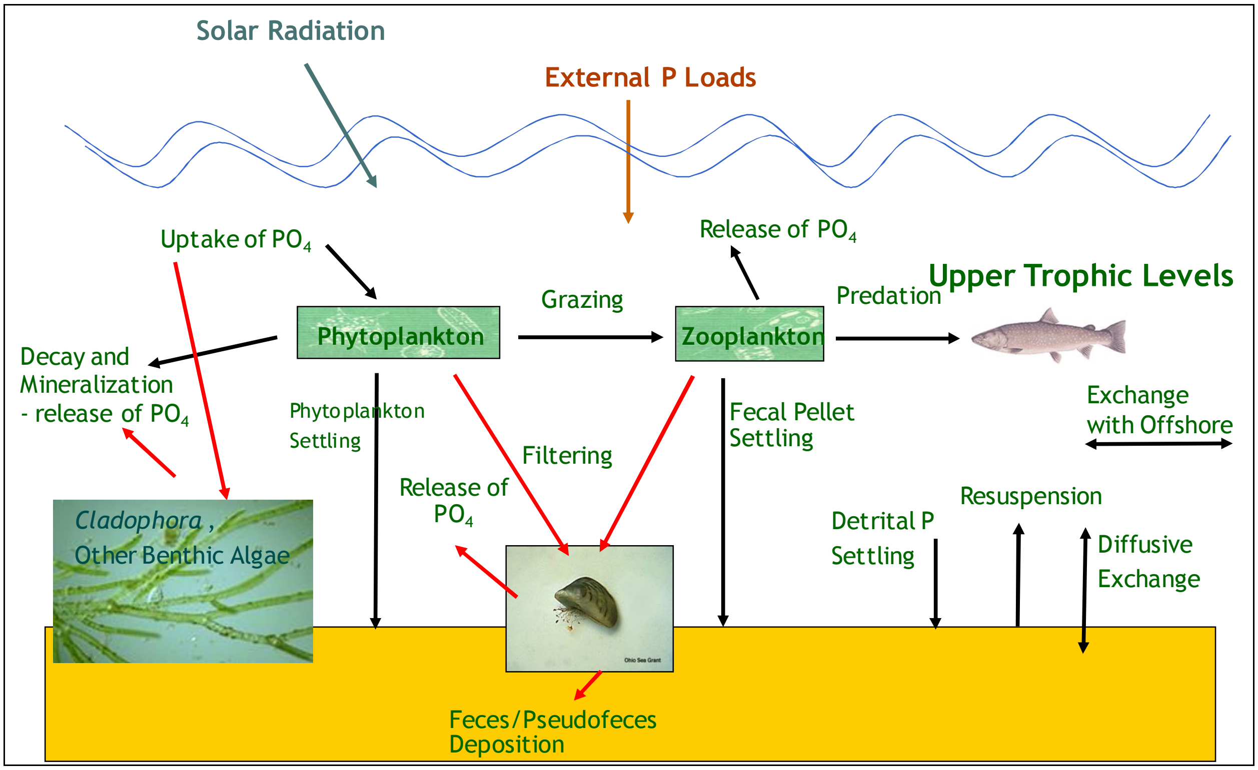

Figure 6.4: Schematic of Phosphorus Cycling Advanced Aquatic Ecosystem Model

APPENDIX: Detailed Description of Eutrophication Model Kinetic Processes

State Variables

Phy_n = Phytoplankton carbon in segment n, $mg \cdot L^{-1}$

Zoo_n = Zooplankton carbon in segment n, $mg \cdot L^{-1}$

UP_n = Unavailable phosphorus in segment n, $mg \cdot L^{-1}$

AP_n = Available phosphorus in segment n, $mg \cdot L^{-1}$

OC_n = Organic carbon in segment n, $mg \cdot L^{-1}$

DO_n = Dissolved oxygen in segment n, $mg \cdot L^{-1}$

C_n =General state variable concentration in segment n, $mg \cdot L^{-1}$

Model Inputs

E_u = dispersion across the interface between segment n_{-1} and segment n, $m^2 \cdot s^{-1}$

E_b = dispersion across the interface between segment $n+_1$ and segment n, $m^2 \cdot s^{-1}$

Q_n = Advective outflow from segment n, $m^3 \cdot d^{-1}$

V_n = Volume of segment n, m^3

d_z = Vertical thickness of segment, m

Z_n = Depth at segment, m

vs_c = Settling rate of state variable C, $m \cdot d^{-1}$

T_n = Temperature in segment n , C

T_{opt} = Optimal growth temperature, C

k_p = Phosphorus half saturation constant

ke_n = Light extinction coefficient, m^{-1}

I_0 = Incident solar radiation, $langley \cdot d^{-1}$

I_{sat} = Saturating solar radiation, $langley \cdot d^{-1}$

$Pg_{\max}$ = Maximum growth rate, d^{-1}

k_{pr} = Base phytoplankton respiration rate, d^{-1}

kg_{zoo} = Zooplankton grazing rate, $L \cdot mg \cdot d^{-1}$

Z_{eff} = Zooplankton grazing efficiency

r_{zoo} = Base zooplankton respiration rate, d^{-1}

kd_{zoo} = Zooplankton death rate, d^{-1}

a_{PC} = Phosphorus to carbon ratio

$k_{\min}$ = Phosphorus mineralization rate, d^{-1}

k_{ox} = Organic carbon oxidation rate, d^{-1}

k_{DO} = Half saturation constant for carbon oxidation

SOD_{20} = Sediment oxygen demand at 20 ^{0}C, $g \cdot m^{-2} \cdot d^{-1}$

a_{OC} = Oxygen to carbon ratio

k_{ox} = Oxygen surface mixing coefficient, $m \cdot d^{-1}$

Common Terms

Mass dispersion across the interface between segment n_{-1} and segment n, $mg \cdot L^{-1} \cdot d^{-1}$

$$Diff_u = \frac{E_u}{{d_z}^2}\left(C_{n-1} - C_n\right)$$

Mass dispersion across the interface between segment n_{+1} and segment n, $mg \cdot L^{-1} \cdot d^{-1}$

$$Diff_L = \frac{E_b}{d_z^{\ 2}}\left(C_{n+1} - C_n\right)$$

Mass advection from model segment n to eastern basin, $mg \cdot L^{-1} \cdot d^{-1}$

$$Out \quad = \frac{C_n \cdot Q_n}{V_n}$$

Mass settling across the interface between segment n_{+1} and segment n, $mg \cdot L^{-1} \cdot d^{-1}$

$$Pvs_n \ = \frac{vs_c}{d_z} \cdot C_n$$

Mass settling across the interface between segment n_{-1} and segment n, $mg \cdot L^{-1} \cdot d^{-1}$

$$Pvs2_n \ = \frac{vs_c}{d_z} \cdot C_{n-1}$$

Temperature Limitation in segment n

$$T\lim_n = \theta_g^{\ T_n - T_{opt}}$$

Phytoplankton

Phosphorus limitation in model segment n

$$P\lim_n \ = \frac{AP_n}{\left(k_P + AP_n\right)}$$

Light limitation in model segment n

$$I\lim_n \ = \left(\frac{2.178 \cdot FP}{ke_n \cdot Z_n}\right) \cdot \left(\exp\left(-\frac{I_0}{I_{sat}} \cdot \exp\left(-ke_n \cdot Z_n\right)\right) - \exp\left(-\frac{I_0}{I_{sat}}\right)\right)$$

Total growth limitation in segment n

$$G\lim_n = Min\left(I\lim_n, P\lim_n\right) \cdot T\lim_n$$

Phytoplankton growth in model segment n, $mg \cdot L^{-1} \cdot d^{-1}$

$$Pg_n = G\lim_n \cdot Pg_{\max} \cdot Phy_n$$

Phytoplankton respiration in model segment n, $mg \cdot L^{-1} \cdot d^{-1}$

$$\mathrm{Pr}_n = T\lim_n \cdot k_{\mathrm{Pr}} \cdot Phy_n$$

Phytoplankton death via grazing in model segment n, $mg \cdot L^{-1} \cdot d^{-1}$

$$Pd_n = kg_{zoo} \cdot T\lim_n \cdot Zoo_n \cdot Phy_n$$

Zooplankton

Zooplankton growth in model segment n, $mg \cdot L^{-1} \cdot d^{-1}$

$$Zg_n = Z_{eff} \cdot kg_{zoo} \cdot T\lim_n \cdot Phy_n \cdot Zoo_n$$

Zooplankton respiration in model segment n, $mg \cdot L^{-1} \cdot d^{-1}$

$$Zr_n = r_{zoo} \cdot T\lim_n \cdot Zoo_n$$

Zooplankton death in model segment n, $mg \cdot L^{-1} \cdot d^{-1}$

$$Zd_n = kd_{zoo} \cdot T\lim_n \cdot Zoo_n$$

Unavailable Phosphorus

Inefficient Zoo Grazing in segment n, $mg \cdot L^{-1} \cdot d^{-1}$

$$GrzIneff_n = a_{PC} \cdot \left(Pd_n - Zg_n\right)$$

Algal death in segment n, $mg \cdot L^{-1} \cdot d^{-1}$

$$UPd_n = a_{PC} \cdot Pd_n$$

Mineralization in segment n, $mg \cdot L^{-1} \cdot d^{-1}$

$$MinP_n = k_{\min} \cdot LimT_n \cdot UP_n$$

Available Phosphorus

Phosphorus uptake by phytoplankton segment n, $mg \cdot L^{-1} \cdot d^{-1}$

$$P_{uptake} = a_{PC} \cdot Pg_n$$

Detrital Carbon

Inefficient Zoo Grazing in segment n, $mg \cdot L^{-1} \cdot d^{-1}$

$$GrzIneff_n = Pd_n - Zg_n$$

Oxidation of organic carbon in segment n, $mg \cdot L^{-1} \cdot d^{-1}$

$$OxidC_n = k_{ox} \cdot LimT_n \cdot OC_n \cdot \left(\frac{DO_n}{DO_n + k_{DO}} \right)$$

Dissolved Oxygen

Sediment oxygen demand (only in bottom segment), $mg \cdot L^{-1} \cdot d^{-1}$

$$SOD_n = \frac{SOD_{20}\left(\theta_{SOD}{}^{T_n - 20}\right)}{dz}$$

Oxidation of organic carbon in segment n, $mg \cdot L^{-1} \cdot d^{-1}$

$$OxidDO_n = a_{OC} \cdot OxidC_n$$

Net Primary Production in segment n, $mg \cdot L^{-1} \cdot d^{-1}$

$$NPP_n = a_{OC} \cdot \left(P_g - P_r\right)$$

Surface reparation (only in top segment), $mg \cdot L^{-1} \cdot d^{-1}$

$$Raerition_n = \frac{k_{ox}}{dz} \cdot \theta_{ra}{}^{T_n - 20} \cdot \left(DO_{sat} - DO_n\right)$$

REFERENCES

Aku, P. M. K. and Tonn, W. M. 1997. Impact of hypolimnetic oxygenation on the vertical distribution of cisco (Coregonus artedi) in Amisk Lake, Alberta. Canadian Journal of Fisheries and Aquatic Sciences 54:2196-2206

Arend, K.K., Beletsky, D., Depinto, J.V., Ludsin, S.A., Roberts, J.J., Rucinski, D.K., Scavia, D., Schwab, D.J. & Höök, T.O. 2011. Seasonal and interannual effects of hypoxia on fish habitat quality in central Lake Erie. Freshwater Biology. 56: 366-383.

Ambrose, R.B., Wool, T.A., and Martin, J.L., 1993. The Water Quality Analysis Simulation Program WASP5, Part A: Model documentation, version 5.10, US Environmental Protection Agency, Env. Research Lab., Athens Georgia

Anderson, Thomas R. (2005) Plankton functional type modelling: running before we can walk? Journal of Plankton Research, 27, (11), 1073-1081

Atkinson, J.F., J.V. DePinto, and D.C.L. Lam. 1999. Water Quality. Chapter in: Potential Climate Change Effects on Great Lakes Hydrodynamics and Water Quality. D.C.L. Lam and W.M. Schertzer (eds). ASCE, Reston, VA.

Auer, M.T., Johnson, N.A., Penn, M.R., Effler, S.W. 1993. Measurement and verification of rates of sediment phosphorus release for a hypereutrophic urban lake. Hydrobiologia 253(1-3), pp 301-309.

Bates, B. C., Kundzewicz, Z. W., Wu, S., and Palutikof, J. P. 2008. Analysing regional aspects of climate change and water resources. IPCC Secretariat, Geneva.

Beeton, A. M. 1963. Limnological survey of Lake Erie 1959 and 1960.Great Lakes Fisheries Commission Technical Report. No. 6.

Beletsky, D., Schwab, D.J., 2001. Modeling circulation and thermal structure in Lake Michigan: Annual cycle and interannual variability. J. Geophys. Res. 106, 19745ï 19771.

Beletsky, D., N. Hawley, Y.R. Rao, H. A. Vanderploeg, R. Beletsky, D. J. Schwab and S.A. Ruberg. 2012. Summer thermal structure and anticyclonic circulation of Lake Erie, Geophysical Research Letters 39:L06605

Bertram, P. E. 1993. Total Phosphorus and Dissolved Oxygen Trends in the Central Basin of Lake Erie, 1970-1991. Journal of Great Lakes Research 19:224-236.

Bierman, V.J., Jr. and D.M. Dolan. 1976. Mathematical modeling of phytoplankton dynamics in Saginaw Bay, Lake Huron. In: Environmental Modeling and Simulation. Proceedings of a Conference sponsored by the U.S. Environmental Protection Agency and held at Cincinnati, Ohio, April 19-22, 1976.pp. 773-779.

Bierman, V.J., Jr., D.M. Dolan, E.F. Stoermer, J.E. Gannon and V.E. Smith. 1980. The development and calibration of a multi-class, internal pool, phytoplankton model for Saginaw Bay, Lake Huron. J. Great Lakes Res.

Bierman, V. J., Kaur, J., Depinto, J.V., Feist, T. J., Dilks, D. W. 2005. Modeling the role of zebra mussels in the proliferation of blue-green algae in Saginaw Bay, Lake Huron. J. Great Lakes Res. 31:32ï 55. 2005

Blumberg, A. F. and Di Toro, D. M. 1990. Effects of Climate Warming on Dissolved Oxygen Concentrations in Lake Erie. Transactions of the American Fisheries Society 119:210-223.

Blumberg, A. F., Mellor, G. L. 1987. A description of a three-dimensional coastal ocean circulation model. In Three-Dimensional Shelf Models, Coastal and Estuarine Sciences, ed. N. S. Heaps, pp. 1-16. American Geophys. Union.

Bocaniov, S.A., Smith, R.E.H., Spillman, C.M., Hipsey, M.R., Leon, L.F. 2013. The nearshore shunt and the decline of the phytoplankton spring bloom in the Laurentian Great Lakes: insights from a three-dimensional lake model. Hydrobiologia. DOI 10.1007/s10750-013-1642-2

Borsuk, M., Higdon, D., Stow, C. and Reckhow, K. 2001. A Bayesian hierarchical model to predict benthic oxygen demand from organic matter loading in estuaries and coastal zones. Ecological Modelling 143:165ï 181.

Bricker S, Longstaff B, Dennison W, Jones A, Boicourt K, Wicks C, Woerner J. 2007. Effects of Nutrient Enrichment in the Nationôs Estuaries: A Decade of Change, National Estuarine Eutrophication Assessment Update. NOAA Coastal Ocean Program Decision Analysis Series No. 26. National Centers for Coastal Ocean Science, Silver Spring, MD. 322 pp

Breitburg, D. 2002. Effects of Hypoxia, and the Balance between Hypoxia and Enrichment, on Coastal Fishes and Fisheries. Estuaries 25:767-781.

Bridgeman, T.B., J.D. Chaffin, and J.E. Filbrun. 2013. A novel method for tracking western Lake Erie Microcystis blooms, 2002ï 2011. Journal of Great Lakes Research, 39(1):83-89.

Burns, N. M., Rockwell, D. M., Bertram, P. E., Dolan, D. M., and Ciborowski, J. J. H. 2005. Trends in Temperature, Secchi Depth, and Dissolved Oxygen Depletion Rates in the Central Basin of Lake Erie, 1983-2002. Journal of Great Lakes Research 31:35-49.

Calhoun, F. G., Bigham, J. M., and Slater, B. K. 2002. Relationships among Plant Available Phosphorus, Fertilizer Sales, and Water Quality in Northwestern Ohio. Journal of Environmental Quality 31:46.

Chapra, S.C. 1977. Total phosphorus model for the Great Lakes. Journal of the Environmental Engineering Division, American Society of Civil Engineers. l03(EE2): 147-161.

Chapra, S. C. 1997 Surface Water Quality Modeling, Hardbound: McGraw Hill.

Chapra, S. C. and David Dolan. 2012. Great Lakes total phosphorus revisited: 2. Mass balance modeling. Journal of Great Lakes Research 28(4):741-754.

Charlton, M. N. 1980a. Oxygen Depletion in Lake Erie: Has There Been Any Change? Can. J. Fish. Aquat. Sci. 37(1): 72-80.

Charlton, M. N. 1980b. Hypolimnion Oxygen Consumption in Lakes: Discussion of Productivity and Morphometry Effects. Can. J. Fish. Aquat. Sci. 37(10): 1531-1539.

Charlton, M.N., Lean, D.R.S. 1987 Sedimentation, Resuspension, and Oxygen Depletion in Lake Erie (1979), Journal of Great Lakes Research. 13(4):709-723

Chen, C., R. Ji, D.J. Schwab, D. Beletsky, G.L. Fahnenstiel, T.H. Johengen, H.A. Vanderploeg, B.J. Eadie, M. Bundy, W. Gardner, and J. Cotner. 2002. A model study of the coupled biological and physical dynamics in Lake Michigan. Ecological Modeling, 152, 145-168

Cook, G. D., Welch, E. B., Peterson, S., and Newroth, P. 1993. Restoration and Management of Lakes and Reservoirs. Boca Raton, FL: Lewis Publishers.

Croley, T. E. I. 1990. Laurentian Great Lakes double-CO2 climate change hydrological impacts. Climatic Change 17:27-47.

Depew, D.C., Guildford, S.J, Smith, R.E.H. 2006. Nearshoreï offshore comparison of chlorophyll a and phytoplankton production in the dreissenid-colonized eastern basin of Lake Erie. Canadian Journal of Fisheries and Aquatic Sciences, 63:1115-1129

DePinto, J.V., Young, T.C., McIlroy, M., 1986. Great Lakes water quality improvement: the strategy of phosphorus discharge control is evaluated. Environ. Sci. Technol. 20 (8), 752ï 759

Di Toro, D.M., D.J. O'Connor, J.L. Mancini and R.V.Thomann, 1973. A preliminary phytoplankton-zooplankton-nutrient model of Western Lake Erie. In Systems Analysis & Simulation in Ecology. Volume 3. Academic Press.

Di Toro, D. M., Thomas, N. A., Herdendorf, C. E., Winfield, R. P., and Connolly, J. P. 1987. A Post Audit of a Lake Erie Eutrophication Model. Journal of Great Lakes Research 13:801-825.

Di Toro, D.M. and W. Matystik, Jr. 1980. Mathematical models of water quality in large lakes. Part I: Lake Huron and Saginaw Bay model development, verification, and simulations. U.S. Environmental Protection Agency Ecological Research Series. EPA-600 / 3 -80 -056

Di Toro, D.M. and W. Matystik, Jr. 1980. Mathematical models of water quality in large lakes. Part I: Lake Huron and Saginaw Bay model development, verification, and simulations. U.S. Environmental Protection Agency Ecological Research Series. EPA-600 / 3 -80 -056

Di Toro, D., and J. Connolly. 1980. Mathematical models of water quality in large lakes. Part 2: Lake Erie. Report to EPA. EPA-600/3-80-065, July 1980.

Di Toro, D.M., N.A. Thomas, C.E. Herdendorf, R.P. Winfield, and J.P. Connolly, 1987. A post audit of a Lake Erie eutrophication model. Journal of Great Lakes Research. 13:801-825

Diaz, R. J. 2001. Overview of Hypoxia around the World. Journal of Environmental Quality 30:275-281.

Diaz, R. J., and R. Rosenberg. 2008. Spreading Dead Zones and Consequences forMarine Ecosystems. Science 321:926-929.

Dolan, D. M. 1993. Point source loadings of phosphorus to Lake Erie: 1986-1990. Journal of Great Lakes Research 19:212-223.

Dolan, D. M. and Chapra, S.C. 2012. Great Lakes total phosphorus revisited: 1. Loading analysis and update (1994ï 2008), Journal of Great Lakes Research, 38(4):730-740

Dolan, D.M., and McGunagle, K.P., 2005. Lake Erie total phosphorus loading analysis and update: 1996ï 2002. J. Great Lakes Res. 31 (Suppl. 2), 11ï 22

ECWSTB (Environment Canada, Water Science & Technology Branch) ftp:// charon.cciw.ca (accessed June 2007)Edwards, W. J., Conroy, J. D., and Culver, D. A. 2005. Hypolimnetic Oxygen Depletion Dynamics in the Central Basin of Lake Erie. Journal of Great Lakes Research 31:262-271.

Edwards, W. J., Conroy, J. D., and Culver, D. A. 2005. Hypolimnetic Oxygen Depletion Dynamics in the Central Basin of Lake Erie. Journal of Great Lakes Research 31:262-271.

Effler, S. W. 1996. Limnological and Engineering Analysis of a Polluted Urban Lake: Prelude to Environmental Management of Onondaga Lake, New York . New York: Springer.

Effler, S. W., Boone, S. R., Siegfried, C., and Ashby, S. L. 1998. Dynamics of Zebra Mussel Oxygen Demand in Seneca River, New York. Environmental Science & Technology 36:807-812.

El-Shaarawi, A. H. 1987. Water Quality Changes in Lake Erie , 1968-1980. Journal of Great Lakes Research 13:674-683.

Fang, X. and Stefan, H. G. 1997. Simulated climate change effects on dissolved oxygen characteristics in ice-covered lakes. Ecological Modelling 103:209-229.

Friedrichs, M.A.M., Hood, R.R., Wiggert, J.D., 2006. Ecosystem model complexity versus physical forcing: quantification of their relative impact with assimilated Arabian Sea data. Deep-Sea Research II 53, 576ï 600.

Goldman, J.C., Oswald, W.J., and Jenkins, D. 1974. The Kinetics of Inorganic Carbon Limited Algal Growth. Journal of Water Pollution Control Federation. Vol. 46, No. 3, Part I (Mar., 1974), pp. 554-574

GLWQA 1978. Great Lakes Water Quality Agreement.

Hagy, J.D., W. R. Boynton, C. W. Keefe, and K. V. Wood. 2004. Hypoxia in Chesapeake Bay, 1950-2001: Long term change in relation to nutrient Loading and River Flow. Estuaries 27:634-658.

Hanson, P. C., A. Pollard, D. L. Bade, K. Predick, S. R. Carpenter, and J. Foley. 2004. A model of carbon evasion and sedimentation in temperate lakes. Global Change Biology. 10: 1285-1298.

Hecky, R.E.H. Smith, D.R. Barton, S.J. Guildford, W.D. Taylor, M.N. Charlton, and T. Howell. 2004. The near shore phosphorus shunt: a consequence of ecosystem engineering by dreissenids in the Laurentian Great Lakes. Can. J. Fish. Aquat. Sci. 61:1285-1293

Helly, J. J. and Levin, L. A. 2004. Global Distribution of Naturally Occurring Marine Hypoxia on Continental Margins. Deep-sea Research I 51:1159-1168.

Howarth, R.W., Marino, R., and Cole, J.J. 1988. Nitrogen Fixation in Freshwater, Estuarine, and Marine Ecosystems. 2. Biogeochemical Controls. Limnology and Oceanography , Vol. 33, No. 4, Part 2: Comparative Ecology of Freshwater and Marine Ecosystems, pp. 688-701

Huang, A., Yerubandi R. Rao, and Youyu Lu. Evaluation of a 3D hydrodynamic model and atmospheric model forcing using observations in Lake Ontario. J. Geophys Res. (in press).

IFYLE 2006. NOAA Great Lakes Environmental Research Laboratory: International Field Years on Lake Erie (IFYLE). http://www.glerl.noaa.gov/ifyle/ 11/12/2006.GLNPO (Great Lake National Program Office. http://cdx.epa.gov/ (accessed February 2007).

Kalff, J., 2001. Limnology. Prentice Hall, 2001

Kantha, L. H. and Clayson, C. A. 1994. An improved mixed layer model for geophysical applications. Journal of Geophysical Research 99:25235-25266.

Keenan, J.D. and M.T. Auer. 1974. The influence of phosphorus luxury uptake on algal bioassays. Journal of the Water Pollution Control Federation , 46:532-542.

King, D. L., 1970, The role of carbon in eutrophication: Water Pollution Control Federation Jour., v. 42, no. 11, p. 2035-2051

Kritzberg, E. S., Cole, J. J., Pace, M. L., Graneli, W., and Bade, D. L. 2004. Autochthonous versus allochthonous carbon sources of bacteria: Results from whole-lake 13C addition experiments. Limnology and Oceanography 49:588-596.

Lam, D.C.L, and W.M. Schertzer. 1987. Lake Erie thermocline model results: comparison with 1967-1982 data and relation to anoxic occurrences. Journal of Great Lakes Research 13: 757-769.

Lampert, W. and Ulrich Sommer. 1998. Limnoecology: The ecology of lakes and streams. 2nd ed. Oxford University Press, 1998

Lehman, J. T. 2002. Mixing patterns and plankton biomass of the St. Lawrence Great Lakes under climate change scenarios. Journal of Great Lakes Research 28:583-596.

Lesht, B.M., Fontaine, T.D., Dolan, D.M., 1991. Great Lakes total phosphorus model: post audit and regionalized sensitivity analysis. Journal of Great Lakes Research 17 (1), 3ï17.

Leon, L.F., Smith, R.E.H., Hipsey, M.R., Bocainov, S.A., Higgins, S.N., Hecky, R.E., Antenucci, J.P. and Guildford, S.J. (2011) Application of a 3D hydrodynamic-biological model for seasonal and spatial dynamics of water quality and phytoplankton in Lake Erie, J. Great Lakes Res 37-1, Mar 2011, pp. 41-53

LimnoTech. 2010. Development, Calibration, and Application of the Lower Maumee River ï Maumee Bay Model. Technical report prepared for the U.S. Army Corps of Engineers, Buffalo District. 113 pp. (December 30, 2010).

Lofgren, B. M., Quinn, F. H., Clites, A. H., Assel, R. A., Eberhardt, A. J., and Luukkonen, C. L. 2002. Evaluation of potential impacts on Great Lakes water resources based on climate scenarios of two GCMs. Journal of Great Lakes Research 28:537-554.

Makarewicz, J. C. 1993. Phytoplankton biomass and species composition in Lake Erie, 1970ï 1987. Journal of Great Lakes Research 19:258-274.

Matisoff, G. and Neeson, T. M. 2005. Oxygen Concentration and Demand in Lake Erie Sediments. Journal of Great Lakes Research 31:284-295.

McCormick, M.J. and Meadows, G.A., 1988. An Intercomparison of Four Mixed Layer Models in a Shallow Inland Sea. Journal of Geophysical Research, Vol. 93, No. C6, pp. 6774-6778.

Mellor, G. L. and Blumberg, A. F. 2004. Wave breaking and ocean surface layer response. Journal of Physical Oceanography 34:693-698.

Mellor, G. L., and T. Yamada, Development of a turbulence closure model for geophysical fluid problems, Rev. Geophys., 20, 851ï 875, 1982.

Mellor, G.L. 2001. One-dimensional, ocean surface layer modeling: a problem and a solution. J. Phys. Ocean., 31; 790-809.

Ostrom, N.E., Russ, M.E., Field, A., Piwinski, L., Twiss, M.R., Carrick, H.J. 2005a. Ratios of Community Respiration to Photosynthesis and Rates of Primary Production in Lake Erie Via Oxygen Isotope Techniques, Journal of Great Lakes Research, Volume 31, Supplement 2. 138-153

Ostrom, N.E., Carrick, H.J., Twiss, M.R., Piwinski, L. 2005b. Evaluation of primary production in Lake Erie by multiple proxies. Oecologia (2005) 144: 115ï 124

Otsuki, A., Wetzel, R.G., 1972. Coprecipitation of phosphate with carbonates in a marl lake. Limnol. Oceanogr. 17, 763ï 767.

Nixon, S.W., 1995, Coastal marine eutrophication--A definition, social causes, and future concerns: Ophelia, v. 41, p. 199-219.

Park, K., Kuo, A.Y., Shen, J., Hamrick, J.M. 1995. A three-dimensional hydrodynamic-eutrophication model (HEM-3D): Description of water quality and sediment process submodels. Special Report in Applied Marine Science and Ocean Engineering No. 327. Virginia Institute of Marine Science, VA 23062

Park, R.A. and Jonathon S. Clough. 2004. AQUATOX Release 2: Modeling environmental fate and ecological effects in aquatic systems. Volume 2: Technical Documentation. U.S. Environmental Protection Agency Office of Water. January 2004.

Paulson, C. A. and Simpson, J. 1977. Irradiance measurements in the upper ocean. Journal of Physical Oceanography 7:952-956.

Rao, Y. R., N. Hawley, M. N. Charlton, and W. M. Schertzer. 2008. Physical processes and hypoxia in the central basin of Lake Erie. Limnology and Oceanography 53:2007-2020

Redfield A.C., 1934. On the proportions of organic derivations in sea water and their relation to the composition of plankton. In James Johnstone Memorial Volume. (ed. R.J. Daniel). pp. 177-192.Rabalais, N.N., R.E. Turner, and W.J. Wiseman, 2002. Gulf of Mexico hypoxia, aka "The dead zone". Annual Review of Ecology and Systematics. 33:235-263.

RCA. 2002. Userôs Guide for RCA: Release 3.0. June 2004. HydroQual, Inc.

Richards, R. P. 2006. Trends in sediment and nutrients in major Lake Erie tributaries, 1975-2004. In *Lake Erie Lakewide Management Plan 2006 Update* pp. 22.

Richards, R. P. and Baker, D. B. 2002. Trends in water quality in LEASEQ rivers and streams, 1975-1995. Journal of Environmental Quality 31:90-96.

Ro K.S., Hunt, P.G., Poach, M.E. 2007. Wind-driven surficial oxygen transfer. Crit. Rev. Environ. Sci. Technol., 37 (6) pp. 539ï 563

Roberts, J.J. T.O. Höök, S.A. Ludsin, S.A. Pothoven, H.A. Vanderploeg, and S.B. Brandt. 2009. Effects of hypolimnetic hypoxia on foraging and distributions of Lake Erie yellow perch. Journal of Experimental Marine Biology and Ecology. 381: S132-S142.

Roberts, J.J., P.A. Grecay, S.A. Ludsin, S.A. Pothoven, H.A. Vanderploeg, and T.O. Höök. 2012. Evidence of hypoxic foraging forays by yellow perch (Perca flavescens) and potential consequences for prey consumption. Freshwater Biology. 57: 922-937.

Rosa, F. 1985. Sedimentation and Sediment Resuspension in Lake Ontario, Journal of Great Lakes Research 11(1): 13-25

Rosa, F. and Burns, N. M. 1987. Lake Erie Central Basin Oxygen Depletion Changes from 1929-1980. Journal of Great Lakes Research 13:684-696.

Rucinski, D. K., D. Beletsky, J.V. DePinto, D.J. Schwab, and D. Scavia. 2010. A simple 1-dimensional, climate based dissolved oxygen model for the central basin of Lake Erie. Journal of Great Lakes Research, 36:465-476.

Scavia, D. 1980. An ecological model of Lake Ontario. Ecological Modeling, 1980, 8: 48-78

Scavia, D., J. D. Allan, K. K. Arend, S. Bartell, D. Beletsky, N. S. Bosch, S. B. Brandt, R. D. Briland, I. Daloĵ lu, J. V. DePinto, D. M. Dolan, M. A. Evans, T. M. Farmer,D. Goto, H. Han, T. O. Höök, R. Knight, S. A. Ludsin, D. Mason, A. M. Michalak, R. P. Richards, J. J. Roberts, D. K. Rucinski, E. Rutherford, D. J. Schwab, T. Sesterhenn, H. Zhang, Y. Zhou (in review) Assessing and addressing the re-eutrophication of Lake Erie: Central Basin Hypoxia

Schertzer, W.M.,J.H. Saylor, F.M. Boyce, D.G. Robertson, and F.Rosa. 1987. Seasonal thermal cycle of Lake Erie. Journal of Great Lakes Research 13: 468-486.

Schloesser, D. W., Stickle, R. G., and Bridgeman, T. B. 2005. Potential Oxygen Demand of Sediments from Lake Erie. Journal of Great Lakes Research 31:272-283.

Schwab, D. J., Bedford, K. W. 1999. The Great Lakes Forecasting System. In In Coastal Ocean Prediction, Coastal and Estuarine Studies, ed. C. N. K. Mooers, pp. 157-173. Washington, D.C.: American Geophysical Union.

Snodgrass, W. J. 1987. Analysis Of Models And Measurements For Sediment Oxygen Demand In Lake Erie. Journal of Great Lakes Research 13:738-756.

Snodgrass, W. J. and Fay, L. A. 1987. Values of sediment oxygen demand measured in the central basin of Lake Erie, 1979. Journal of Great Lakes Research 13:724-730.

Smith, R.E.H., Hiriart-Baer, V.P., Higgins, S.N., Guildford, S.J., and Charlton, M.N. 2005 Planktonic Primary Production in the Offshore Waters of Dreissenid-infested Lake Erie in 1997. Journal of Great Lakes Research, Volume 31, Supplement 2. 50-61.

Stern, K. R., Jansky, S., and Bidlack, J. E. 2003. Introductory Plant Biology. McGraw Hill.

Thomann, R.V., D.M. DiToro, R.P. Winfield and D.J. O'Connor. 1975. Mathematical modeling of phytoplankton in Lake Ontario I. Model development and verification. U.S. Environmental Protection Agency Ecological Research Series. EPA-660/3-75-005. 177 p,

Thomann, R.V., R.P. Winfield , D.M. Di Toro and D.J. O'Connor, 1976. Mathematical modeling of phytoplankton in Lake Ontario. 2. Simulations using LAKE 1 Model. EPA-660/3-76-065, USEPA ERL, Duluth, MN.

Twiss, M.R., R.M.L. McKay, R.A. Bourbonniere, G.S. Bullerjahn, H.J. Carrick, R.E.H. Smith, J.G. Winter, N.A. D'souza, P.C. Furey, A.R. Lashaway, M.A. Saxton, S.W. Wilhelm. 2013. Diatoms abound in ice-covered Lake Erie: An investigation of offshore winter limnology in Lake Erie over the period 2007 to 2010. Journal of Great Lakes Research, 38(1):18-30.

Urban, N.R., M.T. Auer, S.A. Green, X. Lu, D.S. Apul, K.D. Powell, and L. Bub (2005), Carbon cycling in Lake Superior, Journal of Geophysical Research 110, C06S90.

Walker, R.R. and W.J. Snodgrass. 1986. Model for Sediment Oxygen Demand in Lakes. Journal of Environmental Engineering 112(1): 25-43

Vanderploeg, H. A.; Ludsin, S. A.; Ruberg, S. A.; Hook, T. O.; Pothoven, S. A.; Brandt, S. B.; Lang, G. A.; Liebig, J. R.; Cavaletto, J. F., 2009.Hypoxia affects spatial distributions and overlap of pelagic fish, zooplankton, and phytoplankton in Lake Erie. J Exp Mar Biol Ecol 381, S92-S107.

Vitousek, P.M., K. Cassman, C. Cleveland, T. Crews, C.B. Field, N.B. Grimm, R.W. Howarth, R. Marino, L. Martinelli, E.B. Rastetter,and J.I. Sprent. 2002. Towards an ecological understanding of biological nitrogen fixation. Biogeochemistry 57/58:1ï 45.

Vollenweider R. A. (1975) Input-output models Input-output models with special reference to the phosphorus loading concept in limnology,. Schweiz. Z. Hydrol. 37, 53-84.

Vollenweider, R. A., Rast, W., Kerekes, J. 1980. The phosphorus loading concept and Great Lakes eutrophication. In *Phosphorus Management Strategies for Lakes*, eds. R. C. Loehr, C. S. Martin, and W. Rast, Ann Arbor, MI: Ann Arbor Science Publishers Inc.

Wang, W., 1980. Fractionation of sediment oxygen demand. Water Research, 14(6): 603-612

Wetzel, R.G., 2001. Limnology: Lake and River Ecosystems, 3rd ed. Academic Press, 2001

Whitledge TE. 1985. Nationwide review of oxygen depletion and eutrophication in estuarine and coastal waters. Executive Summary. Report to U.S. Dept. of Commerce, NOAA, National Ocean Service. Rockville, MD. 28 p.

Wool, T.A., Ambrose, R.B., Martin, J. L, and Coormer, E.A. 2002 Water Quality Analysis Simulation Program (WASP). Version 6.0

Zhang, H., Culver, D.A. and Boegman, L. 2008. A two-dimensional ecological model of Lake Erie: Application to estimate dreissenid impacts on large lake plankton populations. Ecological Modelling. 214: 219-241

Zhou, Y., Obenour, D.R., Scavia, D., Johengen, T.H. and Michalak, A.M., 2013. Spatial and Temporal Trends in Lake Erie Hypoxia, 1987-2007. Environ Sci Technol. 47, 899-905.